Collapse Analysis and Selective Retrofitting
using the Applied Element Method, AEM

Cosimo Pellecchia
* * * * * *

Supervisors
Prof. G.P. Cimellaro, Supervisor
Prof. A. Cardoni, Co-Supervisor

Politecnico di Torino
March 31, 2024

I hereby declare that, the contents and organisation of this dissertation constitute my own original work and does not compromise in any way the rights of third parties, including those relating to the security of personal data.

Cosimo Pellecchia
Turin, March 31, 2024

Summary

The main purpose of this research was to develop a strategy for selective retrofitting against progressive collapse, using high-fidelity numerical models to reproduce collapse propagation. In other words, the purpose was to understand if it can be possible to detect any specific path in collapse propagation, and if any specific lack of structural details or structural design mistake can be selected and fixed to prevent the initial failure and its spreading to the rest of the structure.

To do so, the research investigated four well-known collapse cases occurred over the last few decades: the collapse of the Polcevera Viaduct in Genoa in 2018, the partial collapse of the Champlain Tower South residential building in Surfside, Miami, in 2021, the collapse of the Pyne Gould office building in New Zealand in 2011, and the collapse of the transept and main dome of the Basilica di Collemaggio in L'Aquila, after the 2009 seismic event. The initial work consisted of retrieving the original construction drawings of the structures. In the case of the Polcevera Viaduct and Pyne Gould Building, most of the original drawings were accessed through online resources. The original drawings of the Champlain Tower South were requested for research purposes to the municipality of Surfside, Miami. The history of the Basilica di Collemaggio was reconstructed by accessing the Office for Preservation of Cultural and Architectural Heritage archive in L'Aquila. Due to the complex geometry, some of the investigated cases also required direct data acquisition through either a terrestrial laser scanner (Basilica di Collemaggio), or trough photogrammetric point cloud generation from aerial and satellite images (Pyne Gould building and the Polcevera Viaduct).

Next, detailed AEM numerical models were developed based on the retrieved data: 3D elements (8-node cuboids) connected through implicit springs were employed to reconstruct the geometry of the buildings; reinforcing bars (RTF), in reinforced concrete (RC) assembly, were introduced by coupling the mechanical contribution of implicit springs having equivalent area. The Maekawa and Okamura

(1983) elastoplastic model was generally considered for matrix springs representing the axial behaviour of the concrete material; the Menegotto and Pinto (1973) cyclic model was employed for equivalent springs representing the reinforcing bars. The work involved the exact reproduction of the reinforcing bars, stirrups, and tendons' shape in ordinary and pre-stressed assemblies. In addition, degradation phenomena were also considered by introducing area reduction factors in specific portions of the structures. Several sensitivity analyses were carried out, considering both non-linear static (degradation stage) and dynamic analyses (collapse stage).

Among others, the time step, the number of increments, and the proper mesh ratio to reliably represent the collapse phenomenon were investigated, trying to strike a balance between analysis accuracy and the use of computational resources.

Initial analyses were carried out comparing different validation cases, from 2D-frame component level to 3D plane problems (Grunwald et al. 2018), while comparing analysis results and experimental data. Preliminary data on analysis parameters were acquired by comparing actual collapse test results, carried out at Politecnico di Torino's laboratory on an RC beam sample, to AEM analysis results using the Digital Image Correlation, DIC, technique. Results were presented at the Tenth International Conference on Bridge Maintenance, Safety and Management (IABMAS 2020), held in Sapporo, Hokkaido, Japan, in 2021, and later published in 2021 in Bridge Maintenance, Safety, Management, Life-Cycle Sustainability and Innovations edited by Taylor & Francis (Marco Domaneschi et al. 2021). Specific time steps, mesh ratios, and material parameters were defined considering both the initial crack propagation and the collapse phase when element separation and collision occur.

A thin section correction factor in the case of one-element dept in the mesh was considered in the full collapse analysis; in addition, an RTF bending ratio was also introduced to replicate the actual shear stiffnesses of bars in cracking concrete. A micro-modelling approach was adopted in the development of the numerical model of the Basilica di Collemaggio, introducing equivalent springs representative of the combined behaviour of units and mortar, while also replicating the actual stagger pattern of the original masonry.

The initial approach was a forensic one: it consisted of applying to the structures the collapse load which could have determined the observed collapse; the Pyne Gould building and the Basilica di Collemaggio, were subject to the same ground motion acceleration recorded from a nearby station the day of the collapse; the Polcevera viaduct and the Champlain Towers building, which apparently collapsed without any significant external load applied to the structure, were highly degraded till collapse occurred.

In all the cases a series of "what if" scenarios were investigated: in the case of the Polcevera viaduct, which essentially consisted of macro-elements composed in a "balanced system" (the tower, the deck, the trestle, and the strands), a series of degradation analyses were carried out considering the residual capacity of each macro-element. Analysis shows that both the deck, the trestle, and the tower itself would have been able to withstand levels of degradation that far exceeded what was reported in the report about the condition of the structure. However, the collapse of the structure was easily achieved when degrading the strands. In addition, it was observed how the loss of one of the strands would have induced a torsional force in the deck which was not considered in the original design. Finally, the derived collapse mechanism was compared with the actual footage of the collapse and found to be reasonably in accordance. A comparison between the actual debris distribution obtained by reconstructing the 3D point cloud of the area from aerial images and the actual analysis results was also discussed and the final findings of the research were published in Engineering Structures edited by Elsevier: "Collapse analysis of the Polcevera viaduct by the applied element method", M. Domaneschi, C. Pellecchia, E. De Iuliis, G.P. Cimellaro, M. Morgese, A.A. Khalil, F. Ansari (M. Domaneschi et al. 2020). The collapse of the Champlain Towers condo in Miami was investigated by assuming both differential foundation settlement and localized degradation scenarios. During the research, it was observed how the building was sensitive to the loss of perimeter columns, due to the reduced load redistribution capacity at the perimeter of the building.

The analysis found the hypothesis of differential foundation settlement unrealistic, as it would have involved a significant number of columns with no actual evidence of such diffuse damage.

On the other hand, while testing different degradation scenarios, it was observed how the collapse of a single slab at the basement level would have initiated a disproportionate collapse of the structure. In fact, the one-floor basement was composed of high-depth beams directly connected to the perimeter columns of the twelve-story building. The deep beams were functioning as "slab drops", covering the different elevations at the perimeter of the pertinent area of the building. Their failure, due to degradation, would have induced a significant bending moment on the perimeter columns, which were not designed to sustain it.

In addition, the resultant collapse dynamic was found to be reasonable in accordance with what was recorded by a surveillance camera on the day of the collapse. The findings of this research were published last year in the Journal of Structural Engineers edited by ASCE: "Progressive Collapse Analysis of the Champlain Towers South in Surfside, Florida", C. Pellecchia; A. Cardoni, G. P.

Cimellaro, M. Domaneschi, F. Ansari, A.A. Khalil. In the case of the Pyne Gould Building, it was observed how the time-history record of the 6.3 Magnitude earthquake that occurred the 22 February 2011, would have induced a flexural/buckling failure in the RC core of the building. In fact, a vertical discontinuity was found in the east core wall of the building, most probably due to architectural distribution reasons. Such discontinuity would have induced a failure just above the ground floor of the building, where the core wall was missing. Additional analysis carried out employing several different time-history records showed a collapse mechanism originating always from that specific point of the structure. Analysis results were validated by comparing a 3D point cloud derived from satellite images of the actual debris distribution to the actual collapse shape resulting from the analysis. The deviation between the two models was found to be within acceptable range and the findings of the research were later published in Engineering Structures edited by ELSEVIER: "Reliability of collapse simulation - Comparing finite and applied element method at different levels", C. Grunwald, A.A. Khalil, B. Schaufelberger, E.M. Ricciardi, C. Pellecchia, E. De Iuliis, W. Riedel (Grunwald et al. 2018).

Most of the research was carried out on themes related to progressive collapse and collapse simulation; however, slightly different was the work carried out to assess the spreading of damage in the Basilica di Collemaggio, as a consequence of the 5.9 Magnitude earthquake that struck the city of L'Aquila the 6 April 2009. The Basilica di Collemaggio is one of the most known and iconic examples of architectural heritage in L'Aquila. As most of the architectural heritage, is the result of centuries of transformation and overlay of different construction techniques and peculiar structural details. The research investigated the capabilities of the AEM technique to reliably replicate the seismic behavior of the Basilica by employing a micro-modeling approach, considering the different staggered patterns in the different masonry specimens, the presence of voids, cavities in the masonry walls, as well as the actual unit distributions in vaults and columns. In addition, the presence of steel bars and RC beams was also considered and explicitly introduced in the numerical model either by means of 3D elements or implicit springs. The actual staggered pattern of masonry and the complex geometry of the Basilicas were reconstructed via terrestrial laser scanning. The point cloud was transposed into 3D elements representing the same units while equivalent springs were introduced to replicate the combined behavior of unit and mortar. The obtained numerical model was able to replicate crack patterns and in-plane/out-of-plane behavior of the Basilica. The final damage pattern obtained through non-linear dynamic analysis, employing the time-history record of a nearby station on the day of the strike, was

finally compared to the actual damage observed using an ortho-photo technique. The analysis has shown an overall damage state comparable with what was observed after the earthquake and the results of the research were presented at COMPDYN 2023, 9th ECCOMAS Thematic Conference on Computational Methods in Structural Dynamics and Earthquake Engineering, "*Damage pattern analysis of the Basilica di Collemaggio using AEM micro-modeling*", C. Pellecchia, A. Cardoni, G.P. Cimellaro, A. A. Khalil (Pellecchia et al. 2023).

Acknowledgment

I would like to dedicate this thesis to my colleagues at ASI.

To Edward Di Girolamo and Steven Scoba, who believed in me when I couldn't speak a word in English.

To Dr. Ahmed Amir Khalil, Dr. Hatem Tagel-Din, and Dr. Ayman El Fouly, who supported me all the way long, in proving them right.

Finally, to two of the best colleagues one could ever desire to work with, my dear friend Emiliano De Iuliis and my mental coach Samanta Tosolini.

Contents

List of Tables

List of Figures

Chapter 1

Collapse simulation

Introduction

Most of the Reinforced Concrete (RC) structures in our modern society were built between the second half and the end of the 20th century. As a matter of fact, most of the buildings in which we are currently living have passed or are approaching the end of their service life. The effect of degradation, in conjunction with the inherent poor load redistribution capacity of RC frames, is gradually raising the concerns of the engineering community about the aging and the safety of our current buildings and infrastructures. Designed with a component-based approach, no provisions were considered in the past construction codes concerning the risk of progressive collapse. Among others, the recent collapse of the Morandi Bridge in Genoa in 2018 and of the Champlain Towers South in Surfside, Miami, in 2021 are representative examples of the consequences of a catastrophic collapse, both in terms of lives and economic losses.

The attention to the progressive collapse of structures dates back to the collapse of the Ronan Point building in UK in 1968. Over the last decades, several methodologies were developed for progressive collapse assessment. However, the presence of key construction details and structural peculiarities, as well as overall load redistribution capacity, and crack propagation effects were often neglected due to the computational burden.

Nowadays, while constituting an increasing requirement in modern structural assessment procedures, explicit collapse simulation can still be considered an open challenge in numerical modeling.

In fact, based on continuum domain and nodal compatibility, common numerical procedures such as the Finite Element Method cannot be directly applied to collapse simulation. On the other hand, discrete approaches such as the Discrete Element Method, DEM, often require significant computational resources.

Based on a combination of both FEM and DEM approaches, the Applied Element Method, AEM, is among the most promising numerical techniques for

collapse simulation. Compared to FEM, AEM approach does not require nodal compatibility and development of plastic hinges, or crack propagation till separation and subsequent collision are implicitly automated in the modeling technique. Thanks to recent advances in computational capabilities and the development of new numerical methodologies, high-fidelity collapse simulation can nowadays be considered a reasonable approach both to collapse analysis and progressive collapse design.

Collapse analysis

Over the last decades, the number of publications on themes related to the progressive collapse of buildings has exponentially increased (Gerasimidis Simos and Ellingwood Bruce 2023). The attention to the disproportionate effect of a local failure dates back to 1970, when the first regulation related to accidental load was introduced in the UK code, as a consequence of the partial collapse of the Ronan Point building in London (Vrouwenvelder Ton 2021). However, it was after the tragic terroristic attack on the World Trade Center in 2001 that the progressive collapse of structures captured the interest of the academic community (Lalkovski Nikolay and Starossek Uwe 2022). Several definitions of Progressive Collapse were proposed by different authors over the last decades; ASCE 7-05 (ASCE 2013) defines progressive collapse as "the spread of an initial local failure from element to element resulting, eventually, in the collapse of an entire structure or a disproportionately large part of it". Three common points can be identified among the different proposed definitions: the initial failure is local, the failure spreads to other structural members, and the final collapse is disproportionate to the initial failure (Kiakojouri et al. 2021). In the last decades, several countries introduced specific regulations to address the risk of progressive collapse. In the US, the General Service Administration (GSA) code (GSA 2013) was developed for government buildings, while the UFC 4-023-03 code (UFC 2016) was introduced for military buildings. In Europe, Annex A in Eurocode 1 was introduced accounting for the first time for Accidental Actions (CEN 2006).

In contrast with the seismic design of structures, which is largely addressed in worldwide regulations through a more prescriptive code compliance approach, progressive collapse design often requires a performance-based approach, by considering a series of "what if" scenarios (Fiorillo Graziano and Ghosn Michel 2022).

Given that the objective of progressive collapse design is to ensure that a structure can withstand a certain level of local damage and avoid collapse propagation, it is understandable how the prediction of the initial damage effects and its possible propagation can be crucial as well as numerically challenging. Over the past decade, several researchers working on progressive collapse design suggested the introduction of robustness indexes. They can either be based on analytical or simplified numerical approaches, such as alternate load-path methods and push-down analyses (Praxedes Conrado and Yuan Xian-Xun 2021). While both

these approaches can be effective in assessing the risk of progressive collapse of relatively symmetric and homogenous structural systems, the progressive design of complex structural systems may require a more advanced methodology, such as the creation of high-fidelity numerical models (Sadek Fahim et al. 2022). While this approach was considered prohibitive in the past, because of the required computational effort, non-linear dynamic analyses of high-fidelity numerical models are now feasible thanks to the latest advancements in hardware computational capabilities and numerical methodologies (Stylianidis Panagiotis M. and Nethercot David A. 2021) (Le Jia-Liang and Bažant Zdeněk P. 2022).

Among the numerical approaches to progressive collapse analysis, Finite Element Method, FEM, is widely adopted in several published studies. The FEM method can be efficiently used in progressive collapse analysis of frame structures, especially in code-based procedures (Kiakojouri et al. 2020). However, because the FEM solver is based on equilibrium equations, the solution cannot automatically implement element separations. Because of that, the capability to simulate the entire collapse of the structure is limited. Nevertheless, several strategies were developed in recent years to overcome FEM limitations in the analysis of large displacement problems. For example, the smeared crack technique was developed to allow for crack propagation in FEM analyses (Petrangeli Marco and Ožbolt Joško 1996). FEM application to progressive collapse analysis of entire structures often considers bi-dimensional frame elements to reduce the computational burden (Alashker Yasser, Li Honghao, and El-Tawil Sherif 2011). However, researchers also developed a component-level, and multi-scale models approach assuming the refined 3D modeling of only a portion of the structure (Li and Hao 2013), (Mpidi Bita Hercend et al. 2022). Lastly, the recent development of FEM coupling methodology (Lu et al. 2009), and refined numerical procedure for element removal, such as the degree-of-freedom (DOF) release (Xu et al. 2018), overcome the FEM limitations to progressive collapse simulation.

The Discrete Element Method, DEM, was also employed in progressive collapse analysis (Z. Lu, He, and Zhou 2018). Based on the compatibility of displacement, the DEM solver can account for element separation and rigid body collision (Hakuno Motohiko and Meguro Kimiro 1993); however, DEM requires large computational efforts, in particular when dealing with a comprehensive numerical model of the entire structure. To reduce analysis time and increase the accuracy of the results, several FEM-DEM methodologies were also developed over the years (X. Lu, Lin, and Ye 2009).

Among the numerical methodologies for structural analysis, the Applied Element Method (AEM) is considered one of the most efficient numerical approaches to collapse analysis and simulation (Grunwald et al. 2018). The methodology can automatically account for the formation of plastic hinges, development, and propagation of cracks, 3D load redistribution, as well as yielding and failure of reinforcing bars until element separations occur (M. Domaneschi et al. 2020).

Chapter 2

The Applied Element Method, AEM

Introduction to AEM

The AEM consists in discretizing the structure into relatively small rigid elements connected through zero-volume springs (Figure 1).
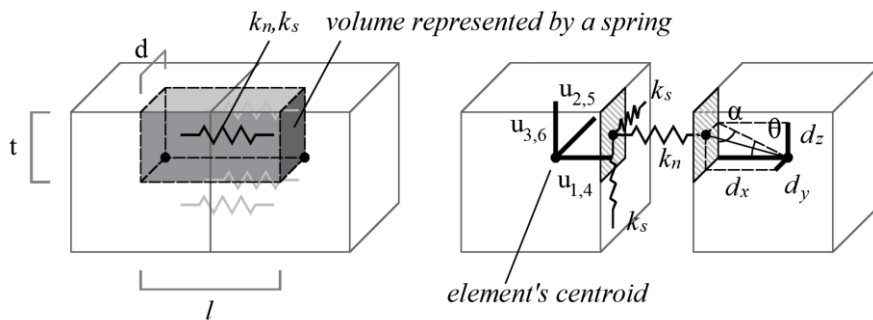
Figure 1. Discretization strategy in AEM approach.

The interface springs, uniformly distributed along the element's surfaces, describe stresses and deformation of a certain volume δV. A geometrical relation is determined between the centroid of the eight-node element and the contact point in which the surface spring is located (Figure 2).
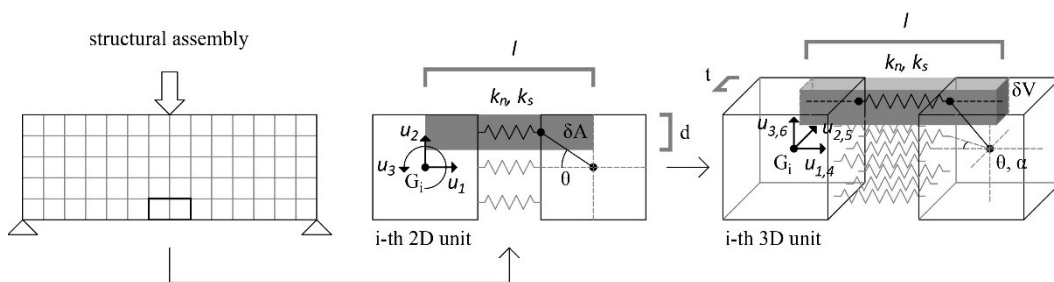
Figure 2. Matrix springs in AEM approach.

The springs represent the linear and non-linear behavior of the constitutive material. The axial stiffness, (k_n) and shear stiffnesses, ($k_{s,1}$, $k_{s,2}$) of the interface springs are determined based on the given elastic moduli, E and G, and the area (d·t) and length (l) of the represented i-volume, as per the following equations:

$$k_n = E_{dt}/l; \quad k_{s,1,2} = G_{dt}/l \qquad\qquad \text{Equation 1}$$

In the AEM approach to the analysis of RC structures, the mechanical behavior of the concrete material is represented by a series of springs distributed along the interface between the two elements (Figure 3, a).
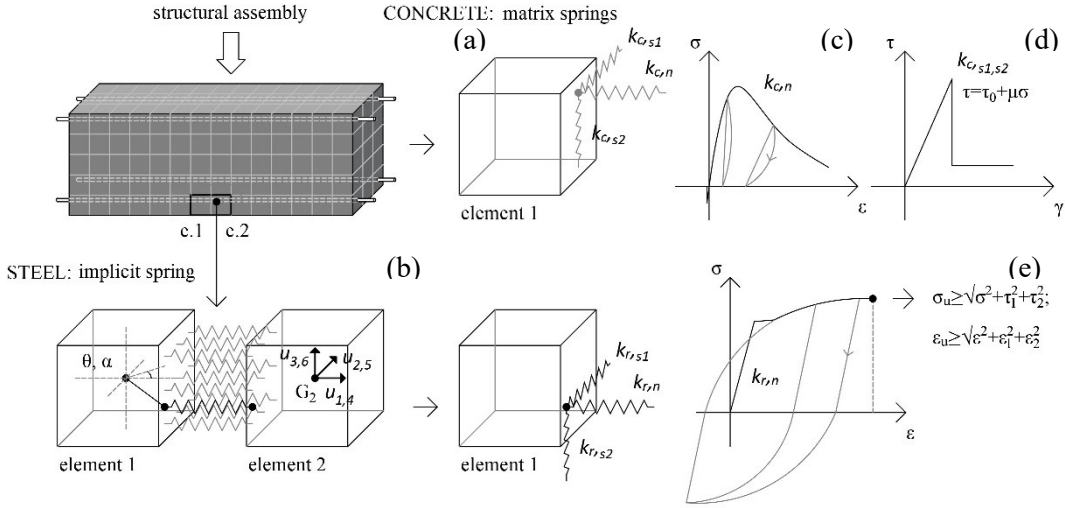
Figure 3. AEM discretization approach of RC assemblies and the corresponding constitutive laws for concrete and steel.

The contribution of steel rebars embedded in the material can be explicitly accounted for by coupling the mechanical contribution of additional springs representing the steel reinforcement. The steel springs are placed in their actual position in the cross-section of the considered structural element (Figure 3, b). As the springs consider the axial stiffness kn, and the shear stiffnesses ks,1 and ks,2, the contribution of both longitudinal and transversal reinforcing bars, for the given constitutive laws, is automatically accounted for in the numerical analysis. In this study, the Maekawa and Okamura (1985) model is considered for representing the axial behavior of concrete (Figure 3, c), while a linear relationship up to failure is assumed for the behavior of concrete subject to combined shear and compressive loads (Figure 3, d). Finally, the Menegotto and Pinto (1973) model is adopted for representing the nonlinear behavior of steel reinforcement (Figure 3, e).

Each 8-node element has six-degrees-of-freedom, three for translations and three for rotations. For each spring connecting two elements, the solver considers a 12×12 stiffness matrix. The dynamic equation and the solution procedure are the same as for the conventional implicit Finite Element Method (Equation 2).

$$[M][\Delta\ddot{U}] + [C][\Delta\dot{U}] + [K][\Delta U] = \Delta f(t) \qquad\qquad \text{Equation 2}$$

In Equation 2, [M] is the mass matrix; [C] the damping matrix; [K] the nonlinear stiffness matrix; $\Delta f(t)$ the incrementally applied load vector; [ΔU] the incremental displacement vector; [$\Delta\dot{U}$] and [$\Delta\ddot{U}$] the incremental velocity and

acceleration vectors. The solution of the equation system is based on the widely known Newmark Beta method. Element separation takes place when the resultant strain of the springs connecting two faces reaches a separation threshold. The connections are subsequently deleted, and the elements respond as free rigid bodies. A penalty-based contact algorithm searches for contact and enables the transmission of shear stresses between contacting elements under compressive loads, hence crack closure can be captured.

More details about the methodology can be found in Tagel-Din and Meguro (Tagel-Din and Meguro 2000).

The commercial software Extreme Loading for Structures (ELS) developed by Applied Science International (ASI) was employed in the present study (ASI, 2021).

Numerical simulations of collapse tests on RC beams

Part of the work described in this chapter has been previously published in Bridge Maintenance, Safety, Management, Life-Cycle Sustainability and Innovations edited by Taylor & Francis Group: "*Numerical simulations of collapse tests on RC beams*", M. Domaneschi, G.P. Cimellaro, G.C. Marano, M. Morgese, C. Pellecchia, A.A. Khalil (Marco Domaneschi et al. 2021).

Before approaching the analysis of a full-scale collapse case, the research focused on a component-level test case. A reinforced concrete, RC, beam was assembled and tested in the Polytechnic laboratories using a four-point bending test. The test was performed in displacement control using a beam designed for ductile behavior (Figure 4, a).

a   b

Figure 4. Test setup (a) and crack pattern at failure (b)

At the end of the test, two types of cracks were detected, due to bending moment and shear (Figure 4, b). Bending vertical cracks were concentrated between the two loading points while shear diagonal cracks developed between the support and the loading point.

Different AEM mesh ratios were considered in the analysis (Figure 5).
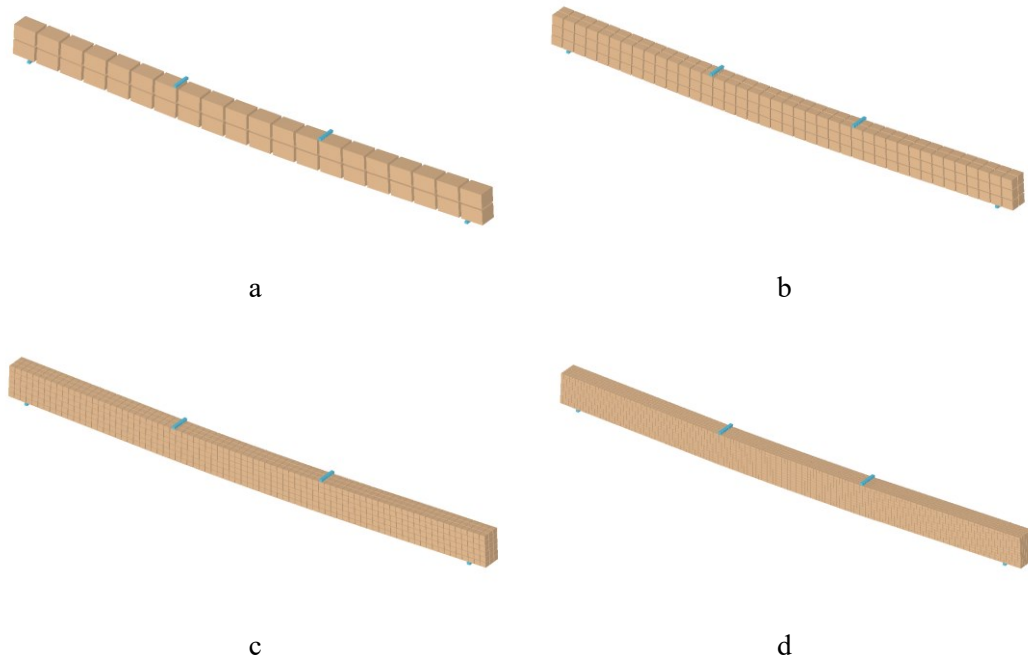
Figure 5. Sensitivity analysis considering a mesh length equal to 20 (a), 10 (b), 5 (c) and 2.5 cm (d).

The comparison between the actual test and the numerical simulation was carried out through the Digital Image Correlation technique, DIC. The DIC technique uses the recorded displacement of a given point pattern to derive the strain distribution of a given surface. A high-resolution camera captures the displacement of the different points, and the images are post-processed using a detection algorithm to compare the position of the different markers and calculate the displacement and strain fields. By using the contour plot technique, the resultant strains valued derived from the experimental test are visually compared with the numerical results at the different loading steps. The accuracy of the DIC technique is generally depending on image acquisition, analysis and image subject (Bomarito et al. 2017). Previous research proved that the deviation between values acquired using DIC and conventional techniques such as strain gauge is less than 5% (Lakshmish Kumar, H B, and Hossiney 2019). The experimental test was carried out considering different loading steps. The numerical results at different loading steps shown a good accordance with the actual strain detected through DIC technique (Figure 6).
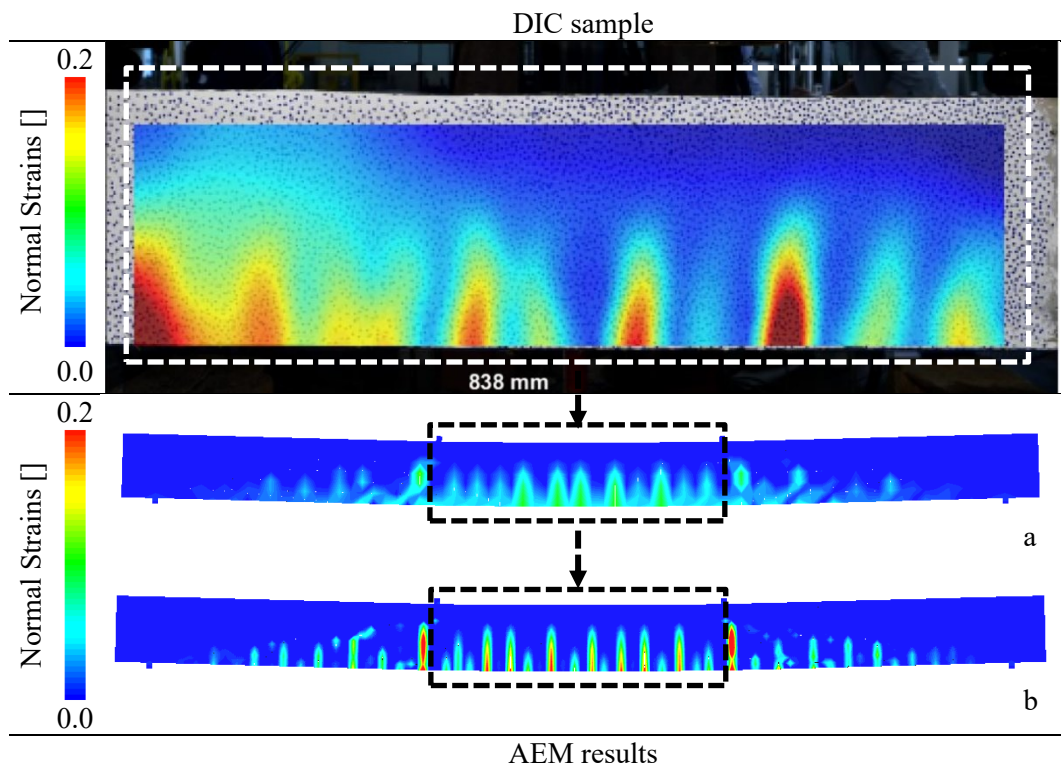
Figure 6. Comparison between DIC and AEM results considering a mesh length of 20 (a) and 2.5cm (b).

It was observed how the reduction of the mesh length from 20 to 2.5cm, passing through the 10 and 5cm length steps, provided an increasing refined representation of the cracks and strain values. For the sake of picture clarity, only the results obtained with the roughest (20cm) and refined (2.5cm) mesh dimensions are included in Figure 6.

In addition, it was observed that even when using a mesh dimension equal to 20 cm (a), rather than 2.5cm (b), the analysis accuracy was still acceptable, both in terms of load-displacement progression and crack representation (Figure 7).
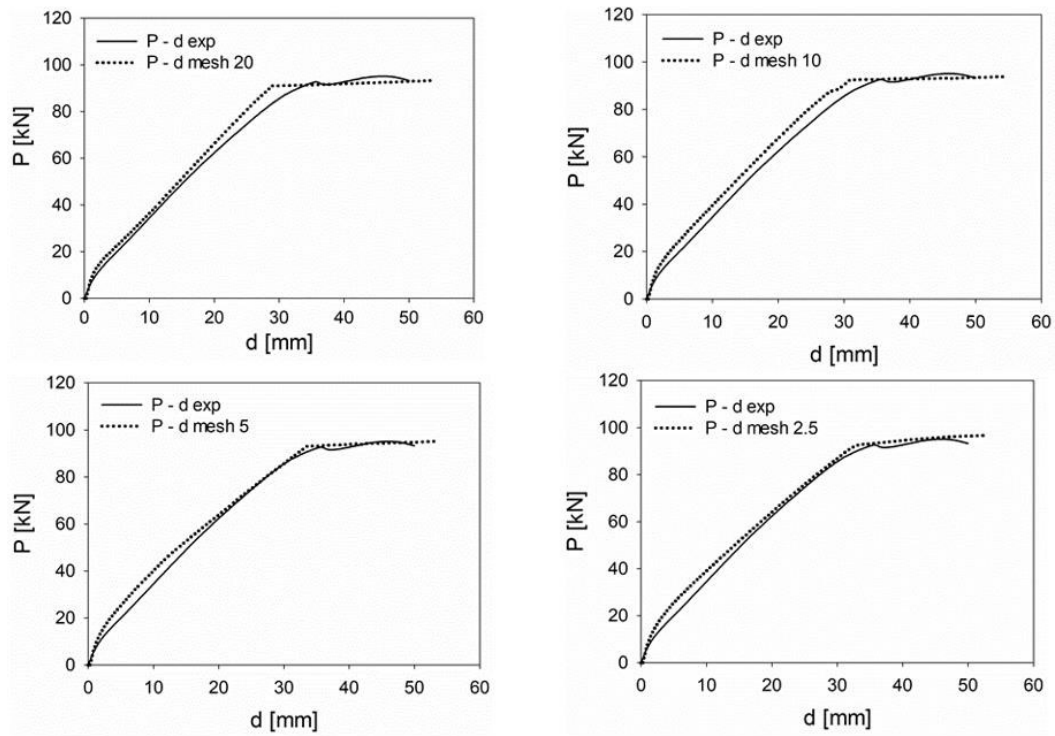
Figure 7. Experimental force displacement curve vs numerical ones.

Because of that, in the full-scale numerical models presented in the following, different mesh sizes were considered in the different portions of the structure, to reduce computational resources. A sensitivity analysis approach was employed to derive the proper mesh ratio in the different portion of the structure. A refined mesh dimensions was generally considered in the areas where the collapse occurred, to capture the initial failure. The different results for the different mesh ratios were compared and the mesh manually resized in the different portion of the structure to assure analysis reliability and reduce analysis time.

Chapter 3

The collapse of the Champlain Tower South Condo in Surfside, Miami, in June 2021

Part of the work described in this chapter has been previously published in Journal of Structural Engineers edited by ASCE: "*Progressive Collapse Analysis of the Champlain Towers South in Surfside, Florida*", C. Pellecchia; A. Cardoni, G. P. Cimellaro, M. Domaneschi, F. Ansari, A.A. Khalil (Pellecchia Cosimo et al. 2024).

Introduction

This chapter focuses on the progressive collapse analysis of the Champlain Towers South condominium using the AEM method. The 2021 collapse of the Champlain Towers (Surfside, Florida) was one of the most catastrophic collapses that ever occurred to reinforced concrete (RC) residential buildings. Built-in 1982 as a part of a three-building complex, namely the Champlain Towers North, South, and East, the Champlain Towers South consisted of an L-shaped, twelve-story RC structure with flat slabs and a basement floor covering the entire footprint of the building area. What makes this event particularly interesting from the point of view of progressive collapse analysis, is that the evidence infers that the collapse was caused by a localized failure of a singular structural element. Specifically, the failure of a slab due to punching shear would spread to the center of the building first, and then to the eastern wing a few seconds later (X. Lu et al. 2021).

To simulate collapse scenarios and investigate the behavior of the building, a high-fidelity AEM numerical model was developed. Several sensitivity analyses and different collapse scenarios were replicated to study the collapse behavior of the building and evaluate the most probable reason for its collapse. Finally, the progressive collapse performance of the structure was enhanced by introducing two different modifications to the original design, which could have prevented the collapse, under the studied hypotheses.

It should be noted that the causes of the collapse are currently unknown and a comprehensive failure investigation by an agency of the US government is underway to provide a definitive answer as to its causes. The present work is based only on publicly available material, which mostly refers to the original drawings of

the structure without considering eventual discrepancies in the final realization of the building. In addition, the analyses presented in this work are based on assumed loads, and degradation conditions which have not been verified.

This work assesses different scenarios that could have hypothetically caused the collapse of the Champlain Tower South Condo in Surfside, Florida, in 2021, one of the most catastrophic progressive collapse events ever occurred. The collapse analysis was performed using the latest developments in the Applied Element Method. A high-fidelity numerical model of the building was developed according to the actual structural drawings. Several different collapse hypotheses were examined, considering both column failures and degradation scenarios. The analyses showed that the failure of deep beams at the pool deck level, directly connected to the perimeter columns of the building, could have led to the columns' failure and subsequent collapse of the eastern wing of the building. The simulated scenario highlights the different stages of the collapse sequence and appears to be consistent with what can be observed in the footage of the actual collapse.

Structure description and material properties

The Champlain Towers South structure consists of RC flat slabs supported by RC columns. The thickness of the slab is 23 cm (9") on the basement floor, 24 cm (9 ½") at the Lobby level, and 20cm (8") for typical floors. Different concrete compressive strengths were considered in the design of the building: columns and shear walls were designed with strength varying from 41 MPa (6000 psi) to 28 MPa (4000 psi), while the slabs were designed with compressive strength varying from 28 MPa (4000 psi) to 21 MPa (3000 psi), (Figure 8). The longitudinal reinforcement of columns is varying from size Ø36 mm (#11) at the lower floors to Ø25 mm (#8) at the upper floors. The reinforcement of the two shear walls includes two columns at each edge and a reinforcement Ø13 mm (#4) mesh, spaced at 30 cm (12"). Ø13 mm (#4) stirrups were used for Ø36 mm (#11) longitudinal reinforcement while Ø10 mm (#3) stirrups were used for the rest of the bar sizes, (Figure 9).

a: Color map of concrete strength

Component:	Columns			Shear walls			Slabs	
Strength:	41 (6)	34 (5)	28 (4)	41 (6)	34 (5)	28 (4)	28 (4)	21 (3)
Color:								
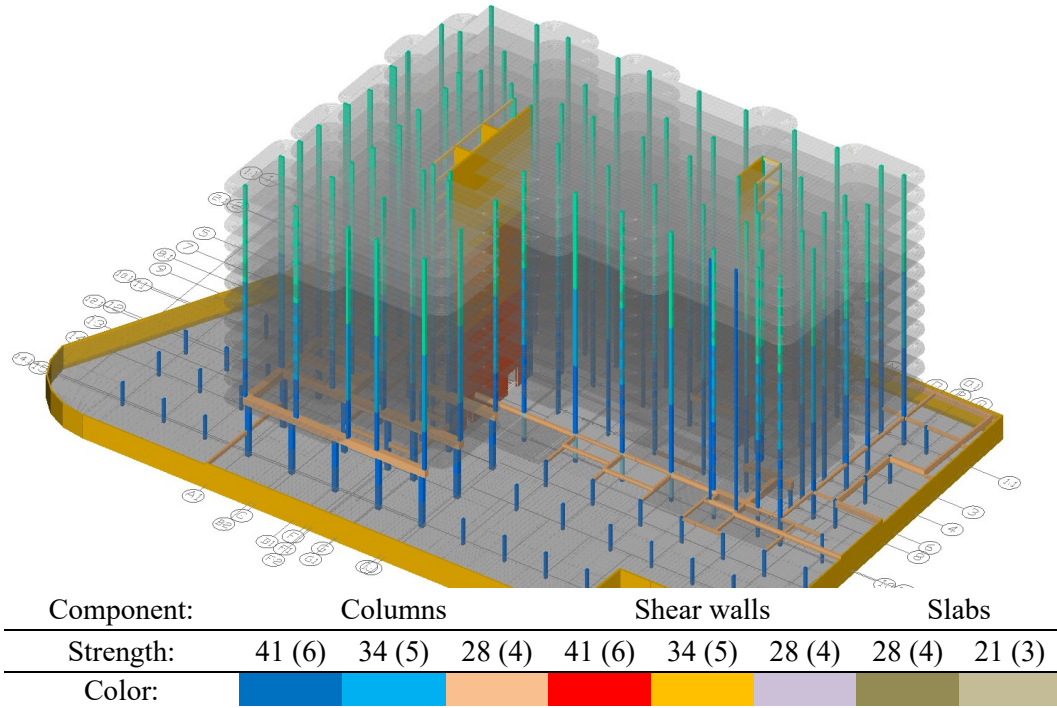
Figure 8. Color map of concrete strength in columns, shear walls, and slabs (a) [MPa (ksi)]

Color map of reinforcement

Diameter of reinforcing

10	13	16	19	22	25	29	32	36
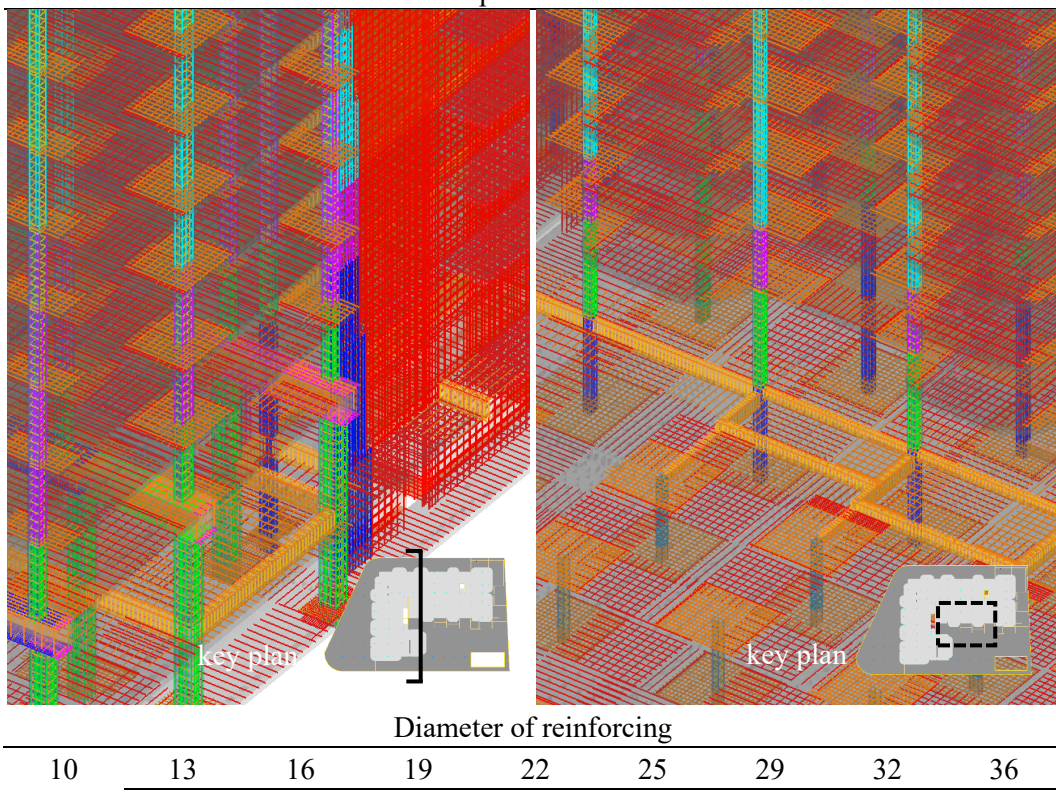
Figure 9. Diameter of reinforcement bars implemented in the numerical model [mm]

Table 1 shows the concrete properties considered for the AEM numerical model.

Table 1. Concrete material properties introduced in the AEM numerical model
[Stresses in MPa (ksi), Elastic Modulus in GPa (Mpsi)]

Concrete	f_c	$f_t^{(a)}$	$\tau_s^{(b)}$	μ [-]	$E^{(c)}$	$G^{(d)}$
6000psi	41 (6)	4 (0.6)	13 (1.9)	0.8	32 (4.7)	13 (1.9)
5000psi	34 (5)	3 (0.5)	12 (1.8)	0.8	29 (4.3)	12 (1.8)
4000psi	28 (4)	3 (0.4)	11 (1.6)	0.8	26 (3.8)	11 (1.6)
3000psi	21 (3)	2 (0.3)	10 (1.5)	0.8	23 (3.3)	9 (1.4)

Note: [a] $f_t = f_c/10$; [b] $\tau_s = 3.8 f_c 0.33$; [c] $E_c = 5000*(fck^{(1/2)})$, [Mpa]; [d] $G = E/(2(1+v))$, $v = 0.2$

The bottom reinforcement of the flat slab consists of a uniform rebar mesh of Ø13 mm (#4) spaced at 30 cm (12") in the basement and Lobby floors, and 33 cm (13") at the 2nd and typical floors. The punching shear reinforcement at the top side of the slab consists of Ø16 mm (#5) rebars with variable spacing. The area covered by the punching shear reinforcement also varies based on the column's section and location. Rebars having a diameter of Ø13 mm (#4) and different spacings were provided, in one direction only, at the top side of the slabs, in the transition zones between the areas covered with punching shear reinforcement (Figure 10).

Example of reinforcement modeling at Lobby Level
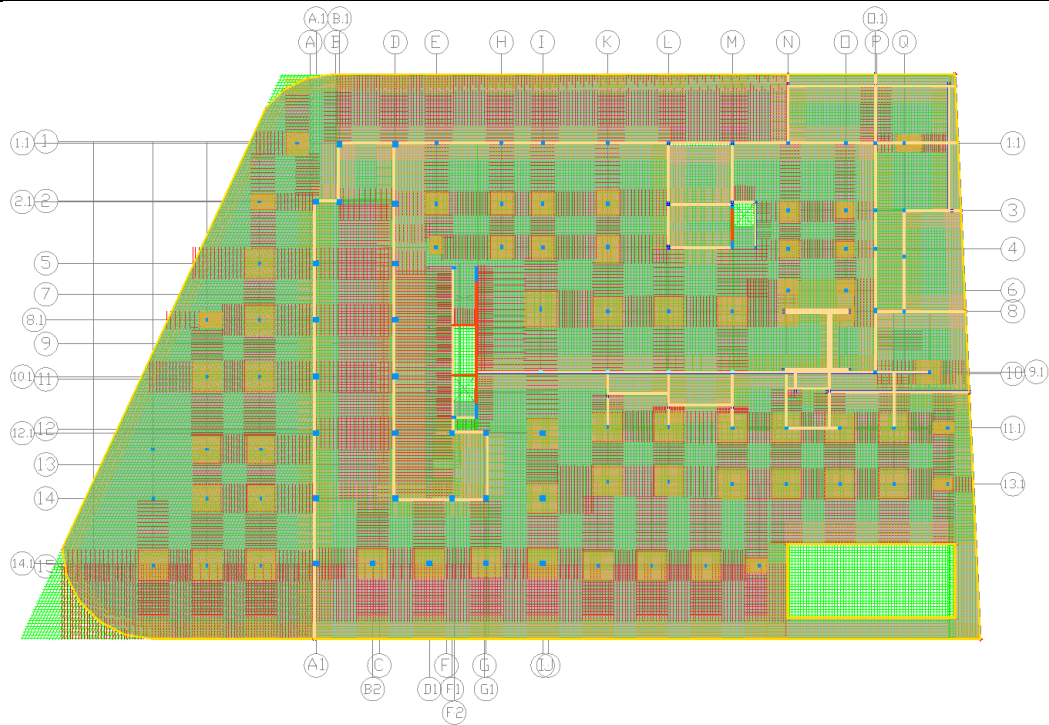
| 2nd Floor | Typical Floor |
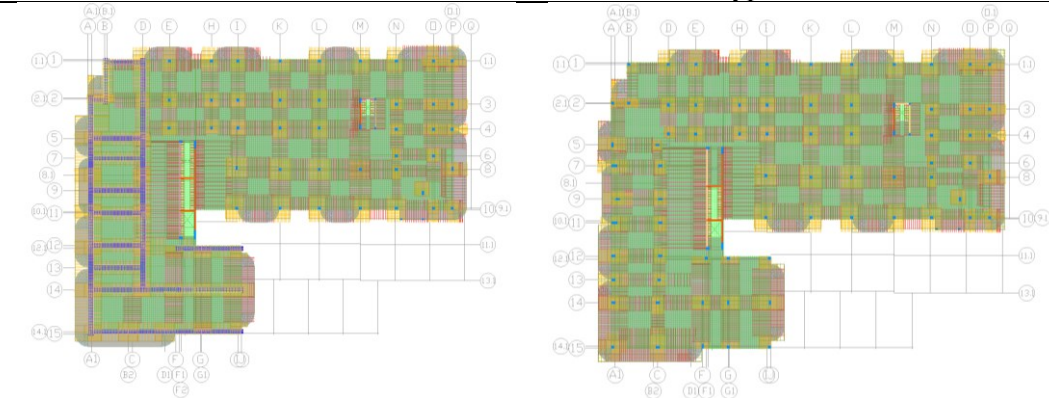
Legend:
━━ Ø16 mm (#5) top   ━━ Ø13 mm (#4) top   ━━ Ø13 (#4)/30cm (12") bottom   ▲ Nord

Figure 10. AEM numerical model view of the punching shear reinforcement in the lobby slab, basement, 2nd floor, and typical floor.

RC girders can be found in the Lobby and 2nd floor only. On the Lobby floor, 30cm (12") width girders with various depths are connecting the Lobby RC slabs at different elevations (also referenced as "slab-drops" in the original drawings of the structure). On the 2nd floor, 91x107 cm (36"x 42") transfer girders are supporting 30,5x61cm (12"x24") columns elevating from the 2nd floor to the roof.

As specified in the as-built drawings notes (William M. Friedman & Associates Architects 1979), reinforcing bars meet ASTM A-615 Grade 60 criteria, with yield strength equal to 414 MPa (60 ksi), (Table 2).

Table 2. Steel material properties introduced in the AEM numerical model [Stresses in MPa (ksi), Elastic Modulus in GPa (Mpsi)]

Steel	σ_y	σ_u	ε_u	E	G
Grade60	414 (*60*)	579 (*84*)	1	200 (*29*)	80 (*12*)

The final developed model, employing 5 matrix springs per element's face, resulted in 7.5 million matrix springs representing the different concrete materials and additional 0.85 million equivalent springs representing the different reinforcement for more than 900,000 degrees of freedom.

The non-linear dynamic analyses were performed considering a time step equal to 0.001 s, using a 3.5 GHz 12 cores processor and requesting approximately 30 Gb of memory. With the given hardware, the AEM solver produced the analysis output of 1 sec in approximately 3 hours of calculations, resulting in overall 48 hours needed to complete one entire collapse simulation of the duration of approximately 16 sec.

Loads

The dead load of the structural elements explicitly introduced in the numerical model is automatically accounted for in the analysis based on the volume and density of the concrete. In addition, the weight of non-bearing walls, finishes, furniture, and any other elements not directly introduced in the numerical model was assumed as distributed on the floor area. As this work aims to compare the numerical results with the actual evidence of the Champlain Tower South collapse, no code-based load combinations are considered in the analysis. In fact, with respect to the DoD and GSA provisions, in which a factor of 1/2 is applied to the prescribed Live Load, LL, only a fraction of 1/4LL is assumed to be in place at the moment of the collapse. The assumption is consistent with ASCE 7-22 Commentary Table C4.3-2, which suggests a mean sustained Live Load of 0.3kN/m2 ($\approx$6 lb/ft2), (ASCE 2021). In addition, because of uncertainties on apartment' finishes, walls and ceilings composition and materials, and overall actual loads at the moment of the collapse, sensitivity analyses were carried out with different loading assumptions, considering a cumulative distributed load (DL+LL) varying from 1.5 kN/m2 ($\approx$30 lb/ft2) to 3.0 kN/m2 ($\approx$60 lb/ft2). In this work, only the analyses with the load assumptions reported in Table 3 are considered for the sake of brevity.

Table 3. Loads [kN/m2 (lb/ft2)]

Floor	Dead load in addition to slab self-weight	Dead Load of walls & partitions	Live Load	Total per floor
Typical	≈1.0 (*20*)	≈0.5 (*10*)	≈0.5 (*10*) [a]	≈2.0 (*40*)
Lobby	≈2.0 (*40*)	≈0.5 (*10*)	≈1.0 (*20*)	≈3.0 (*60*)
Basement	-	-	≈1.0 (*20*) [b]	≈1.0 (*20*)

Note: [a] 1/4 of 2.0kN/m^2 *(≈40lb/ft²)* design load for residential buildings; [b] 1/2.5 of 2.5kN/m^2 *(≈50lb/ft²)* design load for garages.

For the Typical Floor, the following loads were assumed based on the typical weights of the building materials (Breyer, Cobeen, and Martin 2020): dead load in addition to slab self-weight, 1 kN/m2 (20lb/ft2), accounting for the floor finishes, ceilings, façade elements, windows, doors, railings, MEP systems, and any additional load not explicitly introduced in the model; dead load of walls & partitions, 0.5 kN/m2 (10lb/ft2); live load, 0.5 kN/m2 (10lb/ft2); the total considered distributed load results 2 kN/m2 (40lb/ft2).

In addition to the distributed load, an ornamental plant load, estimated on a soil density equal to 16 kN/m2 (≈100 lb/ft3), was introduced in the numerical model at the pool deck level based on the actual plant arrangements at the time of the collapse.

Non-Linear Static & Dynamic Analyses and Collapse Scenarios

Two of the most credited hypotheses raised by media in the aftermath of the collapse of the Champlain Towers South attribute the cause to either differential settlement in the foundations or localized structural failure. In the first stage of this work, several column removal scenarios were carried out to evaluate the sensitivity of the structure to column failure and its consequent load redistribution capacity.

Column removal scenarios

Column removal scenarios were implemented at the locations where the initial failure was observed, considering both perimeter and inner column removal scenarios. To simulate a hypothetical foundation settlement, columns are removed at the foundation pile level, below the basement slab. Thus, the basement slab contributes to the load redistribution till punching shear failure occurs. The column's removal is performed using non-linear static analysis, so the overload determined by the column's loss is redistributed incrementally to the surrounding structural elements. The two considered scenarios, loss of center columns and loss of perimeter columns, were defined to identify the most probable area where the initial failure occurred. Each of the two scenarios was repeated considering the loss

of one column first, and an adjacent one after, keeping removing columns till collapse is reached.

The column removal analyses revealed that the building was more sensitive to the removal of perimeter columns (Figure 11, scenarios C and D) rather than inner columns (Figure 11, scenarios A and B). In fact, under the loading assumption and considering the original properties of steel and concrete, without accounting for material degradation, the building was able to redistribute the loads and avoid progressive collapse, even when three inner columns were removed (Figure 11, Scenario B). Nevertheless, the removal of two perimeter columns was enough to initiate the progressive collapse of the building (Figure 11, Scenario D).
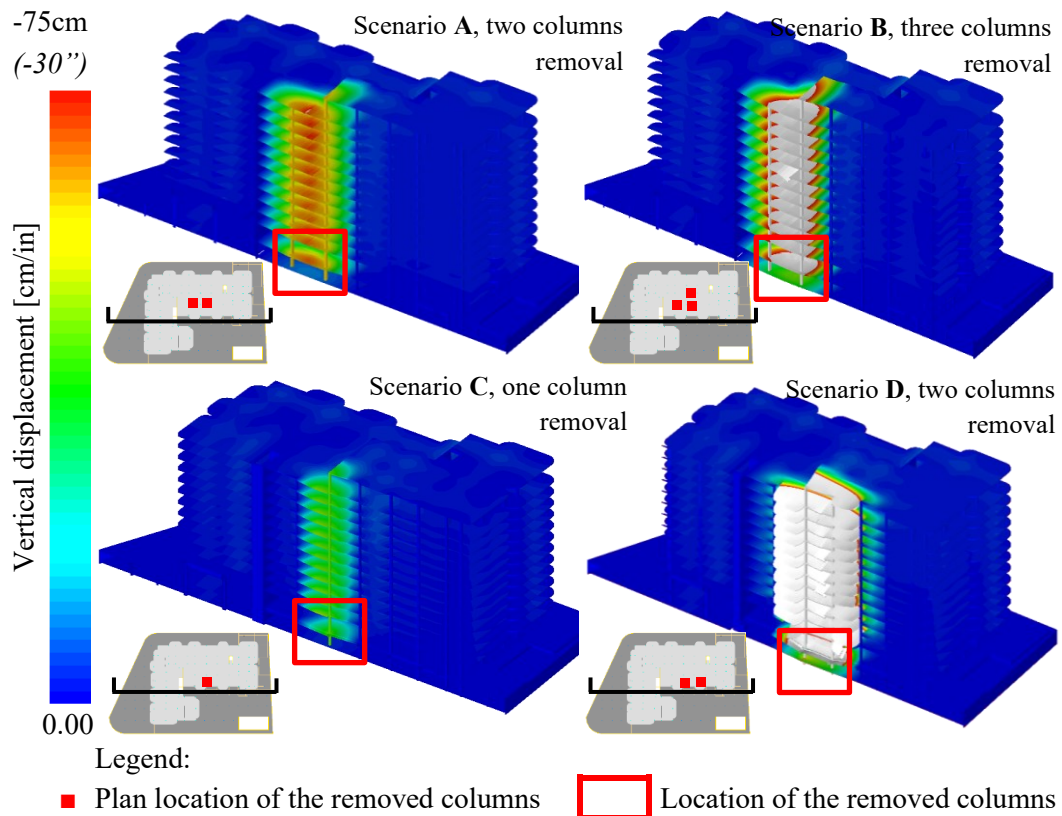
Figure 11. Inner (top) and perimeter (bottom) column removal scenario, Vertical deflection.

A load sensitivity analysis was also carried out showing that the scenario of perimeter column removal remains the most critical one regardless of the entity of load.

Localized degradation scenario

Several media discussed evidence of extensive degradation of the pool deck slab in the immediate aftermath of the collapse. Indeed, the area was partially covered by ornamental plants, which, on top of the additional weight, might also have caused corrosion of the slab steel reinforcement due to watering and lack of proper impermeabilization. Static analyses were performed considering only the vertical dead load, as per load assumptions, without accounting for any degradation.

These analyses showed that the area of the pool deck was substantially weaker and subjected to higher deflections and stresses than the area within the twelve-story building footprint (Figure 12, a). For example, the deflection in the pool deck area reaches 2cm, while it resulted in only fractions of a centimeter in the area pertaining to the twelve-story building itself. The larger spans, together with the limited reinforcement, led to stresses in the punching shear reinforcement substantially higher than in the rest of the structure. The mean value of normal stresses in the punching shear reinforcing bars on the ground floor of the twelve-story building was found to be below 100MPa (≈15ksi). In the pool deck area, the normal stresses in the punching shear reinforcing bars reached 200MPa (≈30ksi), which corresponds to half of the yield stress of the steel, 414MPa (60ksi), according to the original design specification (William M. Friedman & Associates Architects 1979). In particular, the area where the initial collapse occurred, showed the highest stresses, specifically at the top side rebars of the pool deck slab (Figure 12, b).
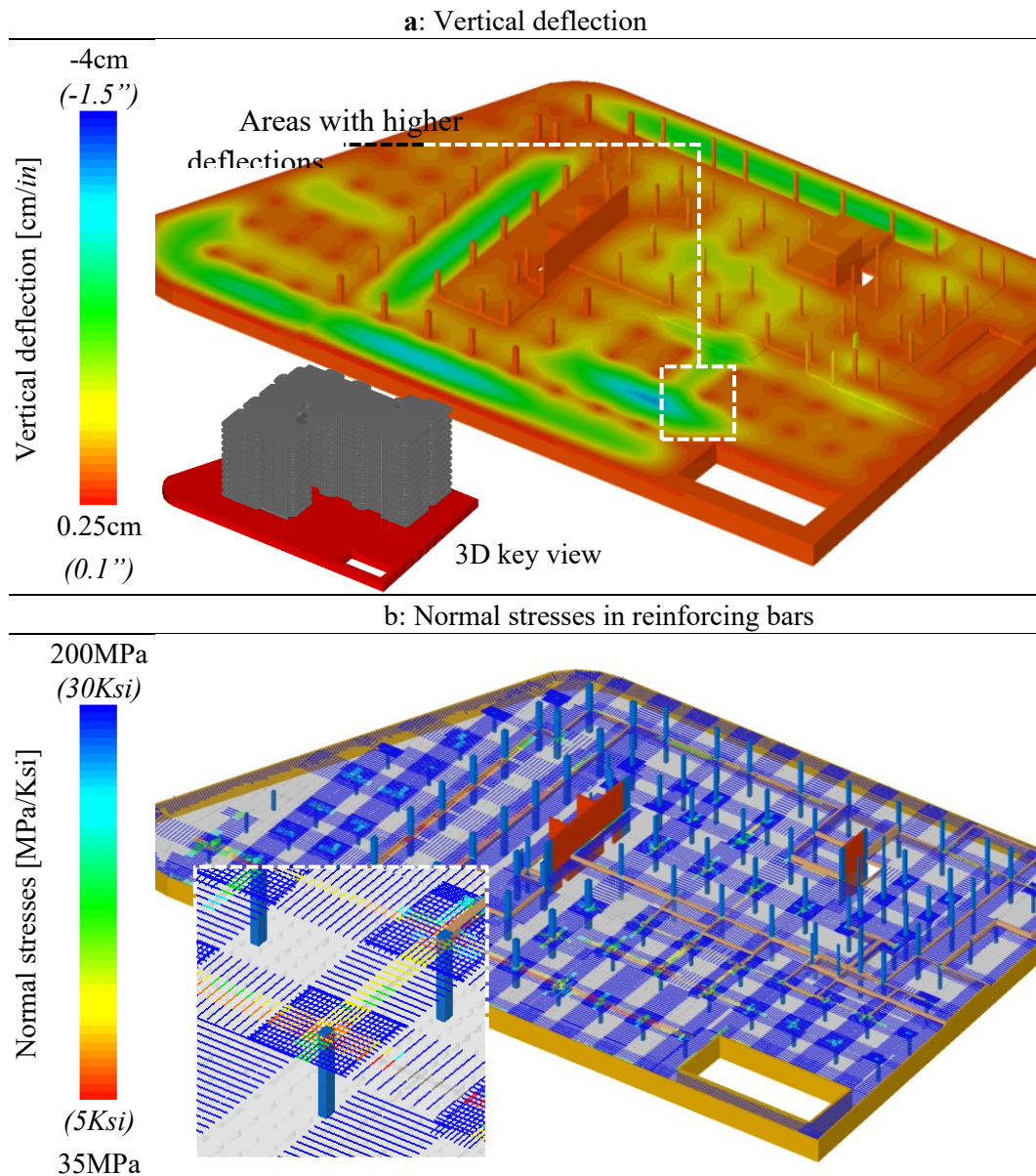
Figure 12. Static analysis, Vertical displacement at basement level [cm (in)] (a), and normal stresses in top punching shear reinforcement [MPa (Ksi)] (b)

To investigate the hypothesis of the pool deck slab degradation, further analyses were performed considering localized steel degradation in the pool deck area (Figure 13).

Degradation analyses were carried out by introducing a progressive area reduction of the slab and beams reinforcement, up to 90%, until collapse is reached. This degradation analysis approach is widely adopted in the literature. For instance, it was used to analyze the collapse of the Polcevera Viaduct in Genoa, Italy (M. Domaneschi et al. 2020).

Figure 13 shows a comparison between the crack distribution resulting from the two considered scenarios, foundation settlement in the center of the building (Figure 13, a) and degradation of the pool deck slab (Figure 13, b).
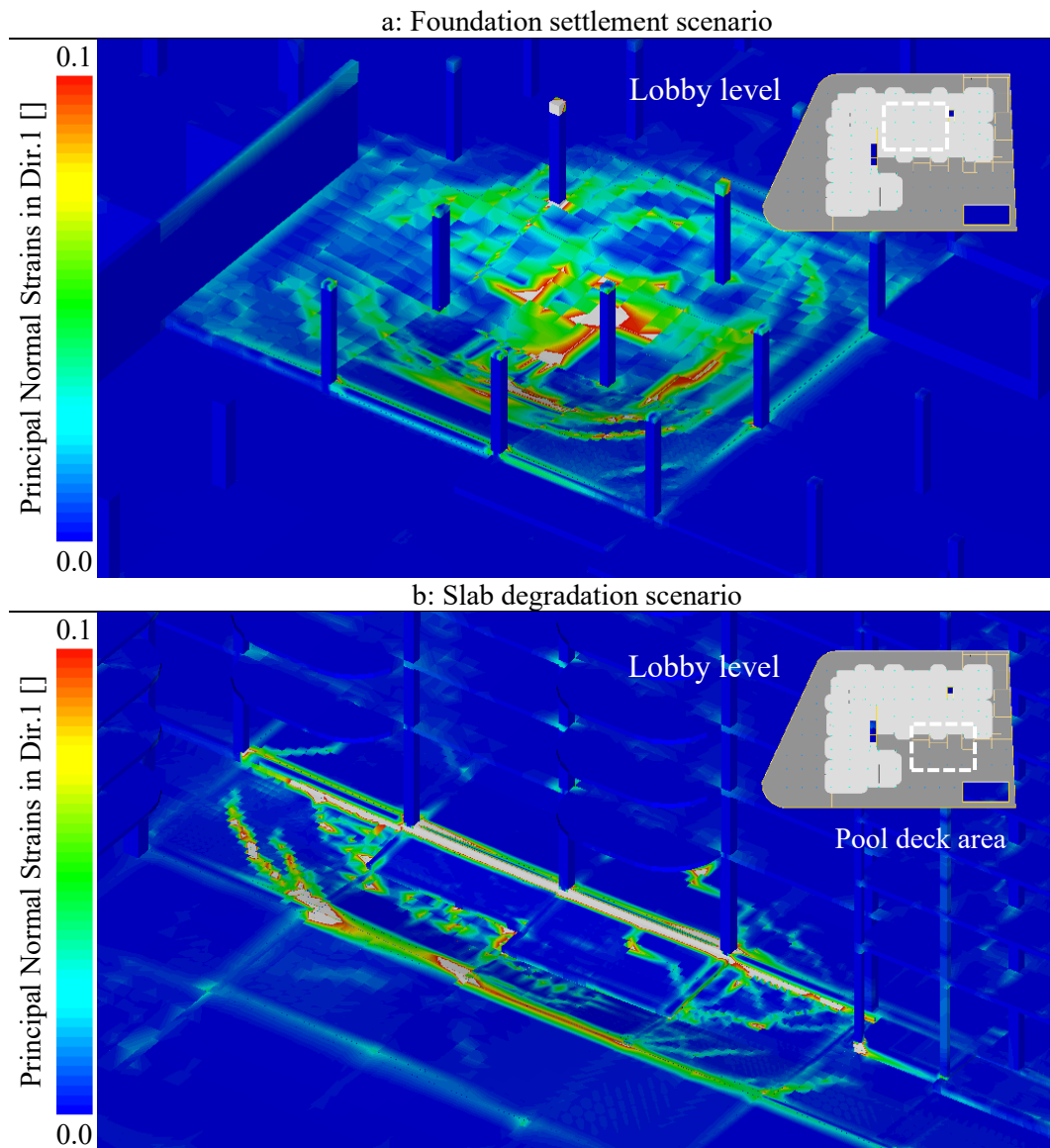
Figure 13. Lobby level, comparison between cracks distribution in case of foundation settlement scenario (left) and pool deck degradation scenario (right), Principal strains in Dir.1 [-]

Cracks are shown based on the plot of principal normal strains, varying from $\varepsilon=0.0$ to $\varepsilon=0.1$. Considering a mesh dimension equal to approximately 30cm ($\approx$1ft), it corresponds to a maximum crack opening of about 3cm ($\approx$1in). It can be noticed how a diffuse foundation settlement, which should have involved at least four columns to result in the disproportionate collapse of the building (see "Columns removal scenarios"), would have caused widespread cracking and concrete spalling at the basement level that by far exceeds what is described in the reports about the structure (Figure 13, a). Evidence of linear cracking at the Pool deck slab, outside the actual footprint of the building, was instead reported by some media and found in the degradation analysis scenario also (Figure 13, b).

In addition, it was noticed that, when applying the degradation to both the spans pertaining to the twelve-story building and the pool deck slab, the pool deck slab area would have shown much more diffuse evidence of cracks compared to the

twelve-story building counterpart, because of the inherent lower residual capacity, deriving from ornamental plant superimposed load and larger spans.

Another aspect worth noticing is that the pool deck structure, designed to carry only one floor rather than twelve stories, while also subject to additional superimposed loads and deterioration, was rigidly connected to the main structure through three beams with a depth of 46cm (18").

These beams were generally used at the pool deck slab level to cover for different elevations and steps, and in fact, called "slab drops".

The three previously mentioned "slab drops" were originally designed to be 59cm (23"), and then reduced to 46cm (18") in a second design revision (William M. Friedman & Associates Architects 1979). The degradation analysis of the pool deck slab shows how the depth of the three girders, resulting from the slab drops, could have played a significant role in propagating the collapse of the slab to the rest of the building. Because the building was particularly sensitive to the loss of perimeter columns, when the slab and connecting beams fail, a concentrated bending moment is transferred to the three perimeter columns, leading to column overload and consequent collapse of the building (Figure 14).

1.00s   1.25s

1.50s   1.75s

Principal Strains in Dir.1 []

0.10

0.00

key plan

2.00s
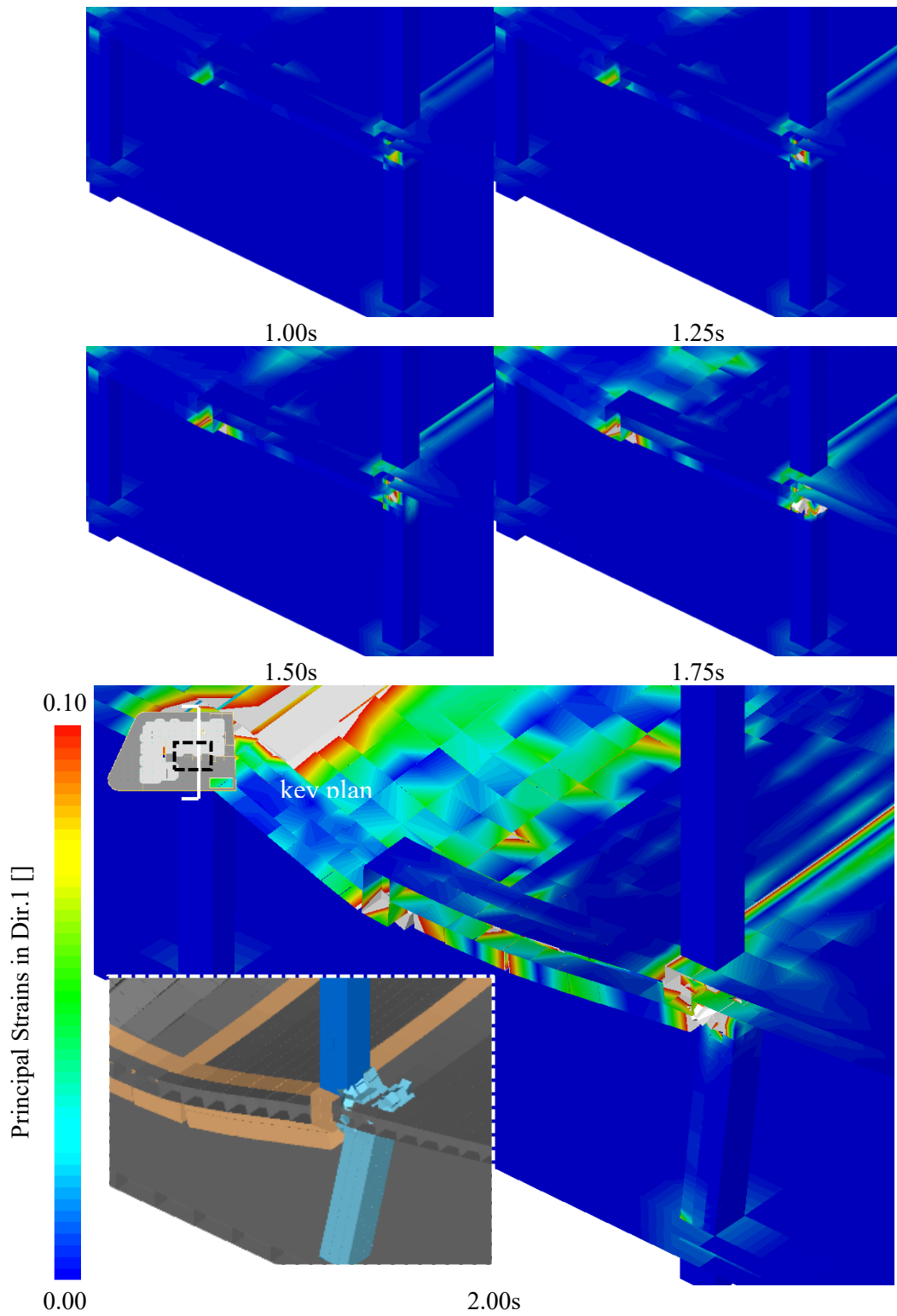
Figure 14. Effect of deep beams in causing the instability of the perimeter columns at 2.0s, Principal strains in Dir.1, Scale color red equal to 0.1 Strain [-], and deformed shape scaled by a factor of 2 (left)

Arch and catenary actions: from the failure of the pool deck slab to the disproportionate collapse of the building

This section describes the identified collapse mechanism, starting from the deck failure, followed by the formation of an arch action and subsequent catenary action, until reaching the failure of the perimeter columns.

Figure 15 shows a time-lapse of the failure at different seconds, describing both the variation of compressive stresses in the concrete, normal stresses in the reinforcing bars, and the variation of internal forces in columns and beams, as the failure progresses. The different instants are identified in the timeline at the bottom of the Figure. The compressive stresses in the concrete are shown in the top row; Also, the stresses in the reinforcing bars are shown in the middle row, together with the related chromatic scale; the compressive stresses in the Finally, the internal forces, bending moment, M, (positive in red and negative in blue), and normal force, N, (in magenta) are shown on the bottom row.
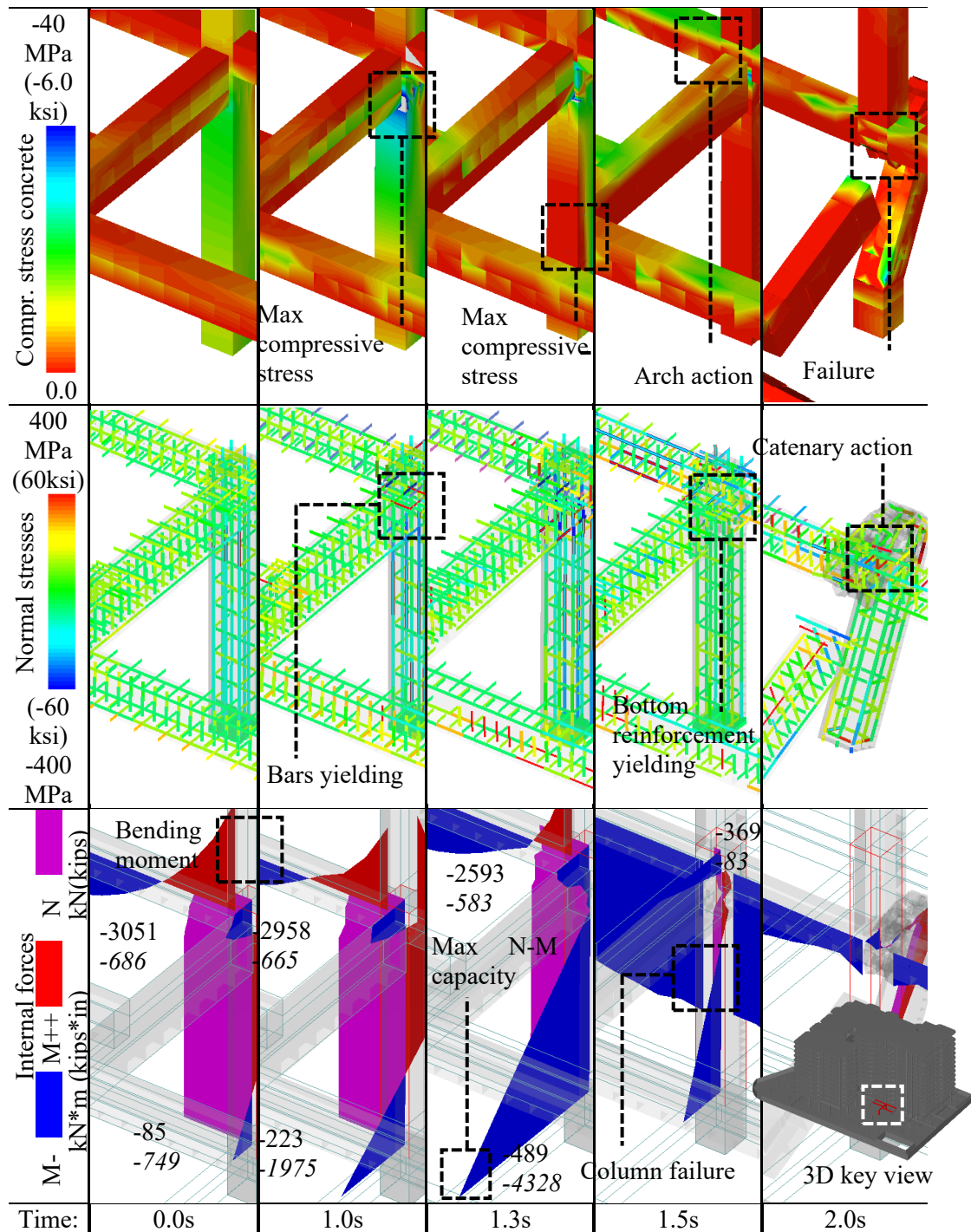
Figure 15. Column 11.1-L, Compressive stresses in the concrete [MPa (Ksi)] (top), normal stresses in beams' and columns' reinforcement [MPa (Ksi)], normal forces [kN (kips)] in the column and bending moments in the beams [kN*m (kips*inch)] (bottom), at different stages of the collapse.

When degradation is introduced, steel rebars start yielding. The slab starts deflecting downwards and the concrete in the perimeter columns reaches its maximum compressive strength at the connection with the pool deck beams (Figure 15, 1.0s). After the concrete fails, as a consequence of the yielding of the longitudinal reinforcement in the pool deck beams, the bending moment in the column increases till reaching the ultimate capacity of the section for the given

combination of axial forces and moment (Figure 15, 1.3s). At this point the column loses its load-bearing capacity, activating an initial arch action, as can be gathered from the increase of compressive stresses at the top of the perimeter beams (Figure 15, 1.5s). Consequently, the column-beam connection fails, generating a catenary action in the perimeter beams that results in both top and bottom longitudinal reinforcement subjected to tensile stresses (Figure 15, 2.0s). At this point, the original degradation introduced in the slab has progressed through slab failure and subsequent column failure, with the only catenary action opposing the propagation of the collapse. Unfortunately, the amount of reinforcement in the beams is not enough to withstand the catenary forces, ultimately leading to the progressive collapse of the building (Figure 16).
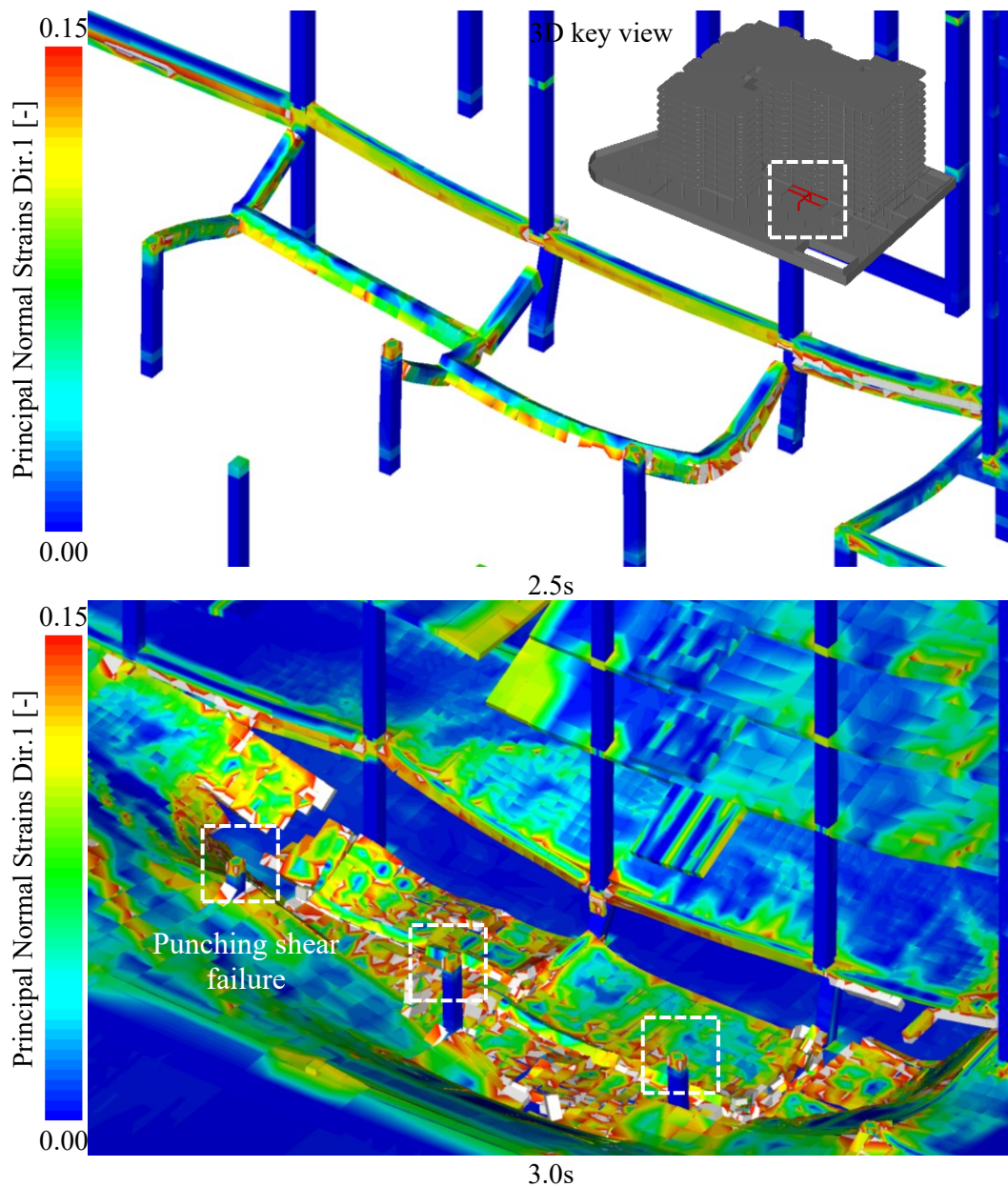
Figure 16. Distribution of Principal Strains [-] after column' failure (left), and punching shear failure at pool deck slab (right)

Side-by-side comparison of the collapse

Fig. 11 shows a side-by-side comparison between the simulation and the footage of the collapse (Slater 2021). The comparison shows a good agreement between the simulations and the actual collapse, both during the initial failure of the central portion of the building, and the initial torsion of the remaining eastern portion of the building, a few instants later. However, a flexural failure at mid-height of the eastern wing of the structure can be observed only in the numerical analysis, occurring when the remaining portion of the structure starts hitting the ground (frame T7 in Figure 17).

EAST WEST
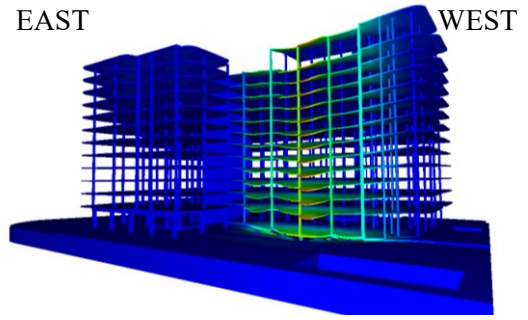
T1
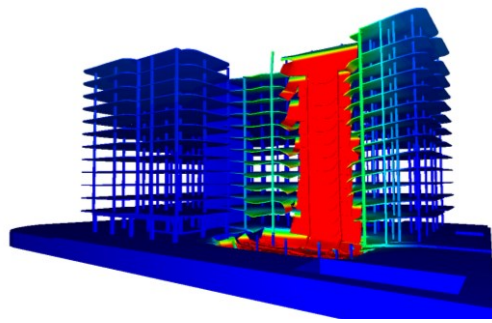
T2
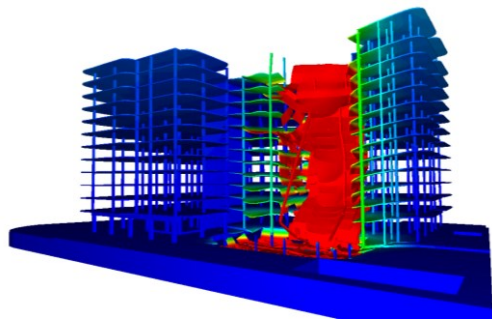
T3
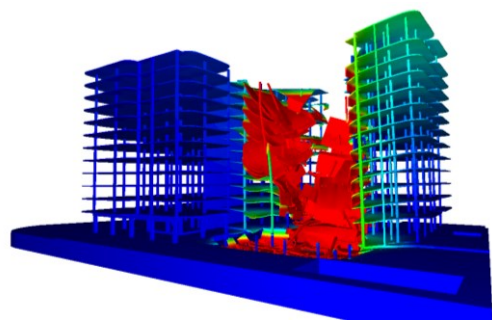
T4
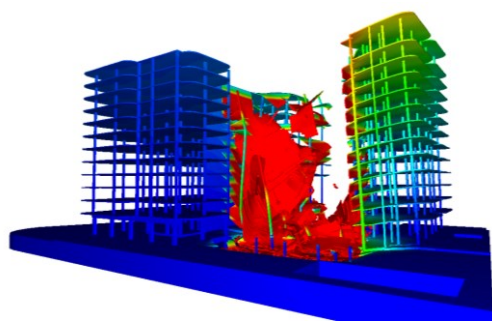
T5
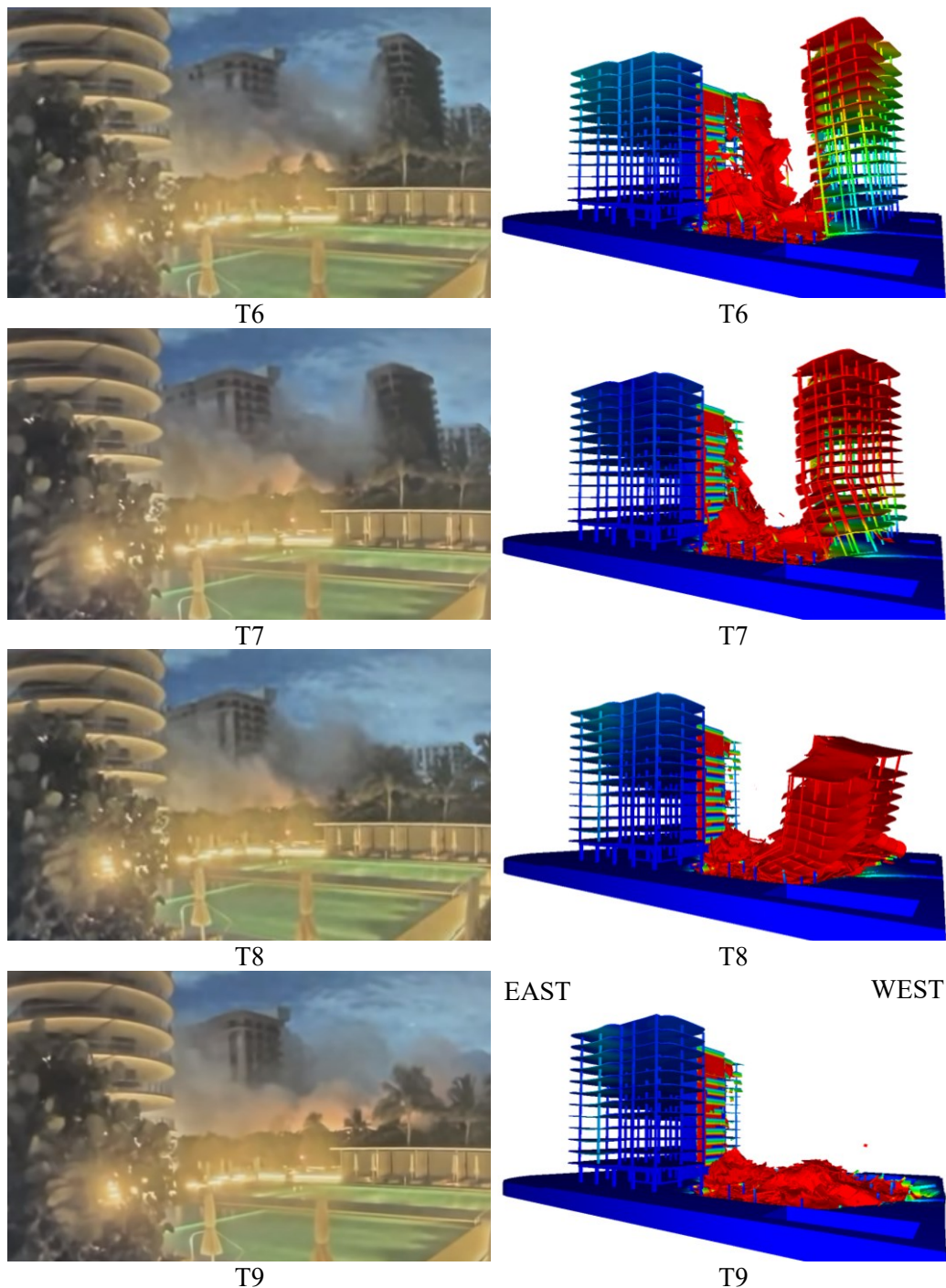
Figure 17. Side-by-side comparison between the collapse footage and the numerical analysis in nine different timestamps; Image courtesy of Slater (2021).

This failure, which takes place approximatively at the middle height of the structure, results in more than half of the eastern core of the building leaning toward the east in the final debris distribution obtained from the numerical analysis. However, this mechanism is not observed in the actual video of the failure, where the eastern wing collapses in on itself, leaning toward the west. The difference in the observed collapse behavior could be explained by a possible divergence of the mechanical properties of the materials, due to either degradation or construction defects, which are not considered in the model.

Figure 18 shows a comparison between the reconstruction of the actual debris distribution resulting after the collapse and the debris resulting from the analysis.

a: Actual debris distribution
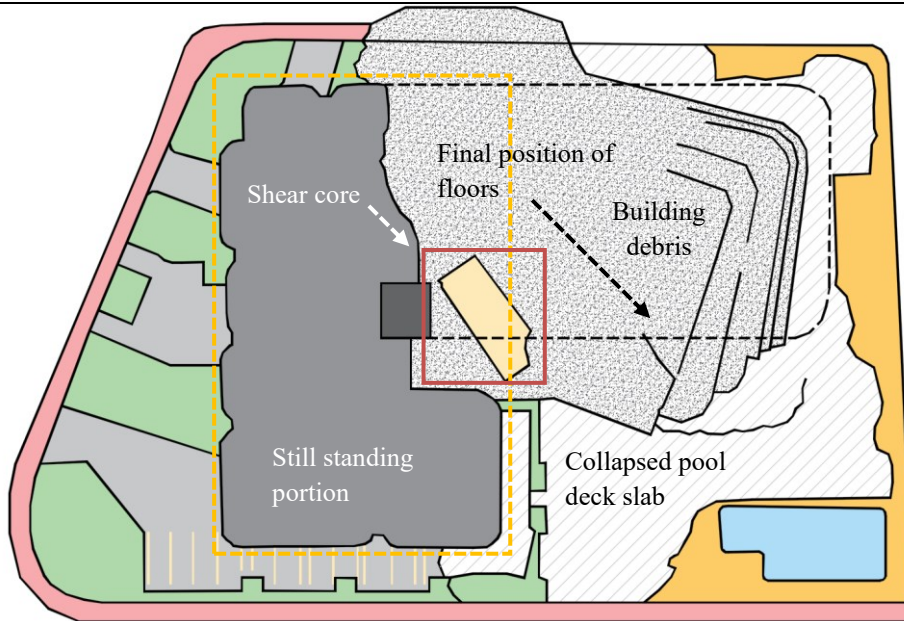
Legend: ▪–▪–▪– Perimeter of the remaining building

b: Analysis results
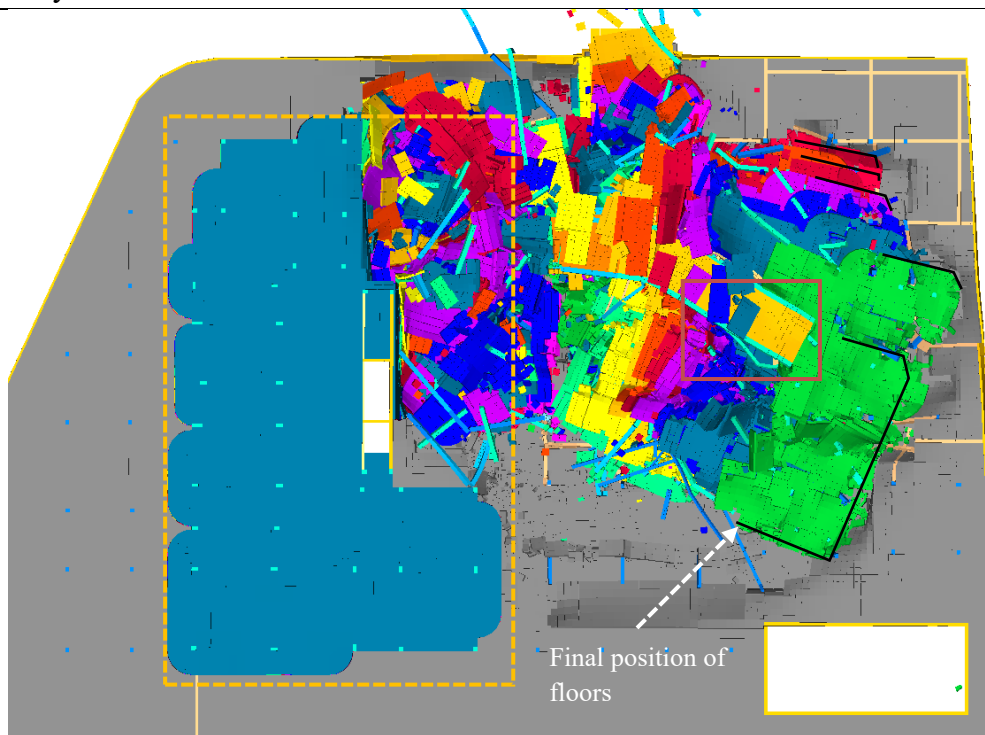
▬▬ East shear core

Figure 18. Comparison between actual debris distribution (a) and analysis results (b); Image (a) reconstructed by the Authors based on available media pictures.

In both cases, the collapse of the building did not spread over the west core of the structure. The initial torsion of the eastern wing is also captured by the numerical analysis, as it can be gathered from the orientation of the slabs, pointing towards the south side. However, because of the flexural failure mechanism described early, which was observed in the numerical simulation only, the final position of the east shear wall core differs, with the half-eastern core leaning east rather than west.

Findings

In this chapter, a series of progressive collapse analyses were performed to analyze the collapse of the Champlain Towers South in 2021 (Surfside, Florida). An AEM high-fidelity numerical model was developed and employed to investigate the possible causes of the collapse. Different column removal scenarios were modeled to simulate foundation settlement, while structural degradation was modeled progressively reducing the reinforcement cross-section area. Column removal analyses revealed that the building was particularly sensitive to the loss of perimeter columns, whose failure could easily propagate to the central block, due to the lack of load redistribution capacity at the perimeter of the structure. In addition, the degradation analysis at the pool deck level showed that the initial failure of the pool deck slab could have caused relevant damage to the connection between the perimeter columns and the pool deck beams, leading to the failure of the perimeter columns. Indeed, the global static analysis revealed that the one-story structure of the pool area was subjected to higher deflections and stresses than those found in the main building. The side-by-side comparison between the simulated collapse through nonlinear dynamic analysis and the actual footage of the event showed a reasonable match.

Chapter 4

The collapse of the Polcevera Viaduct in Genoa, in August 2018

Part of the work described in this chapter has been previously published in Engineering Structures edited by ELSEVIER: "*Collapse analysis of the Polcevera viaduct by the applied element method*", M. Domaneschi, C. Pellecchia, E. De Iuliis, G.P. Cimellaro, M. Morgese, A.A. Khalil, F. Ansari (M. Domaneschi et al. 2020).

Introduction

On August fourteen of 2018, a portion of the highway connection viaduct over the Polcevera Valley in Genoa, Italy collapsed, and resulted in forty-three deaths, and many injuries. In the aftermath of the tragic event, in search of answers, a number of studies focused on various scenarios pertaining to the causes of the collapse, i.e. sustained effects of fatigue and corrosion, lack of redundancy, construction abnormalities, and others. In the study reported herein, the post collapse analysis of the Morandi's Polcevera viaduct was conducted by the applied element method (AEM). AEM made it possible for step-by-step evaluation of the structural response of the bridge model to progressive reduction of the strength capacity of single macro-components. In using the proposed approach, it was not necessary to consider the factors that may have resulted in the capacity degradation of the structural elements, such as fatigue and corrosion. Instead, structural degradations were introduced in the model as an incremental area reduction factor until complete section loss was reached. The results of analysis revealed that the stay cable was the most critical element whose failure would have triggered the collapse. The simulation model further indicated that if sections other than the stay cable had triggered the collapse, such as the main girder, the large visible displacements involved in their collapse, would have warned the authorities of the impending failure. The identified mechanism of collapse was further validated with references to the real debris distribution observed from images and a comparison with a new footage of the bridge collapse, released after the collapse by the Italian Authorities.

The Polcevera viaduct

The viaduct over the Polcevera Valley in Genoa, Italy, was built between 1963 and 1967. It was about 1100 m long and 18 m wide, supported by twelve piers between two bents, from Piers #1 to #12 (Figure 19).

Figure 19. The Polcevera Viaduct [m] (L'Industria Italiana del Cemento, 1967) [2]

To reduce the number of piers between the Polcevera river and the railways, the Italian designer Riccardo Morandi developed the idea of the so called "Balanced system" (Figure 20).

Figure 20. The balanced system (Morandi 1967)

It consisted of A-shaped towers supporting the deck using prestressed concrete stays. The A-shaped towers were 90 m tall, and the deck height above the river was approximately 45 m. The daily traffic count over the 4-lane bridge ranged between 2x104 at the inception to 1.5x105 during the last years of the service life of the bridge (AISCAT 2019; Morandi 1967; 1968).

The Balanced system #9 failed on August 14, 2018, causing the 250 m portion of the deck to collapse into the river and the railway lines beneath. The only major traffic on the bridge at the time of collapse was a 44 tons truck passing by Pier #9 (Gatti 2018). The collapse caused forty-three deaths, and nine injuries including the motorists, and the workers of the municipal waste company below the bridge. Moreover, six hundred people were displaced from their homes near the viaduct.

Several issues concerning the various structural components were cited in the different official reports released in the months following the collapse of the structure (MIT 2018). However, earlier visual inspections of the stays in piers number 9 and 11 during the period between 1991-1992 had already highlighted that "most of the ducts did not have grouts, that supposed to have been injected in during the construction, and strands showed extensive corrosion and some cables had loose strands". For pier number 11, inspections of stays at the top of the A-shaped tower indicated that the "strands were extremely deteriorated with very strong corrosions, many elements were broken with missing injected grouts" (MIT 2018). Subsequent visual inspections in 2015 confirmed further deterioration of the stays. In addition, the dynamic tests of the balanced systems in 2017 indicated "lack of symmetric response in the mode shapes" (MIT 2018). Maintenance of degraded structural elements was planned in 2017. In particular, the maintenance program included retrofitting of the stays in Piers #9 and #10, in a similar fashion to the previous retrofits in Pier 11, where new external cables were added to provide the necessary support. Unfortunately, the bridge collapsed prior to the retrofitting.

 Calvi et al. (2019) first discussed potential reasons for the collapse of the balanced system, prior to the availability of the collapse video footage. They also pointed at some other inadequacies of the bridge. Subsequently, Bazzucchi et al. (2018) reported a description of recent failures for five bridges in Italy including the Polcevera viaduct. The report indicated that lack of information about the structural condition of the bridges was the cause for their failures.

In contrast to the previous contributions from literature, the objective of this study has been to consider the role of each degraded member of the balanced system in the analysis, i.e. tower, deck beams, and the stays, which could have caused the collapse of the bridge. The first step of the work involved building a AEM numerical model of the balanced system of Pier #9; subsequently, the strength degradation of different structural elements was induced to understand their respective contributions to the progressive collapse of the bridge. The Validation of the described iterative approach was accomplished by comparing the analysis results to the debris distribution observed after the collapse; the collapse cinematics was also compared with what was observed in a footage of the bridge collapsing, released by the Italian Police and Fire Brigade Corps (Guardia di Finanza Genova 2019).

Structure description and material properties

The Polcevera Viaduct, also known as Morandi Bridge, was designed by Riccardo Morandi between 1963 and 1967 with extensive use of reinforced concrete and the pioneering use of prestressed concrete (Morandi 1967; 1968). In particular, the stays' cover was built in prestressed concrete as the box girder main deck. Figure 21 shows the AEM numerical model of the balanced system, including the two Gerber 'girders at the ends of the system.
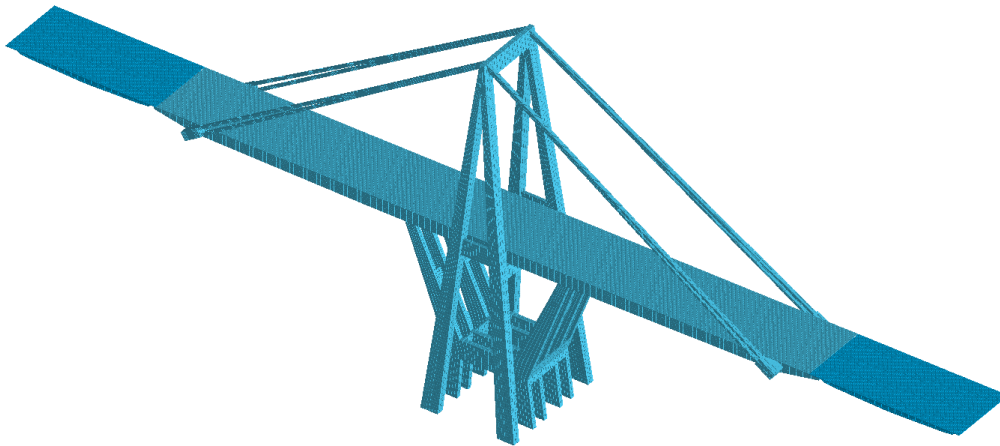
Figure 21. Image of the AEM model of the balanced system

With respect to the balanced system employed in Calvi et al. (2019), as discussed earlier, strands were modelled as an assembly of springs in their actual positions on the cross section of the stays' concrete casing. This provided full bonding between the strands and the stays' concrete elements. The strands continuously running over the saddle at the top of the A-shaped tower were modelled as springs. Thus, their actual curved shape was reproduced.

According to the designer, a maximum compressive strengths of 37, and 50 MPa were assumed for ordinary and prestressed concrete, respectively (Morandi 1967; 1968). Yield stresses of 265, and 431 MPa were considered for corrugated steel bars in ordinary and prestressed concrete elements, respectively. High strength steel with yield strength of 1667 MPa was assumed for strands. Time dependent phenomena were not considered in the AEM model.

In the following, a description of the adopted model with respect to the original design tables of the balanced system is provided. It consists of: (i) a reinforced concrete trestle composed by four H-shaped frames connected by cross girders (Figure 22);
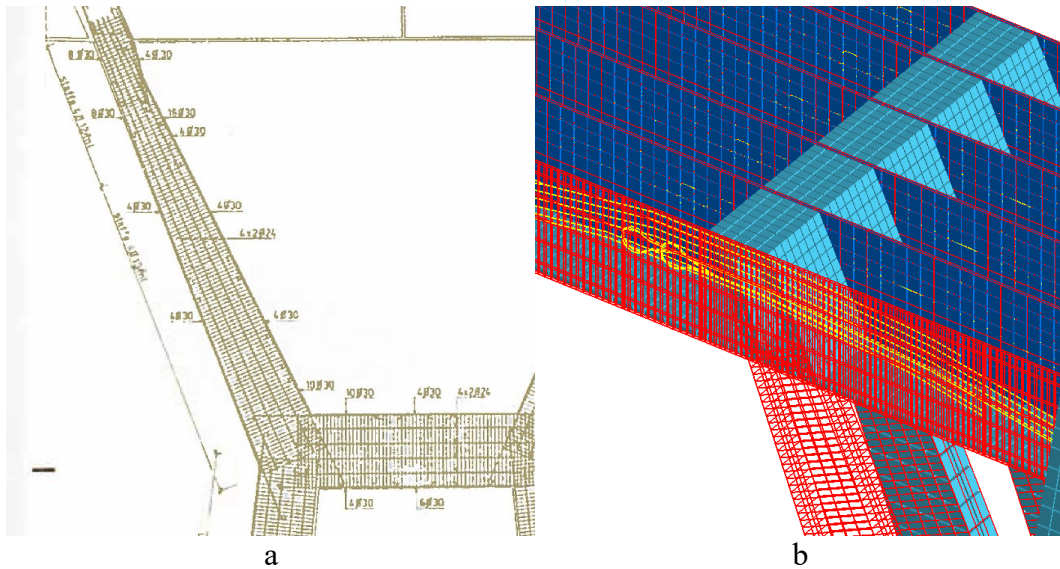
Figure 22. RC trestle reinforcements detail. Comparison between as-built drawings (Morandi 1967) and the AEM model

(ii) An A-shaped tower, completely independent from the trestle, made up of four inclined columns with variable hollow sections (Figure 23);
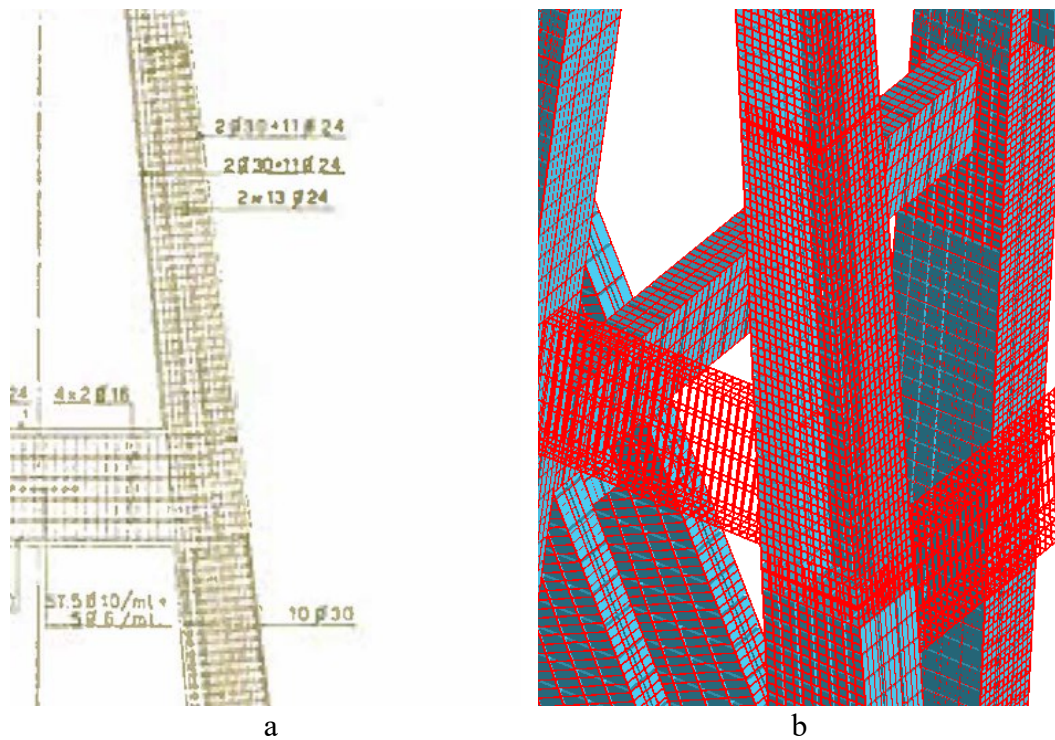
Figure 23. RC A-shaped tower reinforcements detail. Comparison between as-built drawings (Morandi 1967) and the AEM model

(iii) A continuous box girder of prestressed concrete with six longitudinal ribs. Prestressed cables were placed in the ribs at the intersection between the transverse beams and the trestle (e.g. Figure 24). Additional prestressing cables were placed at the bottom of the deck.
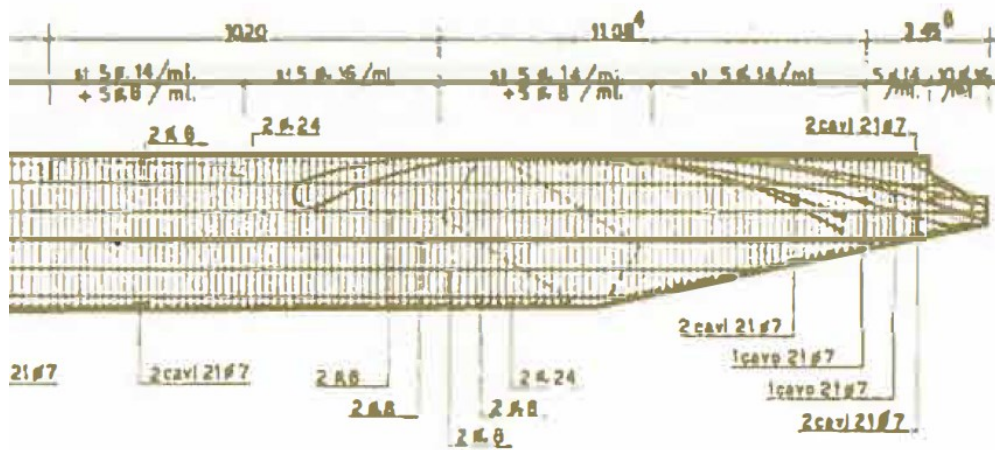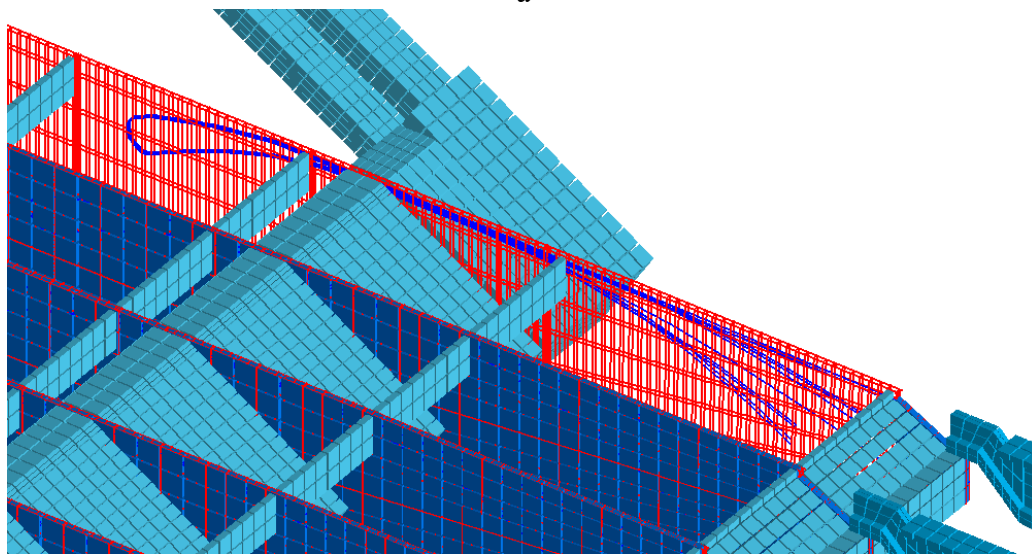
Figure 24. Deck's detail: prestressed cables at the connection with the stays.
Comparison between as-built drawings and the AEM model

The main girder works as a continuous beam on four supports. The trestle provides the first supports on the central portion of the system, while stay-cables passing over the top of the A-shaped tower provide additional supports at both extremities. Different construction phases were considered by the designer (Morandi 1967; 1968):

1. Trestle and A-shaped tower construction by employing the traditional methods in reinforced concrete.

2. Segmental cantilever construction process of the deck from the A-shaped tower. Each new segment was supported by temporary almost horizontal cables.

3. Installation of primary Cables A from the A-shaped tower to the deck extremities for supporting the dead loads, and removal of temporary cables employed in phase

4. Preparation of the form-works for construction of concrete elements surrounding Cables A to be post-tensioned by the embedded secondary Cables B. Such prestressed concrete elements were intended to encase and protect steel Cables

A and B. During this phase, integration of the cables in the system was accomplished by injection of grouts in the ducts.

The stays had variable cross-sections: at the deck connection they were split in two 98x61 cm rectangles to spread the effect of the concentrated force. At the top of the A-shaped tower around the saddle, the cable was composed of a single 98x122 cm rectangle (Figure 25).

a

b
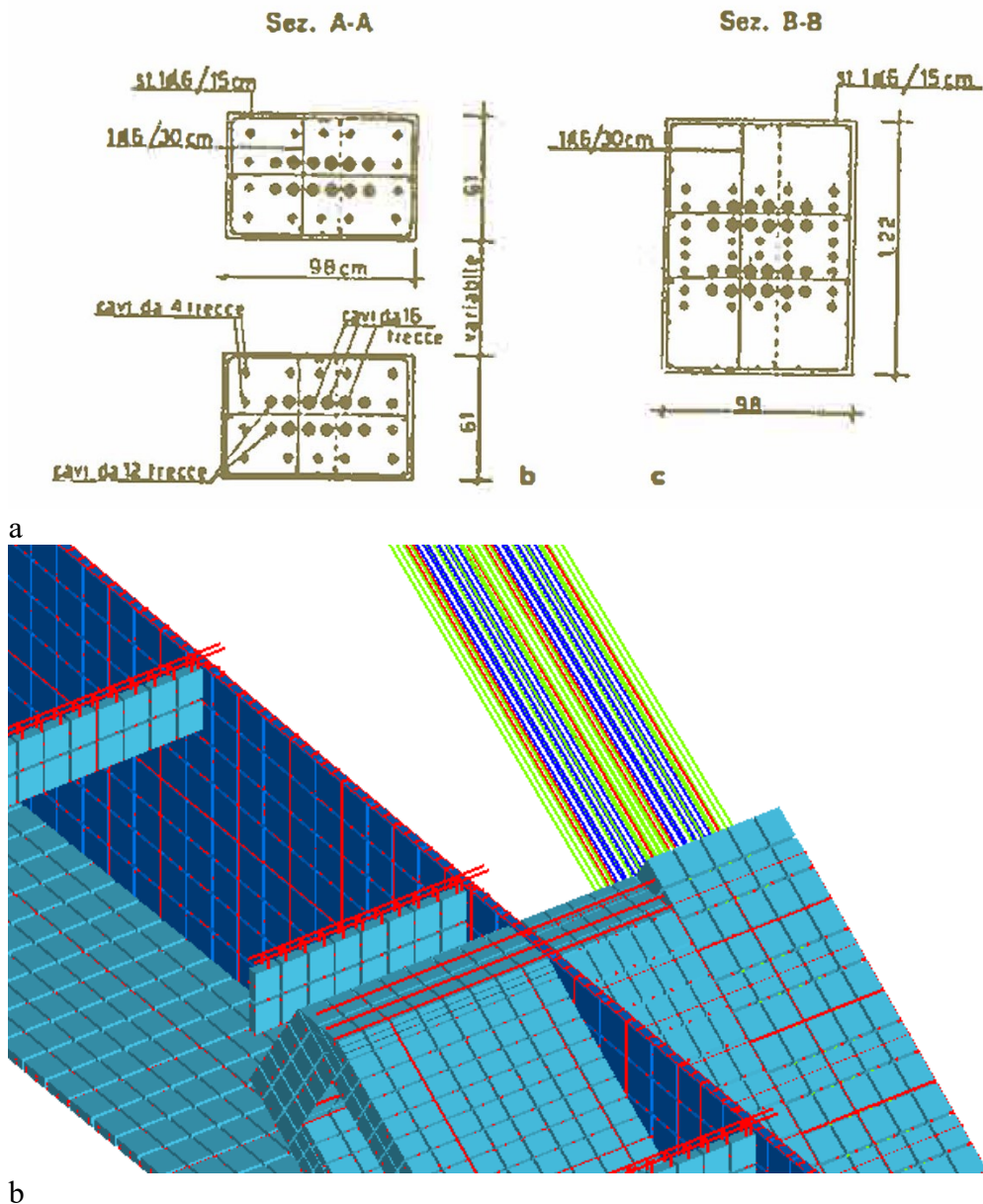
Figure 25. Stay-cables: primary (blue and red) and secondary (green) tendons in the AEM model. Comparison with as-built drawings and the AEM model

The cross-sectional area and the number of strands within each cross section remained the same. Cables A, the inner cables, were the first to be installed and were composed of 8 units of 12 strands each, and 16 units of 16 strands each (352 total strands). Cables B were composed of 28 units of 4 strands each (112 total strands). All the strands had half inch (1/2") diameters.

In the design, the steel cables were encased within the prestressed concrete, mainly for the purpose of reducing the difference between the stiffnesses of the stays and the deck, and to protect the stays against corrosion. Furthermore, injection of the grout in the ducts containing steel tendons were originally planned to monotonize the entire composite structural element.

Gerber beams were installed to connect the adjacent piers (Figure 26).

a

b
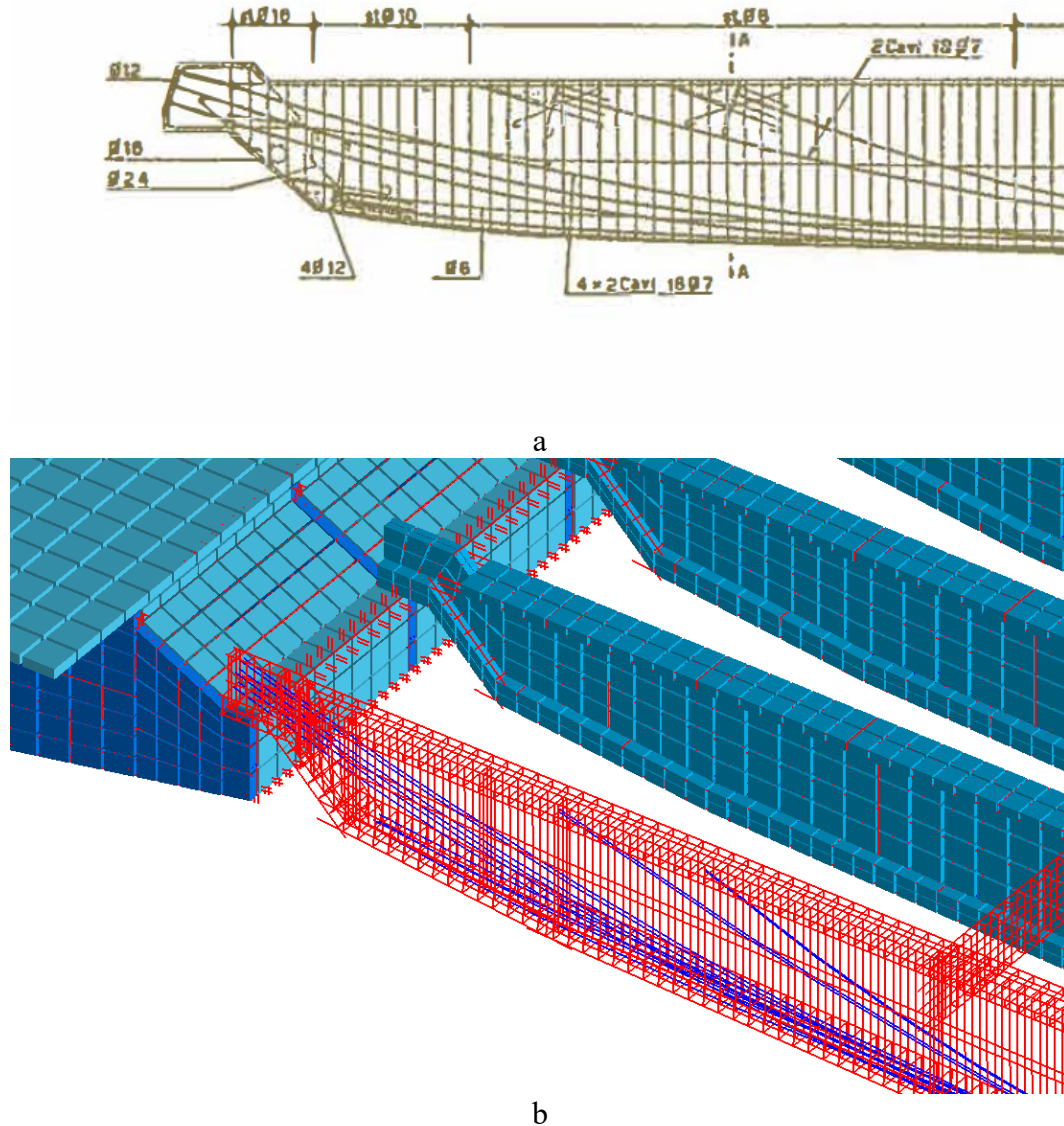
Figure 26. Gerber girders. Comparison between as-built drawings and the AEM model

A bearing material was employed at the interface between the box girder and the Gerber beams in order to allow sliding along the horizontal axes [17]. Therefore, the Gerber beams of the viaduct were considered ads simply supported beams. Sensitivity analyses identified the suitable mesh size and analysis time step parameters. In doing so, both parameters were decreased during the analysis until convergence in the deck's displacement and cable's catenary shape were reached.

Material'models

Fully nonlinear path-dependent constitutive models for reinforced concrete are adopted in the AEM. For concrete compression states, the analysis considered the elasto-plastic and fracture model by Maekawa and Okamura (Maekawa and Okamura 1983). Linear stress-strain relationship is adopted for concrete subjected to tension until the material cracks. The Menegotto and Pinto (Menegotto and Pinto 1973) constitutive relationship was employed for modeling the behavior of reinforcing bars and prestressing strands. Concrete is assumed cracked when the principal tensile stresses reach the cracking strength of concrete.

The AEM code Extreme Loading for Structures was used to perform the collapse simulations of the balanced system ("Extreme Loading for Structures" 2021).

The same code has been also used in a pioneering study on the collapse of Pier #9 (Calvi et al. 2019). In that work, stays were modelled as nonlinear links consisting of special nonlinear springs with capability to connect the centroids of two separate solid elements, carrying axial stresses only. The AEM model consisted of 320000 degrees of freedom.

In the present research, stays' strands were modelled as nonlinear springs in their actual positions on the cross section of the stays within the encased concrete, connecting face-by-face adjacent solid concrete elements. The whole model consists of 900000 degrees of freedom.

Then, a collapses scenario was assumed to determine a suitable time step for collapse behavior. Analysis with time step higher than 0.001 showed unrealistic collapse behavior. Finally, 0.001 s time step and approximately 150000 solid elements were employed for the analyses. This led to a total computation time of almost 48 hours. Each solid element had 8 nodes, 6 degrees-of-freedom (3 translations and 3 rotations), and five springs per elemental face. A 6 core 3.50 GHz processor with 64Gb RAM and SSD drive was employed in the aforementioned computations.

The bridge model was considered fixed at the base; thus no soil-structure interaction was considered in the analysis. The construction sequence in the analysis refers to a simplified scheme with the aim of collapse reproduction. It consists in the application of the post-tensioning forces in the stays' strands, and then in the generation of the simply supported Gerber beams. The other structural components, such as the main deck, were generated at the early stages of the analysis. Vertical loads were applied as lumped masses.

The post-tensioning forces in the stays were calibrated to match the design stresses reported by the designer (Morandi 1967; 1968). Accordingly, the tensile stresses in the stays' strands ranged between 675 to 735 MPa. A rigid interface was assumed between the strands and the concrete. Because of this simplification there was approximately 25 MPa higher compressive stresses in the concrete surrounding the stays with respect to the actual stresses of around 5 MPa. However, this simplification was considered compatible with the aims of this study, which intended to focus on the overall behavior of the system rather than on local

phenomena, such as concrete cover decompression of the bridge stays. Time-dependent phenomena, as well as construction defects were not considered in the analysis scheme described herein. The vertical displacements based on the above-mentioned analysis schemes are shown in Figure 27.
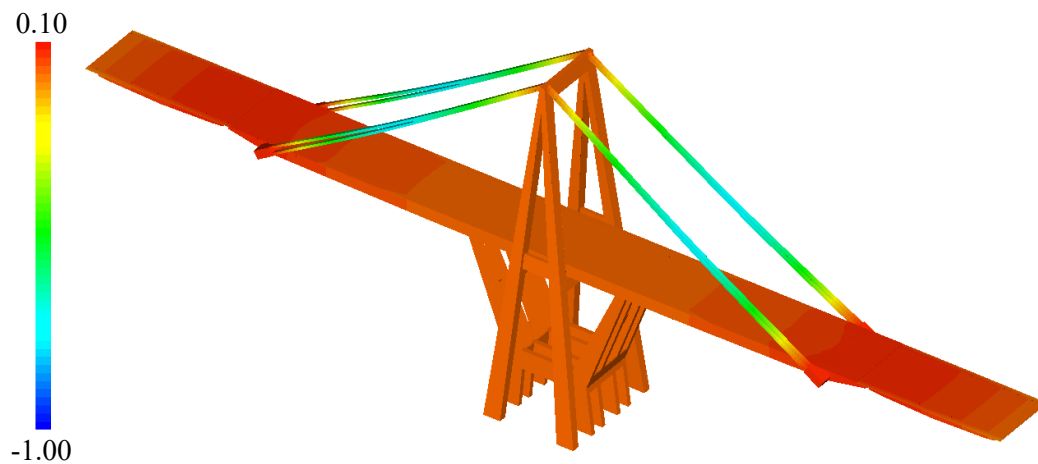
Figure 27. AEM model: vertical displacements due to the dead load after post-tensioning of prestressing cables [cm]

An accurate reproduction of the construction stages for the balanced system can be found in Orgnoni et al (2019), where each stage was reproduced in detail through finite element approach and compared with the original design at several key points in terms of displacements and internal stresses. Furthermore, time dependent effects (i.e. creep and shrinkage), added masses (e.g. Jersey barriers installed during 90s), concrete stays' decompression, and defects (e.g. partial ducts injections) were also considered in order to assess the system's performance during its service life (Orgnoni et al. 2019).

Damping was considered in the AEM model as internal damping (rate-independent). Internal damping is associated with the nonlinear response of the construction materials (e.g. concrete cracking, steel reinforcements unloading after yielding) and contact induced friction between the structural components. Furthermore, the proposed AEM model considers energy dissipation due to collision between elements and soil during collapse.

Focusing on bridge loading conditions that could have contributed to the structural collapse, some considerations were done. Degradation of bridges over the duration of their service lives is usually associated with the effects of increased truck traffic (N. Lu, Noori, and Liu 2017). Therefore, increased frequency of axle loads and amplitudes are amongst major reasons for shortening the service lives or even collapses of existing bridges (Morgese et al. 2020; Invernizzi, Montagnoli, and Carpinteri 2019).

Dynamic AEM analyses were performed taking into account the effect of traffic loading on internal actions, for comparison with the structure's response due to its self-weight. The automobile induced loads were modelled by considering the effects of two axles, exerting a load equal to 2 tons to the bridge. Trucks were modelled by 5 equidistant axles, resulting in a total load of 44 tons. Both

automobiles and trucks were considered travelling along the two traffic directions on the bridge.

The dynamic preliminary analyses indicated that the effects of live loads on internal stresses were minimal compared to the dead loads (2-5% with respect to dead loads). The same outcome can be found in Calvi et al. (2019), where the findings indicated that the live loads consisted of only a small fraction of the permanent loads. Indeed, the box girder of the bridge consists of extremely heavy reinforced and prestressed concrete elements. In essence, the amplitude of the main deck dead load in this structure overshadowed the amplitude of the live loads. For instance, the weight of a 44 tons' truck was estimated less than 1% of the box deck dead load, i.e. about 4500 tons considering a total length of about 170 m between the stays' connections, and a width of 15 m.

Therefore, traffic load could not significantly influence the level of stress and strain demand in the bridge. As shown by the classical influence line analysis in Morgese et al. (Morgese et al. 2020), other factors in combination with truck axle loads may lead to the collapse of the bridge.

Thus, traffic action could be assumed at most as trigger for the collapse of a highly degraded system. In light of these considerations, the self-weight can be assumed as the critical load for the balanced system, and hence, has been considered for the following static collapse analysis.

Collapse assessment

This study did not concentrate on the factors that may have resulted in the capacity degradation of the structural elements. Instead, it followed a macro-structural component approach, evaluating the step-by-step structural response of the model to the progressive reduction of the strength capacity of single macro-components. Hence, the analysis of the collapse was performed through an iterative approach, assuming an increase of local degradation in different sections of the structure. For example, the strength capacities of the deck ribs were progressively reduced, section by section, until the collapse occurred. Degradations were introduced in the model as an incremental area reduction factor, till the complete section loss was reached. This was done without explicit modelling of the degradation processes, e.g. fatigue or corrosion.

Table 4 summarizes the local incremental degradation analysis carried out in this study.
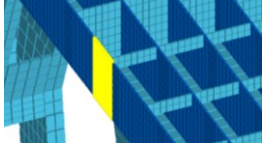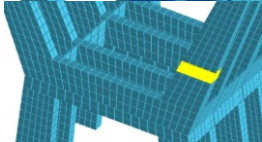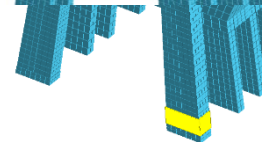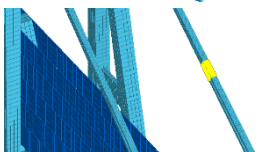
Element	Degraded area	n. of elements	Results
Deck		3	-
		4	Collapse
Trestle		4	-
		5	Collapse
Tower		1	-
Cable		1	Collapse

Table 4. Performed analysis during the first stage of numerical simulations.

For the deck, the trestle and the A-shaped tower, degradation corresponded to the transvers section reduction of both steel reinforcements and concrete. For stays, damage corresponded to the transvers section reduction of steel reinforcements only. The proposed damage analysis approach was implemented through incremental reduction of the properties of the spring elements connecting the rigid elements of the model.

The incremental reduction of the steel properties was limited to 90% to model the largest degraded conditions, allowing for redistribution of stresses, and avoiding the complete and sudden loss of a structural element. For example, when the rib of the main girder reached the 90% damage level without collapse, degradation process would continue on the next rib, and so forth, till failure.

The first outcome of the sensitivity analysis on the progressive collapse of the bridge highlighted the robustness of the A-shaped tower, of the trestle and of the deck. This result was justified in view of the redundancy that characterize these structural elements and their compression state in in-service condition. Indeed, both the A-shaped tower and the trestle elements were predominantly in compression. Similarly, the main girder was subjected to high compressive forces because of the horizontal components of the internal forces in the stays. In essence, all the deck sections were in a prevalent compression state under the working loads (Figure 28).
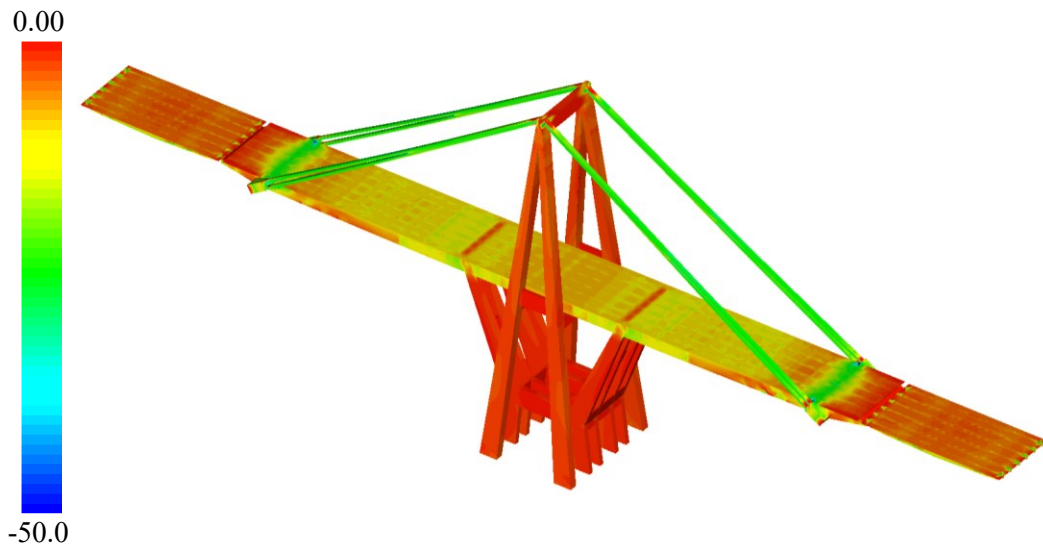
Figure 28. Compressive stresses along the deck in the static analysis [MPa]

The collapse of the balanced system did not occur, even following the reduction in the global capacities of three ribs. The bridge was still able to redistribute the loads, even when the deck deflected by about 1 m (Figure 29).
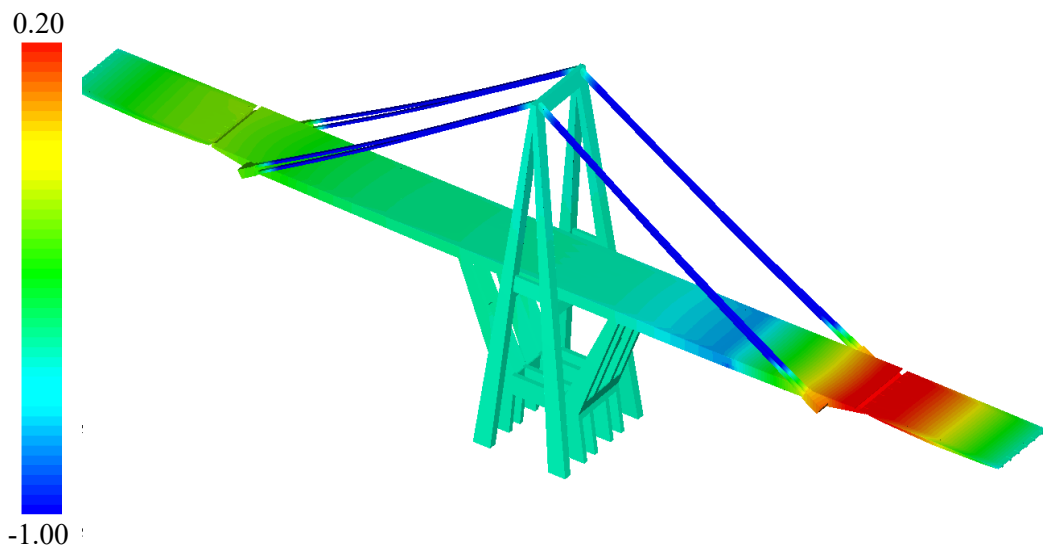
Figure 29. Vertical displacement with degradation to four deck's ribs [m]

The bridge collapsed when four deck ribs reached their maximum degradation limits (Figure 30).
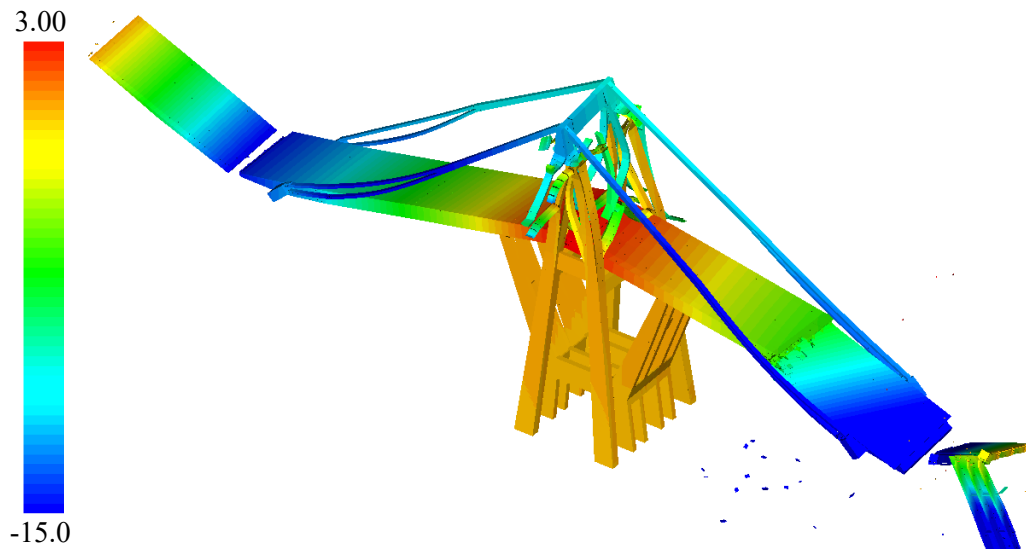
Figure 30. Vertical displacement with degradation to four deck's ribs [m]

Similarly, even full degradation of four out of eight trestle columns did not lead to collapse of the bridge, considering the large vertical displacements as shown in Figure 31.
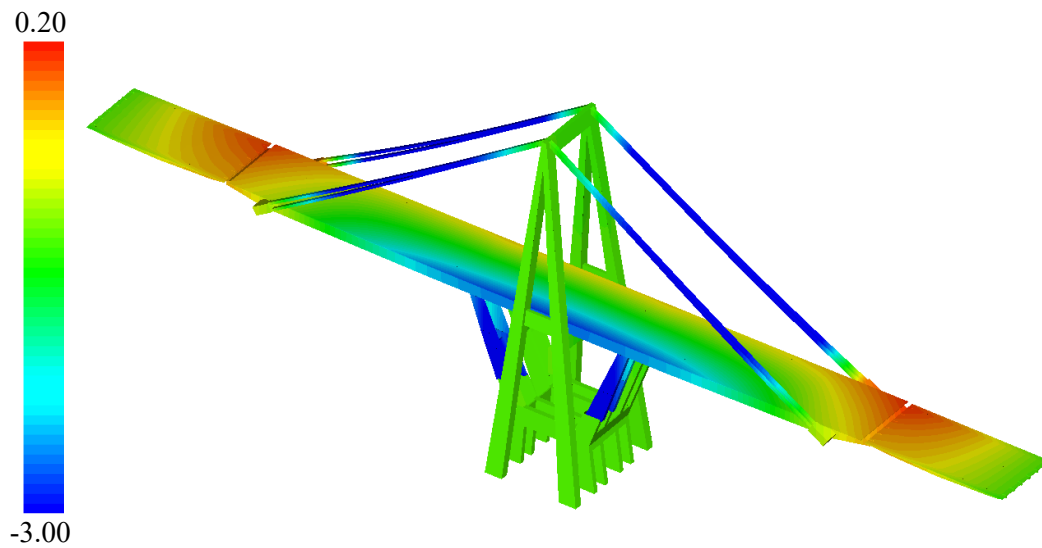
Figure 31. Vertical displacement with degradation to four trestle's sections [m]

The collapse occurred when the fifth trestle section fully degraded (Figure 32).
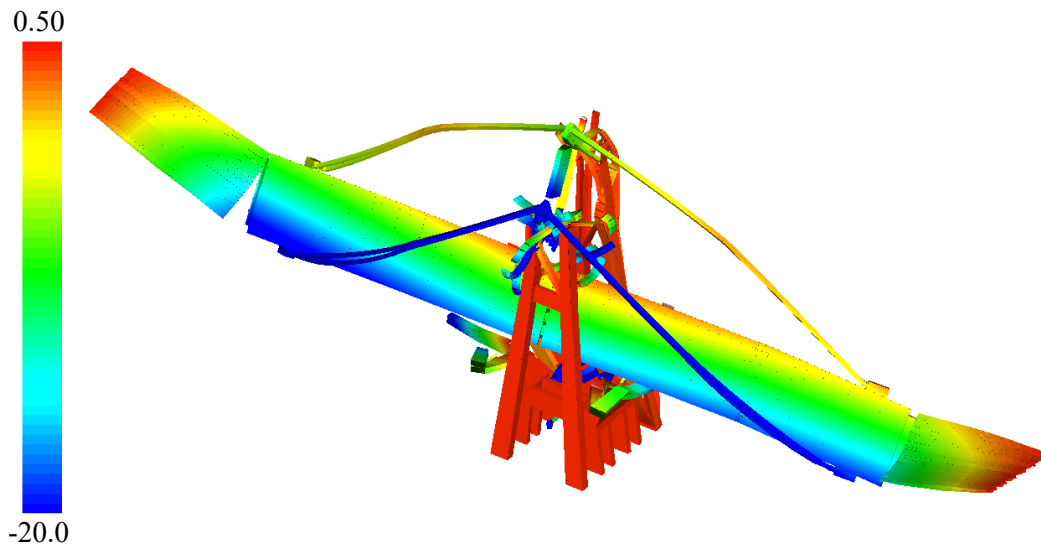
Figure 32. Vertical displacement with degradation to five trestle's sections [m]

Even the failure of one column of the tower would not lead to the total collapse of the bridge. In essence, the bridge was able to redistribute the load and find a new balanced stable state (Figure 33).
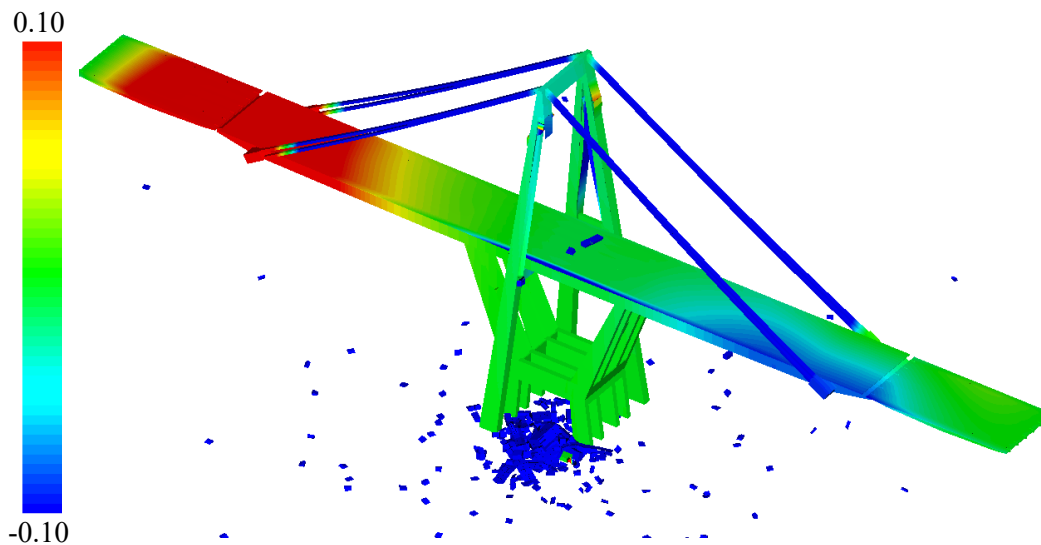
Figure 33. Vertical displacement with applied degradation to one tower's section [m]

Analysis of the results indicated that, the stresses in the remaining columns were compatible with the maximum compressive strength of the concrete (about 35 MPa). The transvers beams that connected the columns of the tower prevented the failed columns from impacting the deck of the bridge. The ground was considered rigid, justifying the fragmentation of the collapsed structural portions after the impact with the ground. It is worth underlining that the provided interpretation, especially in terms of the fate of the columns, stems from the fact that it is not possible to a great degree of certainty to provide the model with exact collapse scenarios. Thus, the analysis is based on such assumptions.

On the other hand, the failure of one cable leads to the failure of the main deck due to lack of torsional capacity, and consequently, the entire structure collapses (Figure 34).
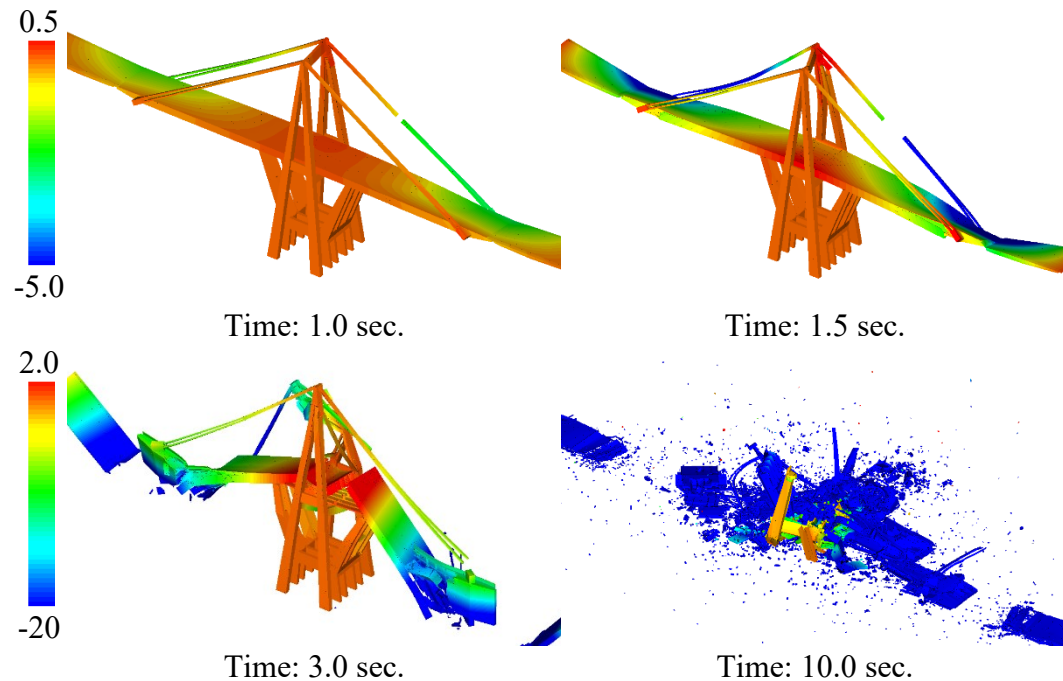
Figure 34. Vertical displacement with applied degradation to one cable's section [m]

Analysis of the incremental degradation in different sections of the structure revealed that stay cable is the most critical element whose failure triggers the collapse. If sections other than the stay cables were responsible for the collapse, large deformations and displacements would have warned the authorities of the impending failure.

To identify the most vulnerable cross section of the stays that culminated in progressive collapse, additional analyses were performed. To accomplish this goal, the incremental degradation approach was also performed along the entire length of the strands within the stays.
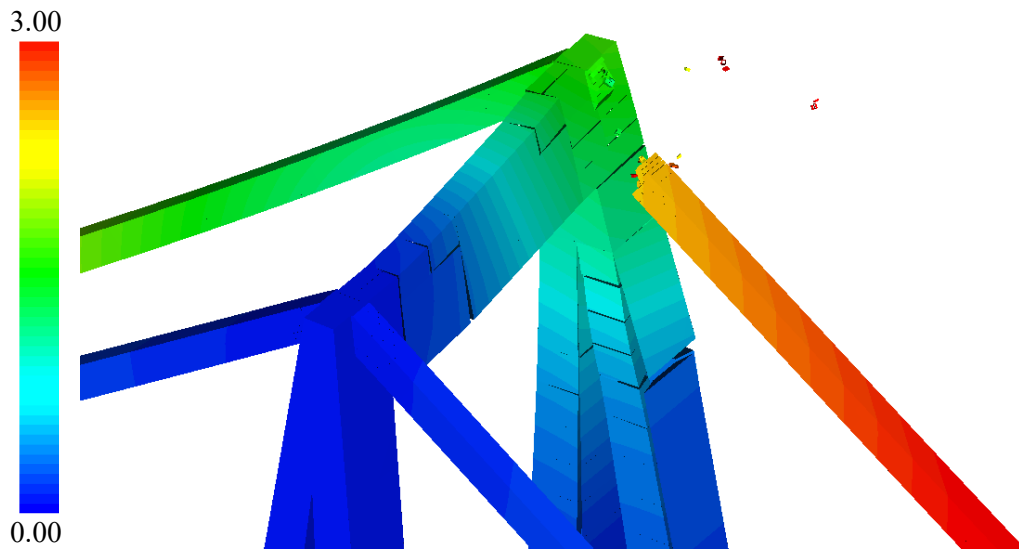
Figure 35. Vertical displacement with applied degradation along the entire length of the stay [m]

The results shed light into the first occurrence of failure at the connection between the stay and the saddle top of the A-shaped tower (Figure 35).

Comparison of the results

The outcomes of the analyses in the previous section of this work allowed for the identification of the component and the section that may have triggered the progressive collapse. The numerical simulations described in this section are focused on the comparison with the available documents, such as the footage recently released by the authorities (Guardia di Finanza Genova 2019). In particular, the failure of the South-East stay was reproduced, by gradually degrading the strands at the connection between the stay and the saddle at the top of the A-shaped tower (Figure 36).
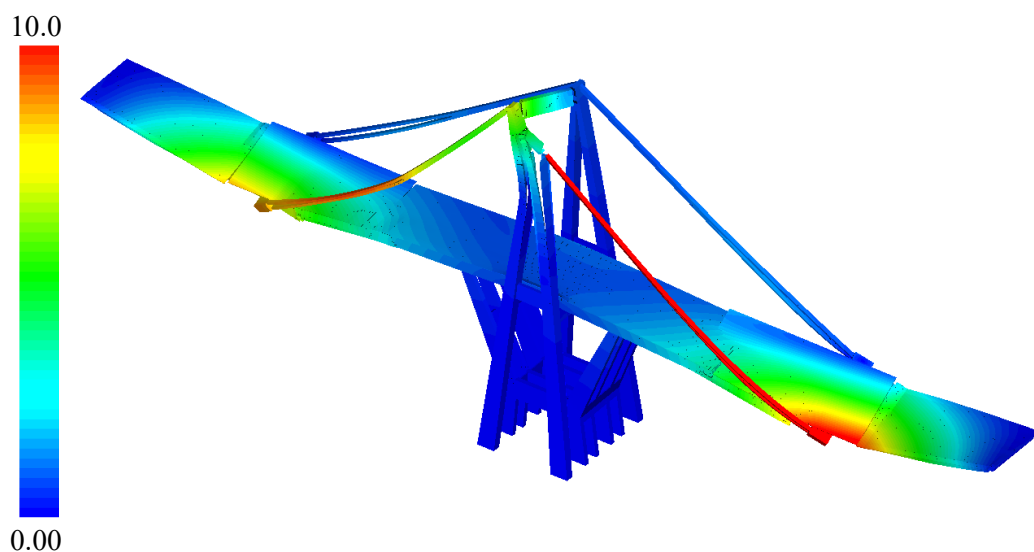
Figure 36. Vertical displacement with applied degradation to the South-East stay [m].

In total around 60 % of the cross section of the strands was removed for simulating the degradation. The simulations were compared, frame by frame, with the images derived from the collapse footage to allow an improved interpretation of the mechanism (Figure 37).
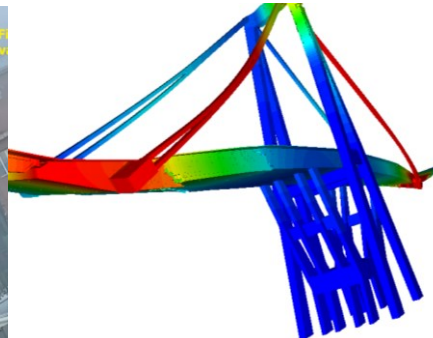
Time: 1.00 sec   Time: 1.00 sec
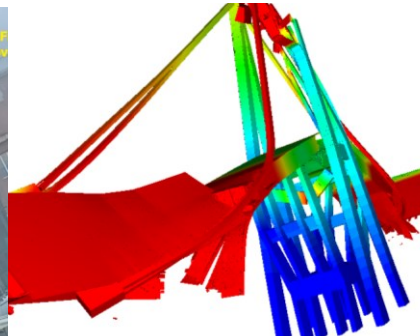
Time: 2.00 sec   Time: 2.00 sec
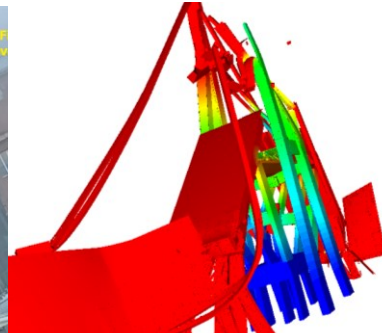
Time: 3.00 sec   Time: 3.00 sec
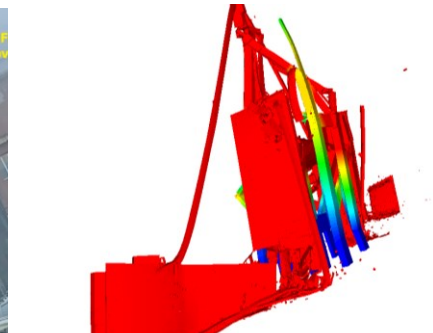
Time: 5.00 sec   Time: 5.00 sec

Time: 6.00 sec   Time: 6.00 sec

Time: 7.00 sec   Time: 7.00 sec

Time: 9.00 sec   Time: 9.00 sec
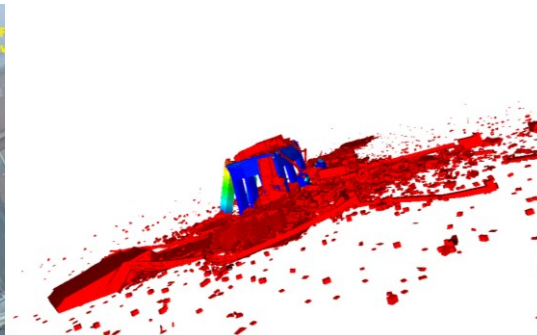
Time: 13.00 sec   Time: 13.00 sec

Figure 37. Side by side comparison of the collapse mechanism of the bridge. Analysis results (left), actual collapse images (right).

The first step at the 1-second time instant in Figure 37 shows the collapsing bridge deck that has lost its support at the South-East stay. The bridge starts to collapse, and the end of the deck at the east side undergoes relevant displacements in vertical direction. The southwest stay breaks the tower, and at the same time, the deck breaks in two points.

At the 2-second time instant, the deck twists around the longitudinal axis because of the pull from the standing support at the north side stay. By the 3-second time instant, the deck has already broken into a "V" shape. The south saddle at the top of the A-shaped tower has also collapsed during this time interval. It is also worth noticing that the western portion of the deck sticks vertically into the ground. However, a discrepancy can be observed in the video footage from the 5 second times instant onwards, when the downstream (South) part of the tower is still standing up until the 9-second time instant, but in the model it collapses much earlier. Correspondence between the computational model and the footage at the 3-second time instant can be also observed by the 180-degrees rotation of the western section of the deck with respect to the transverse axis of the bridge. However, it is impossible to confirm a satisfactory match in the remaining time steps, because the deck portion in the footage is covered by a cloud of dust and debris.

Figure 38 shows the post collapse shape and distribution of the debris by the computational model and the real distribution of the debris. The comparison shows satisfactory agreement between the simulated and actual debris shapes. Slight differences between the two are related to the rigid model adopted for the soil. It does not allow for the penetration of any debris into the ground. Moreover, some site details, such as the railway and the buildings were not modeled and, therefore, they can't interact with the debris distribution.
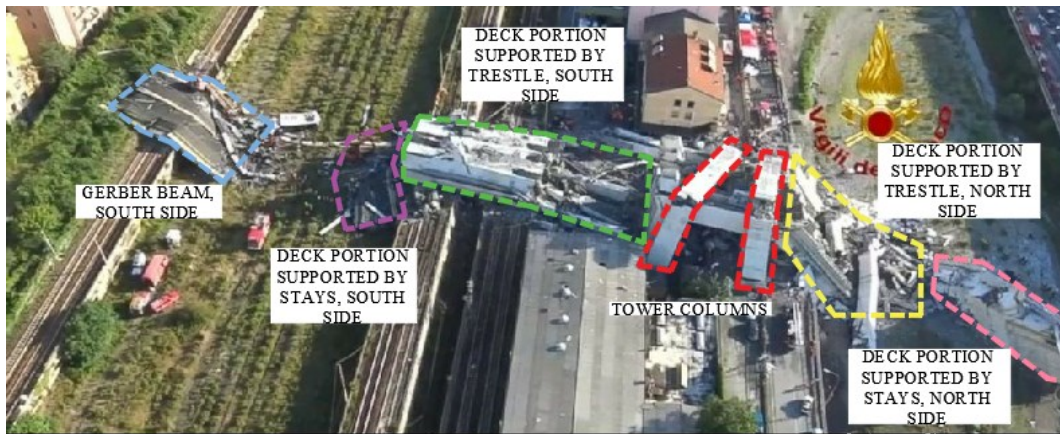
a.: aerial picture
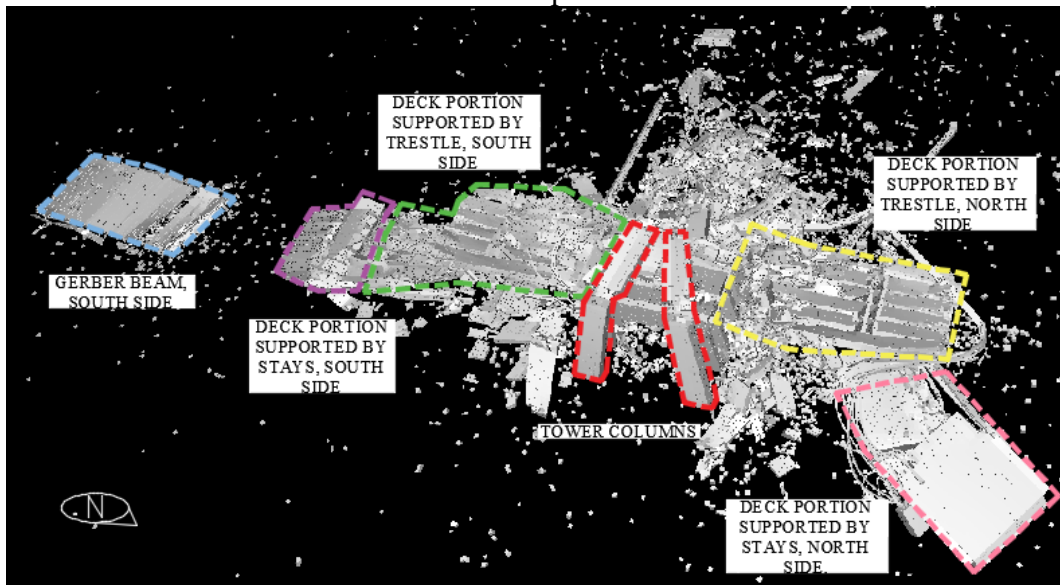
b.: analysis results

Figure 38. Debris heap from a picture of the Italian Fire Brigade Corps (above) [8] and same view of the collapsed shape of the AEM model (below)

A further debris analysis can be performed by overlapping of the actual points cloud of the debris shape, which is based on satellite images (Google Earth® aerial images), and the AEM analysis results. Although at the time of the acquisition of the images (August 27, 2018) the area was already under debris removal operations, a good number of debris were still in their original positions. The overlapped images show a good match between the analysis and the debris positions (Figure 39).
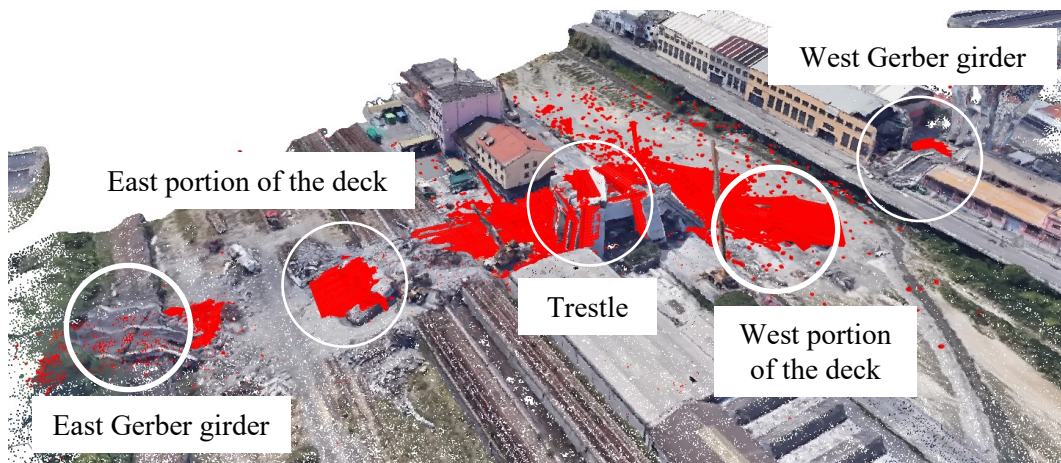
Figure 39. Overlapped images between the point cloud of the area during disposal operations and the results of the AEM analysis (red)

A more detail comparison can be made evaluating the absolute distance between the actual point cloud and a point cloud based on the analysis of results (Figure 40).
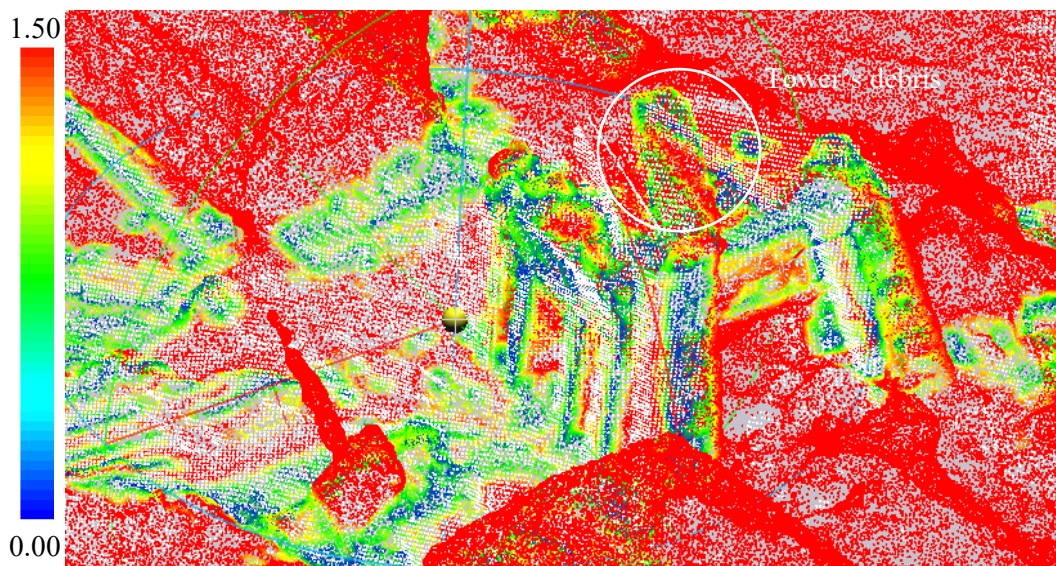
Figure 40. Absolute distance between point cloud based on satellite images and point cloud based on AEM analysis [m]

As it can be seen in this figure, the position of the remaining parts of the A-shaped tower shows a 1-meter spatial deviation with the analysis results. This confirms a pulling of the A-shaped tower towards the southwest side of the bridge, in consonance with the results of the AEM analysis. The absolute distances for this point cloud analysis were computed by using the Cloud Compare software (GPL software 2019, n.d.). Table 1 provides a comprehensive summary of the analysis pertaining to the various sections, and acquired results based in the present study.

Table 5. Summary of the analysis outcomes and their implication

Section/Figure	Analysis	Results/Findings
Section 4	Incremental degradation of cross sections in different components.	The stay is the most critical element for the collapse. Other components show more robustness and redundancy.
Section 5 Figure 20	The failure of the South-East stay has been reproduced. Comparison between AEM simulations and images taken from footage of the real collapse.	Satisfactory agreement of the AEM simulations with the actual images. Validation of the identified mechanism.
Section 5 Figure 21	Comparison between the debris distribution as computed by AEM and the real debris shape.	Satisfactory agreement of the analysis with actual evidence of the debris shape. Validation of the identified mechanism.
Section 5 Figure 22	Overlapping the actual cloud of the debris shape, from satellite images, and the analysis results.	Satisfactory agreement between the analysis and the debris position. Validation of the identified mechanism.
Section 5 Figure 23	Analysis of the absolute distance between the actual point cloud and a point cloud based on the AEM analysis results.	Minor discrepancy between the actual position of the debris and the analysis results. Validation of the identified mechanism.

Findings

This work was focused on the post collapse analysis of the Morandi's Polcevera viaduct. A AEM numerical model of the balanced system of Pier #9 was built, in order to simulate the strength degradation of different structural elements and their respective contributions to the progressive collapse of the bridge segments. The role of each degraded member, such as the tower, deck girders, and the stays within the balanced system was considered in the analysis. The validation of the proposed approach was accomplished by references to the collapsed bridge debris distribution observed from the images and a new footage of the bridge collapse, recently released by the Italian Police and Fire Brigade Corps. A macro-structural component approach in AEM was employed, making it possible for step-by-step evaluation of the structural response of the model to progressive reduction of the strength capacity of single macro-components. Unlike the earlier studies, the present approach did not concentrate on the factors that may have resulted in the capacity degradation of the structural elements. Instead, structural degradations were introduced in the model as an incremental area reduction factor until complete section loss was reached. This was done without explicit modelling for the actual causes of damage, such as fatigue and or corrosion.

The computational approach pertaining to the incremental damage in different sections of the structure revealed that the stay cable was the most critical element whose failure would have triggered the collapse. The simulation model further indicated that the failure of the other sections of the bridge, such as the main girder involved large displacements. Hence, if sections other than the stay cables were responsible for the collapse, large deformations and displacements would have warned the authorities of the impending failure.

Additional analysis of the stay cable by the incremental degradation approach revealed that the stay failure occurred at the connection between the stay and the saddle top of the tower. In particular, a reasonable agreement between the actual collapse mechanism and the simulation model was achieved when the strands in the southeast stay lost 60% of its cross-section at the connection between the stay and the top of the A-shaped tower. The identified mechanism of collapse was further validated with references to the real debris distribution observed from images and a comparison with a new footage of the bridge collapse, recently released by the Italian Authorities. However, the one-to-one correspondence between the official video footage of the collapse and the results of the analysis was fully in agreement only for the first 3-5 seconds of the collapse duration. These results are relevant considering the simplifications in modeling, and the influence of unforeseen conditions at the site of the bridge.

The final steps of the presented study consist of (i) identification of the structural components whose degradation triggered the collapse of Pier #9, and (ii) comparison of the identified failure mechanism with the available media contents (images, videos, etc.).

Chapter 5

The collapse of the Pyne Gould Building in New Zealand, in February 2011

Part of the work described in this chapter has been previously published in Engineering Structures edited by ELSEVIER: "*Reliability of collapse simulation - Comparing finite and applied element method at different levels*", C. Grunwald, A.A. Khalil, B. Schaufelberger, E.M. Ricciardi, **C. Pellecchia**, E. De Iuliis, W. Riedel.

Introduction

During the New Zealand, 22 February 2011 earthquake, the Pyne Gould Corporation (PGC) building at 233 Cambridge Terrace suffered a catastrophic collapse. The structure was designed and built in between 1963 and 1964 (Figure 41).

Figure 41. Pyne Gould Building photographed from the South-East elevation after the 4 September 2011 earthquake.

The structure consists of a reinforced concrete frame and a single shear core centered north-south. The 28 by 28mt plan area was divided into 5,10mt bays with an additional 1.32mt cantilever shifting along the perimeter of the structure.

Retrieved data

The discussed work is based on the following retrieved data:

- Structural drawings dated 1963;
- Additional building retrofit and renovations documents dated 1997, 1998, 2001, 2004, 2005, 2007, 2008, and 2009;
- Photographs from various sources;
- Report: Investigation into the Collapse of the Pyne Gould, Corporation Building on 22nd February 2011, Prepared for Department of Building and Housing (DBH), By Beca Carter Hollings & Ferner Ltd (Beca), 26th September 2011, ©Post-collapse test results for steel reinforcing bar and concrete (Beca Carter Hollings & Ferner Ltd 2011);
- Report: Pyne Gould Corporation Building Site Examination and Material Tests, Report Prepared for Department of Building and Housing, by Hyland Fatigue and Earthquake Engineering, Auckland, New Zealand September 2011(Hyland Fatigue and Earthquake Engineering for the Department of Building and Housing 2011);

Geometry

The typical floor of the building is shown in Figure 42.
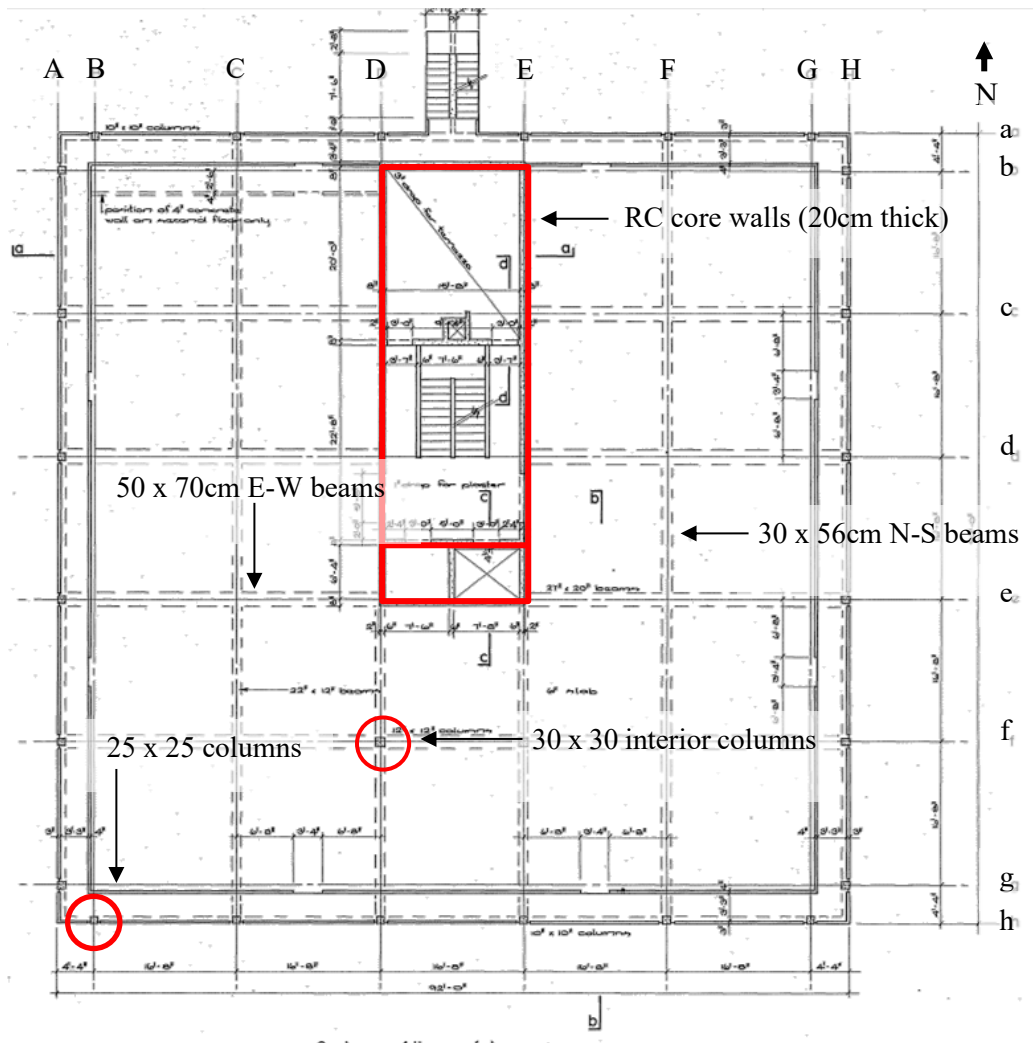
Figure 42. Typical floors (2nd to 4th Floors)

The RC core was 20cm thick; The girders-oriented East-West measured 84x61cm at the first floor and 68.5x51 from 2nd floor up to the roof. The columns dimension was 40x40cm at the ground floor and 30x30cm at the typical floor (Figure 43).

Figure 43. North-South elevation, Grid Line D

Circular columns having a diameter of approximately 40cm were distributed along the perimeter of the building on the ground floor. The columns were enclosed into a steel jacket having a thickness of 3.2mm.

Reinforcement detail

The structure design was based on the New Zealand 1963 code design requirements. Stirrups were provided with a spacing of approximately 23cm (Figure 44).

Figure 44. Perimeter columns reinforcement details.

The core wall reinforcement consisted of a single Ø16mm layer spaced 381mm in both directions. Bars were overlapped approximately 50cm above the floor.
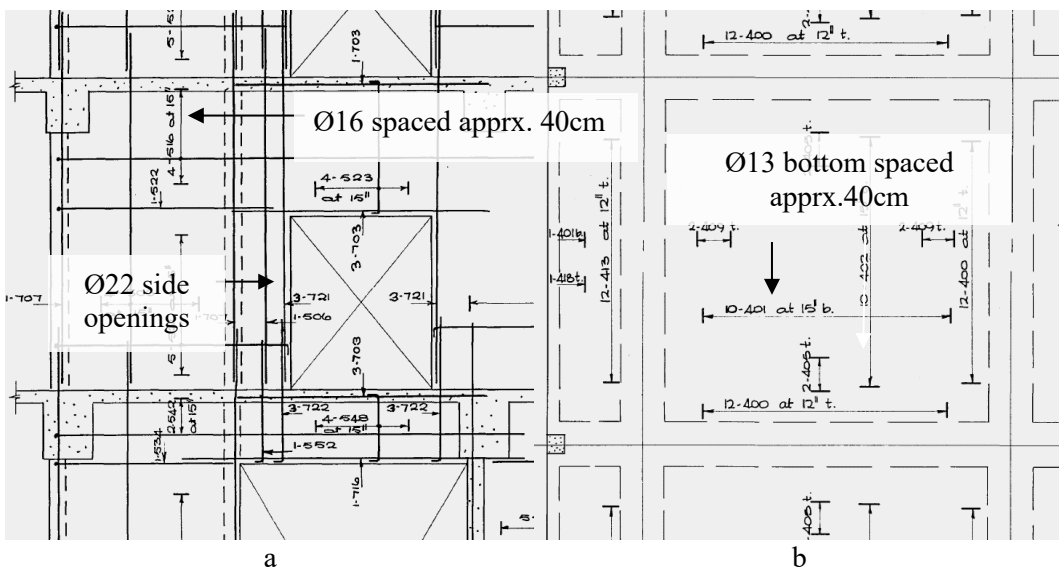
Figure 45. Shear wall (a) and Sabs (b) reinforcement details.

Enclosed steel beams were cast in place at the cantilever perimeter of the building (Figure 46).
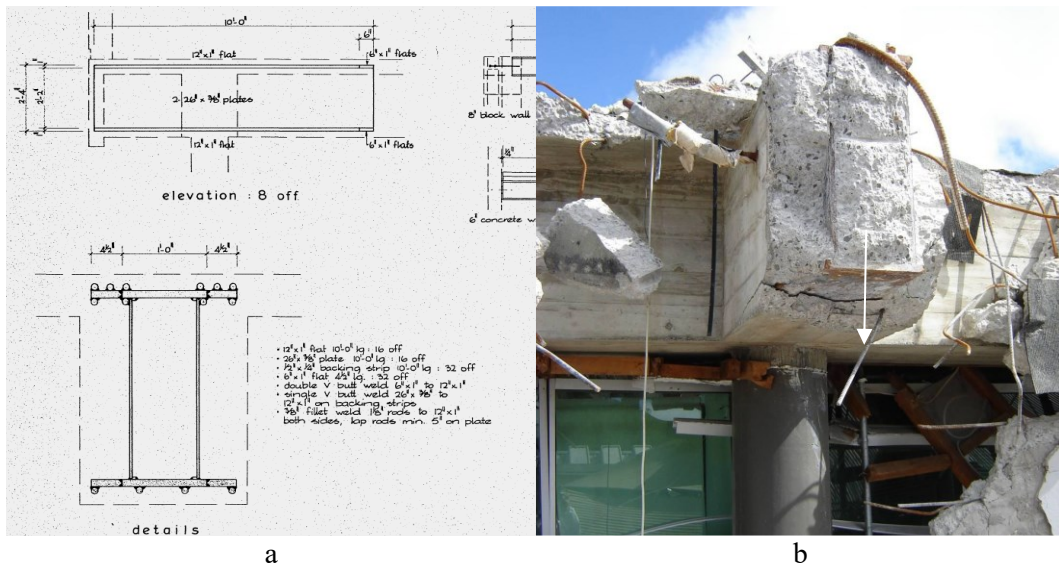
Figure 46. Enclosed steel beam in the original drawings (a) and as photographed after the collapse (b).

Numerical model

The numerical model included the following structural details (Figure 47):

- Reinforcement bars;
- Reinforcement bar overlap;
- Enclosed steel beams;
- RC steel jackets;
- Steel plates;
- Opening and stairs.
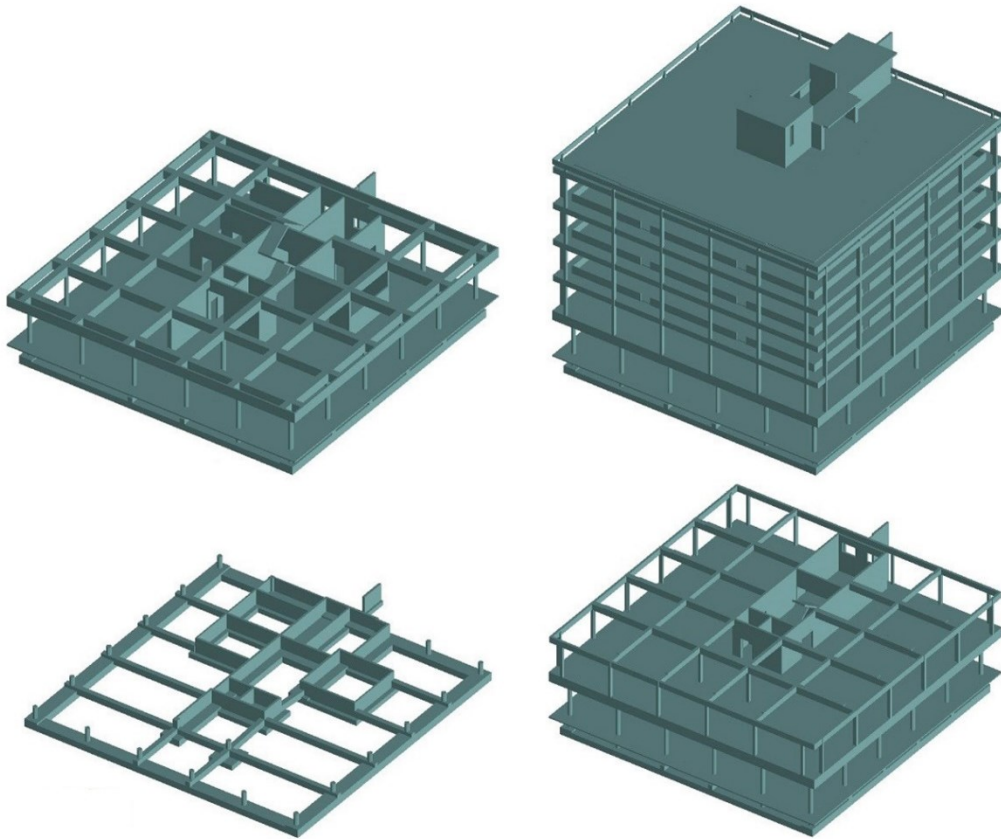
Figure 47. AEM numerical model

The numerical model included the exact reproduction of the structural system including the foundations (Figure 48).
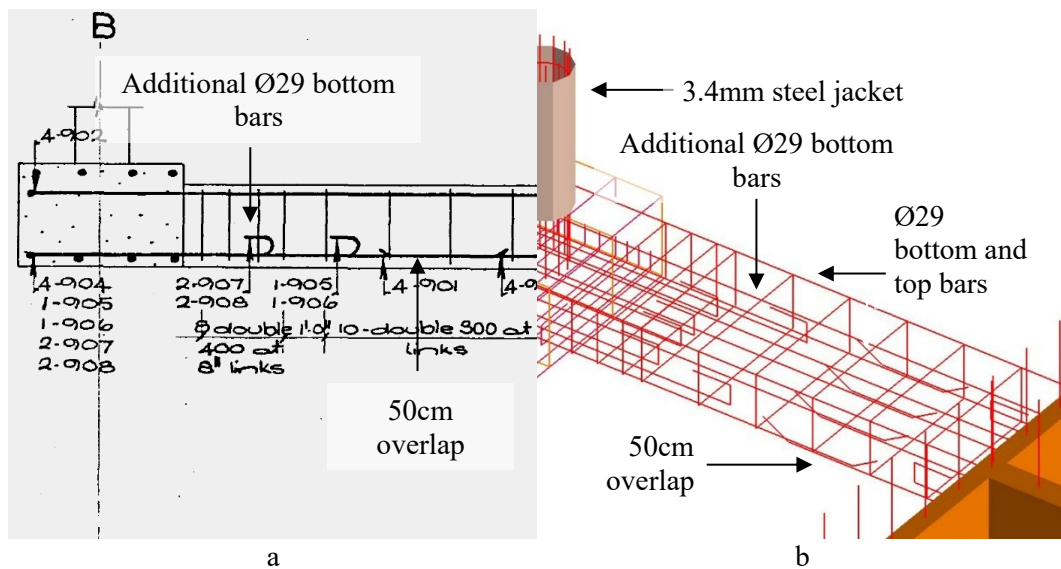
Figure 48. Foundations, original drawings (a) and numerical model (b).

Figure 49 shows the reproduction of the steel beam enclosed into the concrete girder at the perimeter of the building.
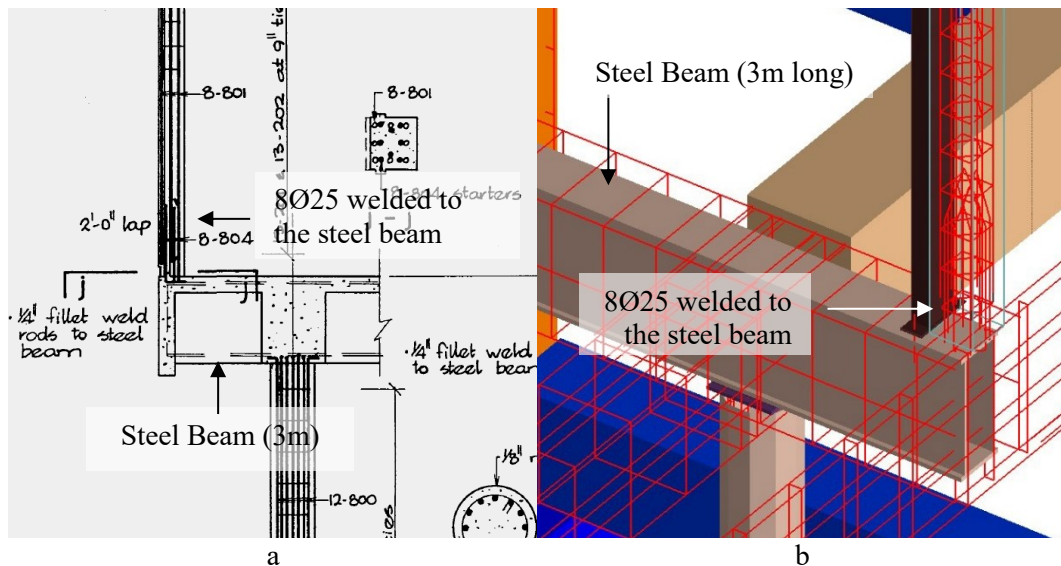
Figure 49. Steel beams enclosed in the concrete girder, original drawings (a) and numerical model (b).

The numerical model also included the circular column' steel jacket and welded steel plates used to connect the longitudinal reinforcement of the circular columns with the girder above (Figure 50).
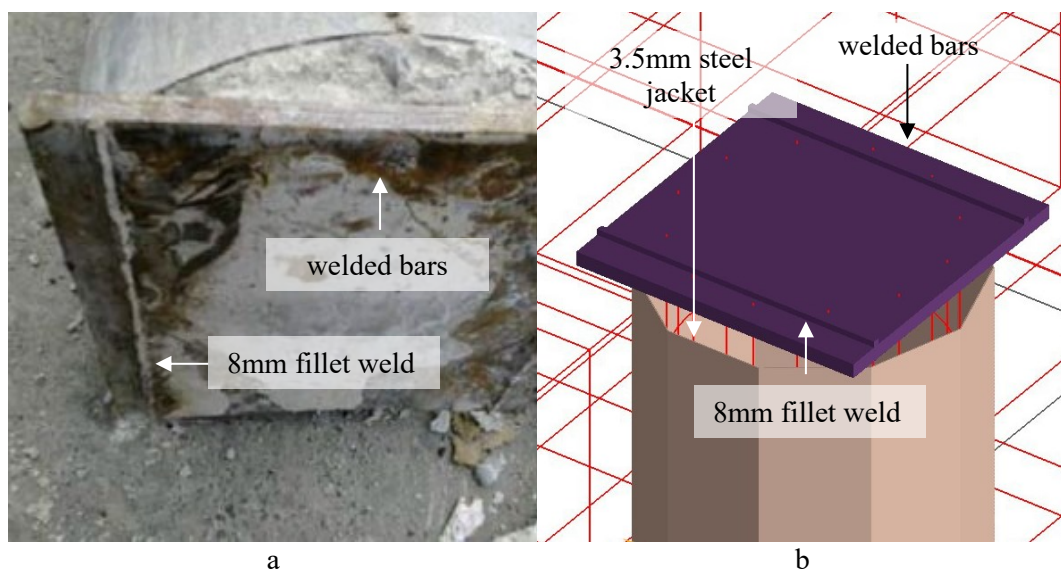
Figure 50. Steel plate and circular column' steel jacket, original drawings (a) and numerical model (b).

Analysis assumptions, material properties, and loads

The available set of structural drawings dated 1963 reports the main mechanical characteristics of the concrete for the different structural elements composing the Pyne Gould building. In addition, specimens were also tested after the collapse of the building. The test results were reported in "*Pyne Gould Corporation Building Site Examination and Material Tests*" (2011). Table 6 reports a comparison between the design value (f_c^k), the expected value considering aging strengthening (f_c), and the test results assumed in the numerical model (f_c^{test}).

Table 6 - Compressive strength of concrete [MPa]

Concrete	f_c^k	f_c	f_c^{test}
2500psi	17.2	26	40.7
3500psi	24.1	36	47.3
4000psi	27.5	41	

Reinforcing steel samples were extracted and tested based on AS/NZS 4671:2001 standards (2001), Table 7.

Table 7. Steel material properties considered in the AEM numerical model [MPa]

σ_y	σ_u	σ_u / σ_y	ε_u
338	497	1.47	1

The analyses were carried out the Maekawa and Okamura (Maekawa and Okamura 1983) elasto-plastic and fracture model for concrete subject to compression state. When subject to tension, a linear stress-strain relationship is considered before reaching crack development. The Menegotto and Pinto (Menegotto and Pinto 1973) constitutive relationship was employed for modeling the cyclic behavior of reinforcing bars.

In terms of seismic loads, the nearest station to the PGC building was the Resthaven Rest Home (REHS), approximately 670 mt northwest of the PGC building site. The record was retrieved from the PEER NGA-East Database (Goulet et al. 2014).

Figure 51 shows the results of the non-linear dynamic analysis using the AEM numerical model.
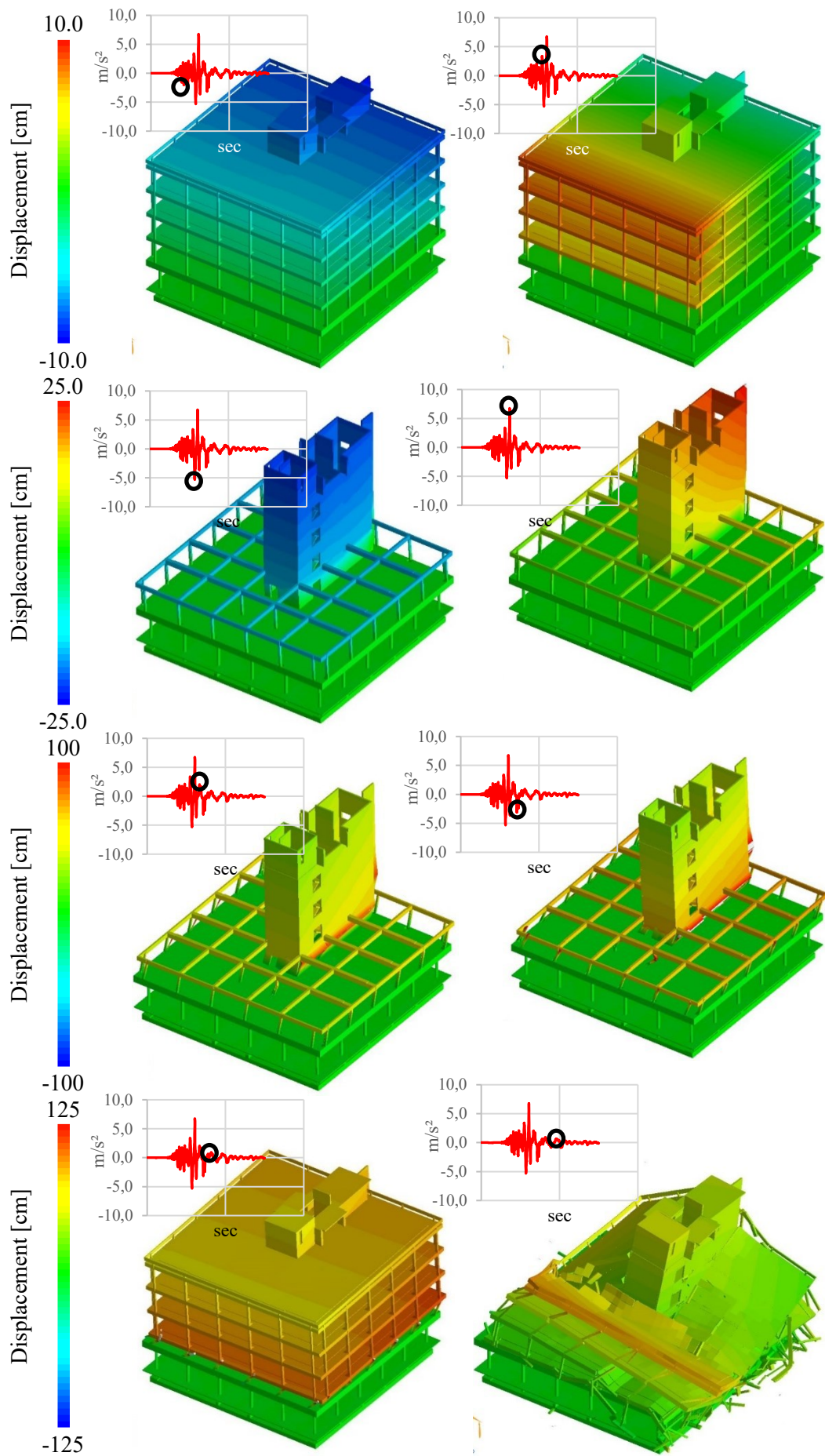
Figure 51. Non-linear dynamic analysis, 2/21/2011 Christchurch Resthaven record.

As it can be observed the collapse propagated from the first floor starting from an initial buckling failure in the shear core of the building.
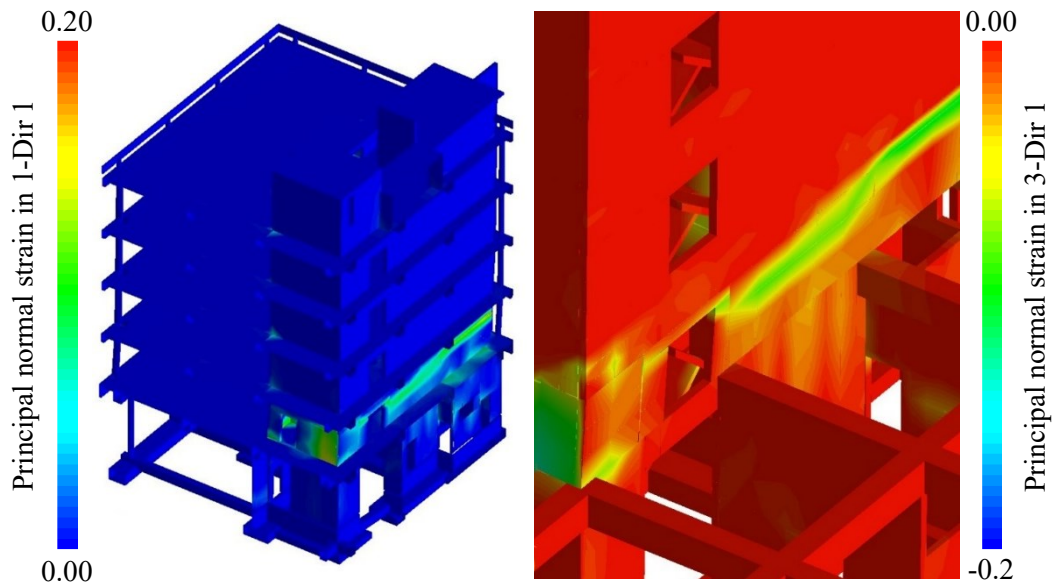
Figure 52. Buckling failure in the shear core of the building at approximately 7.00sec.

In the same area, it was also noticed a vertical misalignment in the RC walls (Figure 53).
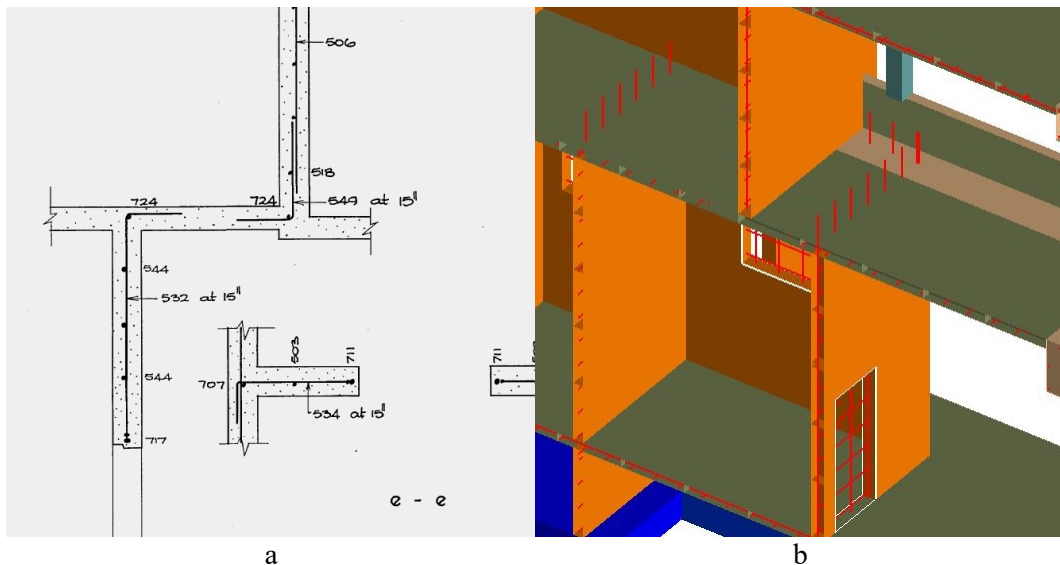
Figure 53. Vertical offset in the shear core wall, original drawings (a), and numerical model (b).

It was found that the vertical misalignment would lead to a principle of buckling failure in the shear core of the building, ultimately leading to the collapse of the building. Figure 54 shows a comparison between the analysis results and a south-west picture captured after the collapse of the PBC building.

<div align="center">a   b</div>
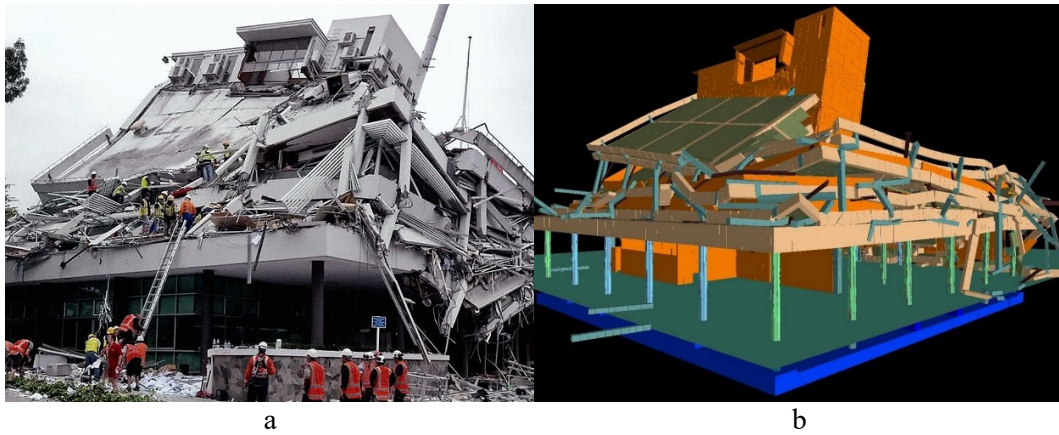
Figure 54. South-west picture of the Pyne Gould Building after the collapse, (a) and analysis results (b).

Findings

This research focused on the collapse analysis of the Pyne Gould Building, a RC office building in Christchurch, New Zealand, collapsed during the 6.3 magnitude earthquake occurred in 2011. The initial work involved the numerical reconstruction of the as-built condition of the building considering reinforcement details, steel elements and retrofitting systems. Non-linear dynamic analyses were carried out applying the signal recorder from the nearby Resthaven Home station (Beca Carter Hollings & Ferner Ltd 2011). It was observed how a vertical discontinuity in the east wall of the RC core could have determined the initiation of a buckling failure in the core of the building, ultimately leading to its collapse. The analysis was validated by comparing the resulting collapse shape with the actual debris distribution captured after the collapse of the building.

Further analyses on this case study are reported in the Chapter "*Collapse prevention and selective retrofit*.".

Chapter 6

The collapse of the main dome of the Basilica di Collemaggio in L'Aquila in April 2009

Part of the work described in this chapter has been previously published as COMPDYN 2023 Proceedings, 9th International Conference on Computational Methods in Structural Dynamics and Earthquake Engineering, edited by ECCOMAS PROCEEDIA: "*Damage Pattern Analysis of the Basilica di Collemaggio using AEM micro-modeling*", Cosimo Pellecchia, Alessandro Cardoni, Gian Paolo Cimellaro, Ahmed Amir Khalil.

Introduction

The 'Basilica Santa Maria di Collemaggio' is a world-known medieval church located in L'Aquila, Italy. The original structure was built in 1270 and then modified and renovated over the centuries. Despite previous retrofit interventions, the 2009 L'Aquila earthquake caused the partial collapse of the central vault and part of the transept.

Ancient masonry structures subject to seismic actions have been the objective of several studies (Tomazevic 1999), (Salonikios et al. 2003) (Belmouden and Lestuzzi 2009). Nevertheless, the reliable representation of structural behavior and damage propagation in ancient masonry buildings is still an open challenge in numerical modeling (Pasticier, Amadio, and Fragiacomo 2008).

Different methodologies, from simplified analytical procedures (Lang and Bachmann 2004), to more complex dynamic methods (Rota, Penna, and Magenes 2010), were developed to study the seismic vulnerability of existing masonry buildings. However, to limit computational resources, numerical models are often simplified or analyzed only in two dimensions (Cardoni and Cimellaro 2020). Nonetheless, many masonry structures have irregular layouts, resulting in complex three-dimensional behavior under seismic action. In addition, the structural system of historical and ancient masonry buildings is typically the result of centuries of transformations, overlay of different structures, technologies, materials, construction techniques, and retrofitting strategies (Croci 1998). As a consequence of that, the seismic assessment of so complex structural systems is often considering conservative assumptions, both in terms of numerical representation of the seismic

behavior and of the overall capacity of the structure (Pasticier, Amadio, and Fragiacomo 2008).

As an example, the actual in-plane stiffness of complex shells and domes may be neglected, while assumptions are made on the rigid or flexible behavior of composite wood and reinforced concrete (RC) slabs. The actual stiffnesses of connections such as masonry-beams connections or dowel-type connections of wooden structures are often conservatively assumed as pinned or rigid connections and local failure mechanisms such as pull-out phenomena and out-of-plane mechanisms are often neglected in the overall seismic assessment of the structure (Admane and Murnal 2017).

The use of simplified methodologies and models, or analyses limited to the two-dimensional behavior, can lead to underestimating the seismic performance of the structure, which in turn results in increasing the seismic retrofitting actions, critical in the case of architectural heritage (Khalil, Pellecchia, and Iuliis, n.d.).

This work focused on developing a high-refined numerical model of the Apse, Nave, and Transept of the 'Basilica di Collemaggio', using the Applied Element Method (AEM) approach. The AEM has advantages both in terms of reduction of computational effort (Grunwald et al. 2018), and accuracy of the results (Malomo, Pinho, and Penna 2020b). By considering a discrete micro-modeling approach it was possible to represent the actual behavior of each structural element, considering peculiar geometry arrangements, edge interlocks, the presence of transversal elements in the masonry, as well as different masonry patterns, deriving from the overlay of different construction techniques over the centuries.

In particular, the nave arches and columns, the choir and apse vaults, and the transept 'columns were detailed and reproduced considering the actual arrangement of the units. Next, non-linear dynamic analyses were performed employing the nearest record of the 2009 L'Aquila earthquake. Finally, the derived damage state was compared with the actual crack distribution observed after the earthquake. It was observed that the crack patterns derived from the numerical analysis were in overall accordance with the actual damaged state of the Basilica.

Numerical approaches

In structural analysis, Finite Element Method (FEM) is the most common methodology adopted in the seismic assessment of the structure. Nevertheless, analysis of existing masonry structures would require employing 3D FEM elements to account for typical damage mechanisms in masonry, such as rocking phenomenal, shear slinging, or diagonal cracking. However, this may lead to a prohibitive computational time when dealing with a comprehensive numerical model of an entire complex structure such as Basilica (Grunwald et al. 2018).

In addition, local collapse mechanisms, often among the primary sources of seismic damage for existing masonry structures, cannot be automatically accounted for in continuous numerical procedures. In fact, in FEM-based analysis, elements are connected at the nodes and two elements cannot displace independently. To reliably account for failure mechanisms, multiple node IDs need to be introduced

in the model, increasing computational resources and the risk of stress singularity at the node separation.

Furthermore, to account for crack propagations and subsequent effects on the overall stiffness of the structure, special techniques need to be introduced in the analysis, such as the "smeared cracks" (Cervera and Chiumenti 2006) or the "discrete crack" modeling (Carol Ignacio, Prat Pere C., and López Carlos M. 1997). However, both techniques require the assumption of locations and directions of cracks' propagation, which is not easily predictable in a complex 3D model of masonry structures.

Nevertheless, most of the research in existing masonry structures employed FEM seismic analysis (Ismail et al. 2009). However, the non-linear range behavior of the structure in a collapse simulation, considering damage propagation and local failures, is generally missing.

Thanks to the significant reduction of computational resources (Grunwald et al. 2018), advanced computational techniques, such as the Applied Element Method (AEM) (Tagel-Din and Meguro 2000), overcome these aspects by considering both in- and out-of-plane behavior of the masonry (Malomo, Pinho, and Penna 2020a), and including the dynamic properties of the entire masonry structure within the non-linear time-history analysis.

AEM numerical approach to modeling of masonry

The most convenient approach, in the AEM framework, to the analysis of the existing masonry structure, is a micro-modeling approach considering the combined properties of unit and mortar.
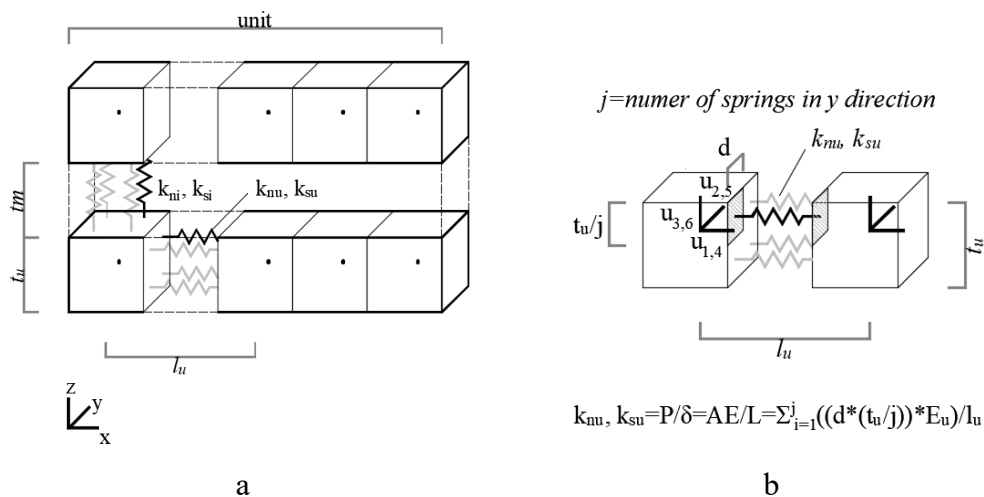
Figure 55. Springs employed in micro modeling of masonry (a) and stiffness of unit springs (b)

For springs connecting elements within the units, normal stiffness k_{nu} and shear stiffness k_{su} are determined according to (Equation 3).

$$k_{nu} = \frac{E_u \cdot d \cdot t_u/j}{l_u}$$

<div align="right">Equation 3</div>

$$k_{su} = \frac{G_u \cdot d \cdot t_u/j}{l_u}$$

Where E_u and G_u represent the Young and Shear modulus of the unit, t_u the height of the unit, l_u the distance between the element's centerline and t_u/j and d respectively the length of the pertinent area of one spring in y and z directions, as per coordinate system reported in Figure 55. The unit behavior and cracks developing within units are defined using those springs. The behavior of the combined unit and interface mortar is represented using equivalent spring properties derived from the spring in-series formulation (Figure 56).

$$\Delta=\Delta_u+\Delta_m > \Delta=P/k=P/k_u+P/k_m > 1/k=1/k_u + 1/k_m > k_i=(1/k_u + 1/k_m)^{-1}$$
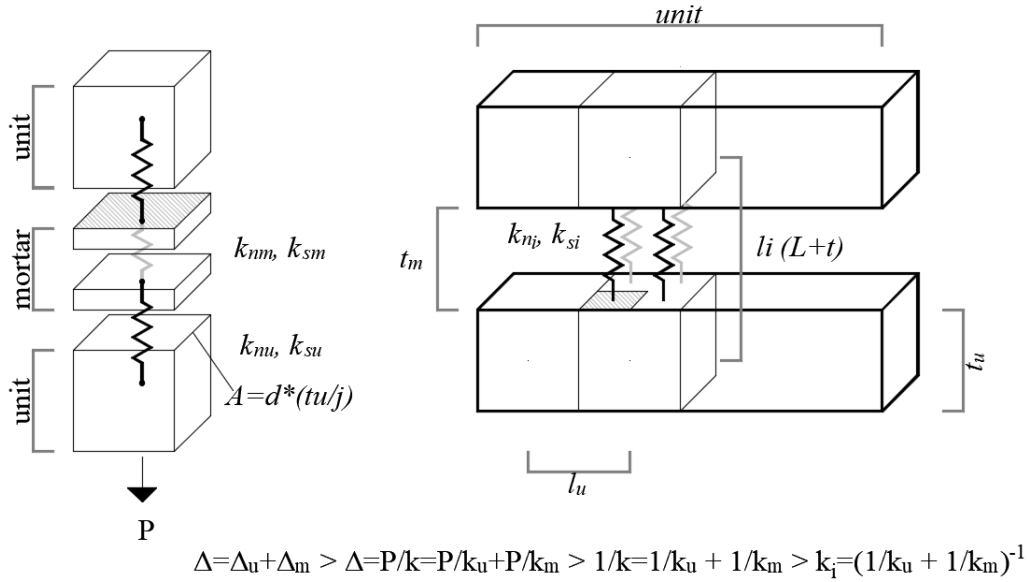
Figure 56. Equivalent springs representing unit-mortar interaction.

The equivalent stiffness of the springs connecting two different units, respectively normal equivalent stiffness k_{ni}, and shear equivalent stiffness k_{si}, are derived as follows (Equation 4).

$$\frac{1}{k_{ni}} = \frac{l_i - t_m}{E_u \cdot d \cdot l_u/j} + \frac{t_m}{E_m \cdot d \cdot l_u/j};$$

<div align="right">Equation 4</div>

$$\frac{1}{k_{si}} = \frac{l_i - t_m}{G_u \cdot d \cdot l_u/j} + \frac{t_m}{G_m \cdot d \cdot l_u/j}$$

Determining the stiffness of both unit and equivalent springs, the stiffness matrix for each set of springs is assembled formulating the geometrical relations between the centroid of each element and the contact point of the spring on the element surface.

Numerical model

The AEM numerical model of the Apse, Transept, and Nave was developed based on a laser scanner survey (Figure 57).
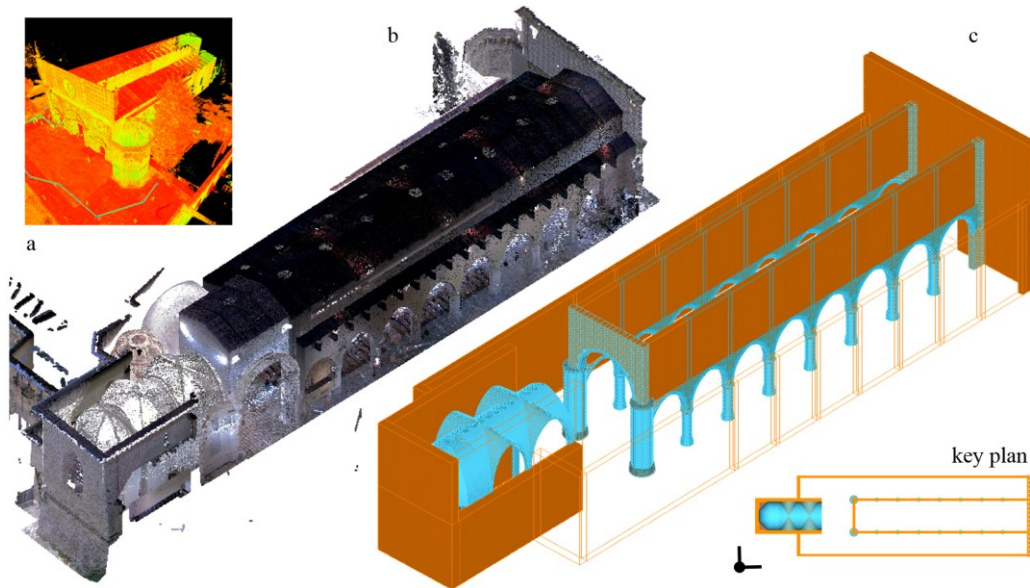
Figure 57. Laser scanner survey of the Basilica (a), processed point cloud (b), and developed numerical model (c).

The nave's columns and arches were modeled following the specific layout derived from the laser scanner survey, including the unit's arrangement and dimensions (Figure 58).
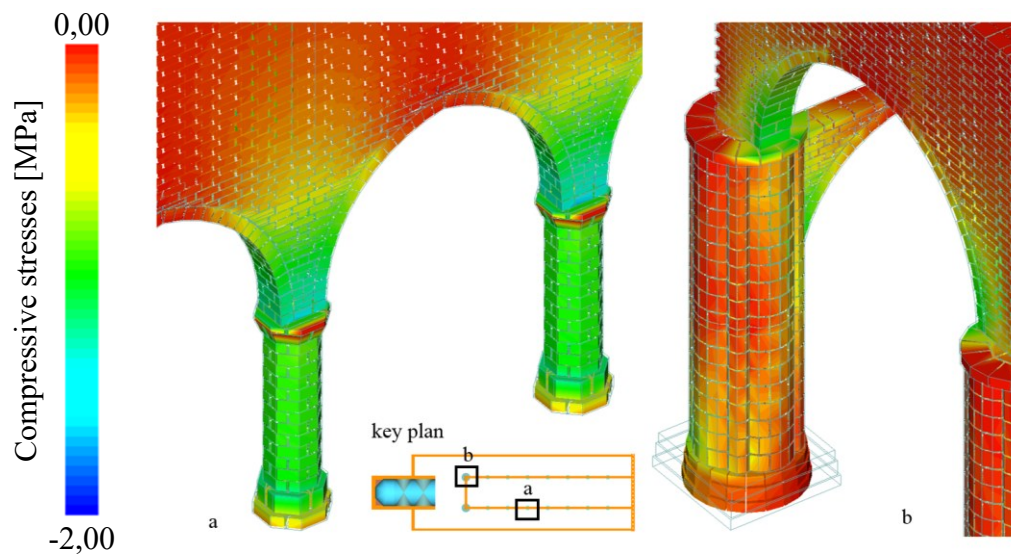
Figure 58. Distribution of compressive stresses in nave's (a) and transept (b) columns, dead load only.

The choir and apse vaults were also reproduced based on the processed point cloud and considering the actual arrangement of units (Figure 59).
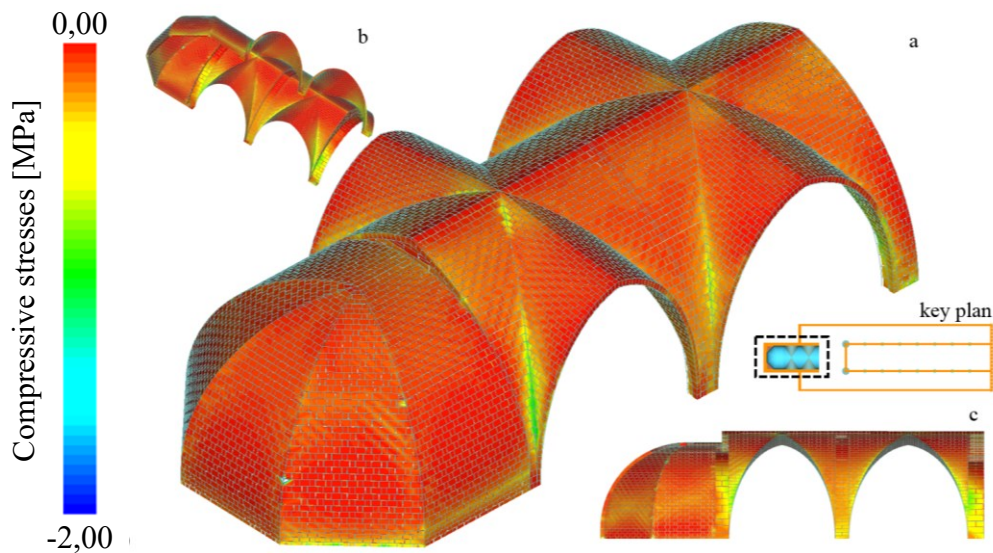
Figure 59. Distribution of compressive stresses in nave's (a) and transept (b) columns, dead load only.

The final numerical model consists of more than 130.000 units and 13.000.000 equivalent springs (5 per element face); non-linear time-history analysis performed the output of one second in approximately 1hour, using a 3.5GHz 6cores and 12threads processor and approximately 42Gb of RAM.

Material models

Two different masonry patterns were considered in the numerical model; the nave walls had one interlock unit for every two longitudinal units and the façade wall had inner voids and interlock units between the two-unit layers (Figure 60).
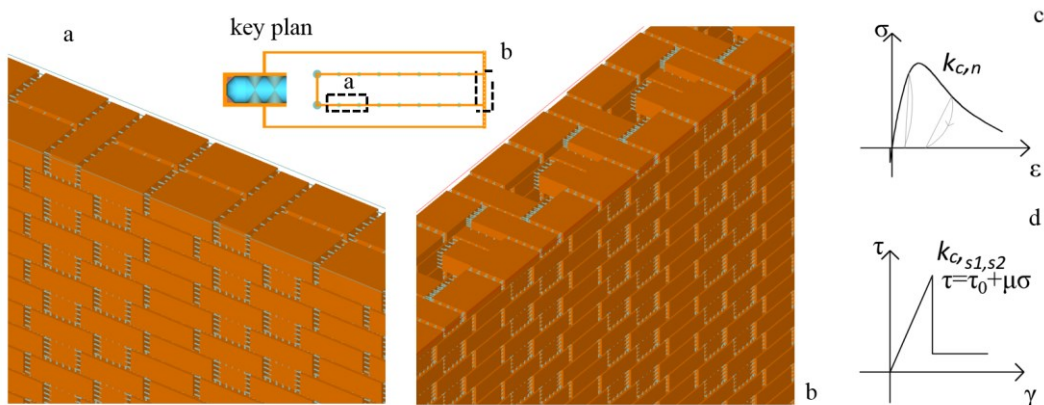
Figure 60. Masonry patterns are considered in the nave walls (a) and in the façade wall (b) and related material models for axial (c) and shear (d) stresses.

The Maekawa & Okamura model (Maekawa and Okamura 1983) is assumed to represent the axial behavior of the masonry subject to normal stresses (Figure 60, c), while the Mohr-Coulomb friction model is implemented for equivalent springs subject to shear (Figure 60, d).

Table 8 shows the assumed material properties for masonry.

Table 8. Material properties of masonry (*Italian Technical Standards Circolare C.S.LL.PP., 21/01/2019, n.7* 2019)

fc [MPa]	τ_0 [MPa]	E [MPa]	G [MPa]	w [kg/m^3]
2.0	0.035	1230	410	2000

Non-linear dynamic analysis and damage pattern assessment

Non-linear dynamic analyses were carried out considering the nearest time history record of the 2009 L'Aquila Earthquake, L_Aquila IT-2009-0009 Station AQK, Data from ESM Database (Russo et al. 2022), Figure 61.
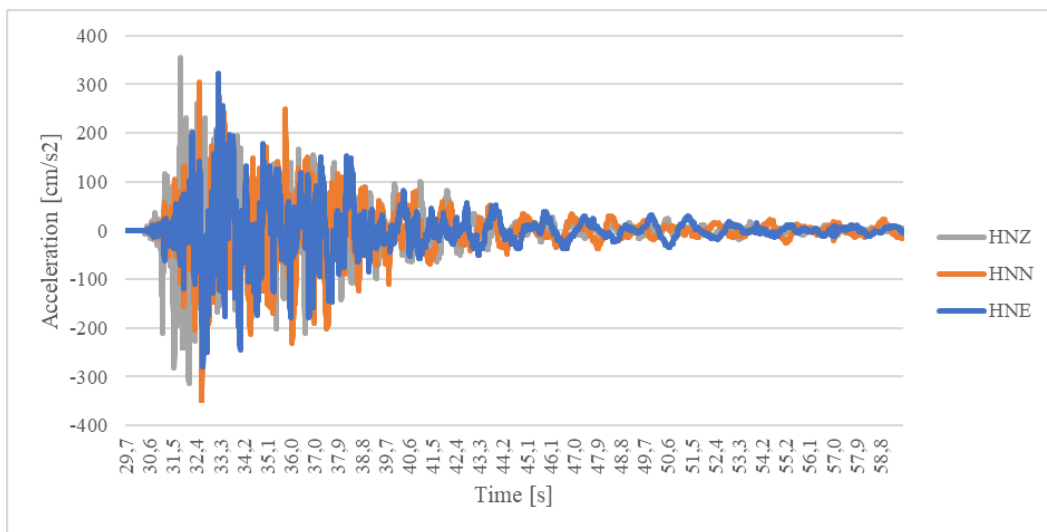
Figure 61. Ground motion at the nearest gauge to the Basilica di Collemaggio. Data from (Russo et al. 2022).

A comparison between the crack pattern derived from the numerical analysis and the actual distribution of cracks observed after the 2009 L'Aquila earthquake is depicted in Figure 62. It was observed that a principal strain of 0.02 is a good criterion for identifying cracks in the masonry structure.
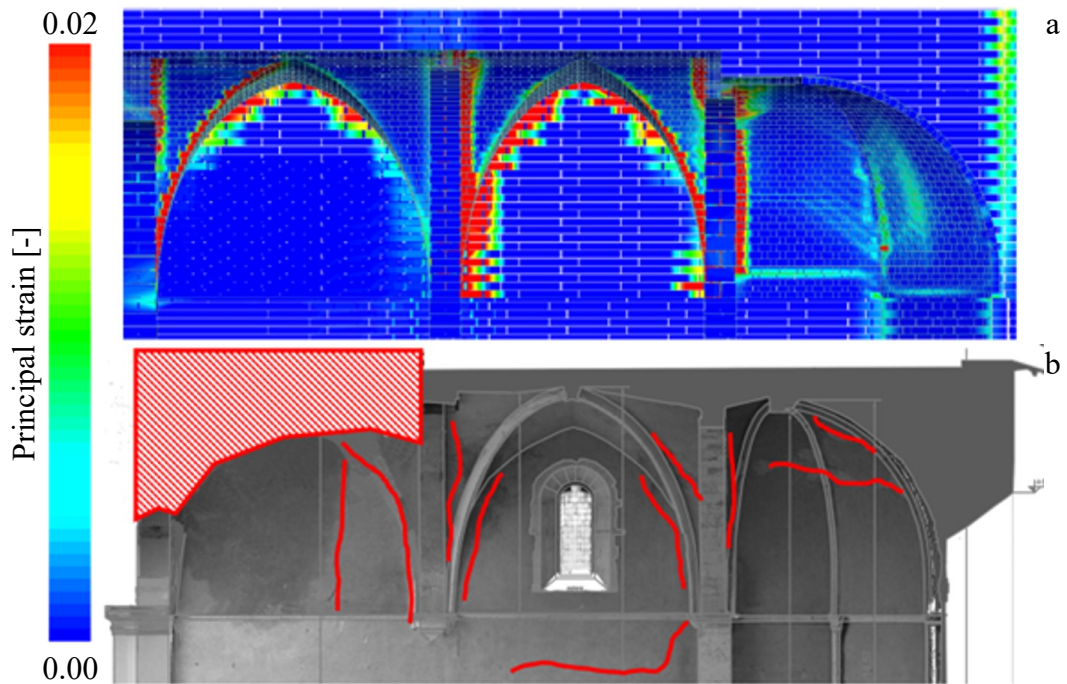
Figure 62. Comparison between the analysis results (a) and actual distribution of cracks observed after the 2009 L'Aquila earthquake (b); orthophoto reproduced with permission from Tracciatori srl (2021).

The analysis results showed good accordance with the actual damage state observed after the shock, except for the collapse of the first of the choir's vault (Figure 63).
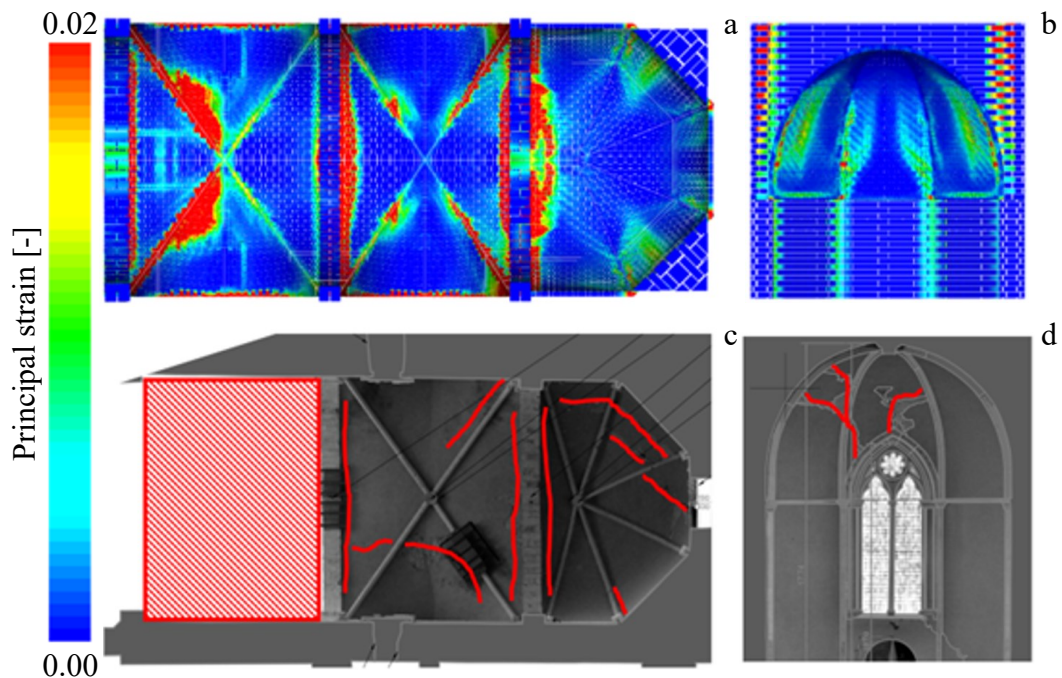
Figure 63. Comparison between the analysis results (bottom view, a, and side view, b) and actual distribution of cracks observed after the 2009 L'Aquila earthquake (bottom view, c, and side view, d); orthophoto reproduced with permission from Tracciatori srl (2021).

However, it is worth noticing that the numerical model did not include the collapsed portion of the transept, which could have induced the subsequent collapse of the choir's vault.
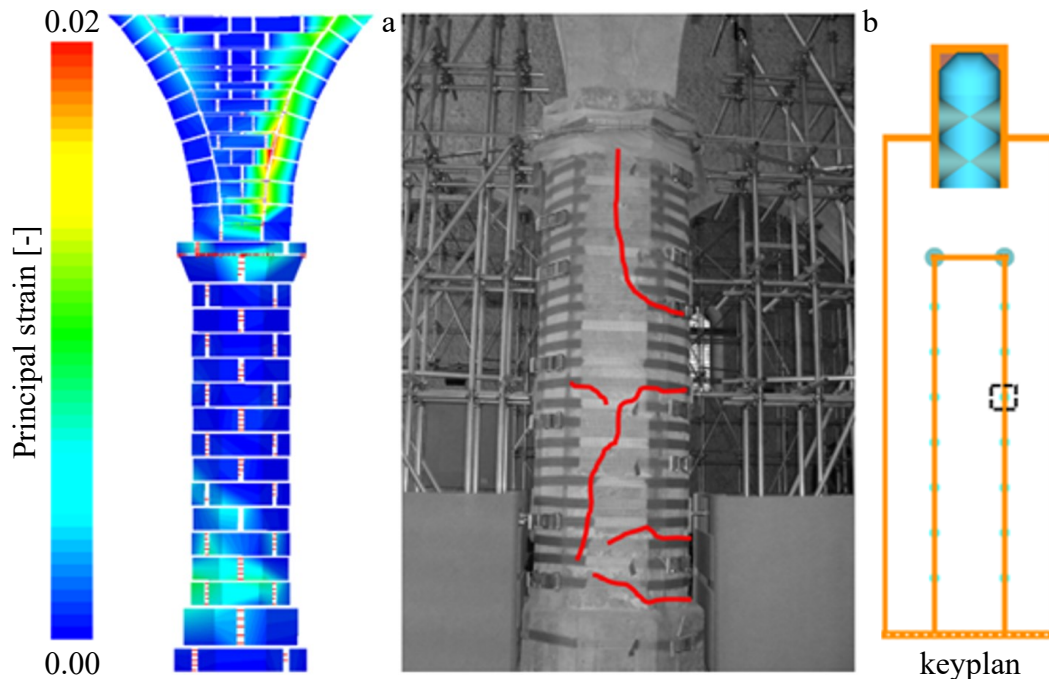
Figure 64. Comparison between the analysis results (a) and actual distribution of cracks observed after the 2009 L'Aquila earthquake (b) in one of the nave's columns.

Finally, a good accordance between the actual damage and the analysis results was also found in observing the springs in a crack state (Figure 64, a, red color) resulting from the analysis in comparison with the actual cracks in one of the nave's column (Figure 64, b).

Findings

Ancient masonry buildings, such as the Basilica Santa Maria di Collemaggio in L'Aquila, are complex structural systems, deriving from centuries of transformation and overlapping of different construction techniques. In seismic retrofit of these monumental buildings, the designer must strike a balance between the effectiveness of the retrofitting actions and the preservation of the architectural heritage. However, the assessment of the seismic performance of so complex structural system is often challenging and the use of simplified procedures and numerical methodologies can lead to the overestimation of the retrofitting strategies.

While prohibitive in the past, a high-refined numerical model of entire monumental buildings is nowadays possible thanks to the advances in computational performance and the development of new computational methodologies. Among others, the Applied Element Method, AEM, has shown promising results in representing the seismic behavior of ancient masonry structures, while accounting for different masonry patterns, complex arrangements

of masonry such as vaults and domes, and peculiar structural details. Automating cracks developments and damage propagation, the methodology can accurately account for local damage prevention and provide a reliable representation of the overall seismic performance of the structure.

In this work, a numerical model of the Basilica di Collemaggio was developed and analyzed using the AEM micro-modeling technique that includes accurate geometry representation based on laser scanning as well as material properties for masonry blocks and mortar joints. Non-linear dynamic analysis carried out using one of the nearest recorded time histories has shown an overall damage state comparable with what was observed after the strike of the 2009 L'Aquila earthquake.

Chapter 7

Collapse prevention and selective retrofit.

Part of the work described in this chapter was presented at EMI 2023, Engineering Mechanics Institute International Conference 2023: "*Seismic-collapse selective retrofitting using the Applied Element Method*", Cosimo Pellecchia, Alessandro Cardoni, Gian Paolo Cimellaro, Ahmed Amir Khalil, Emiliano De Iuliis.

Introduction

The basic idea behind the selective retrofit for collapse prevention is to identify a key element whose failure could lead to the disproportionate collapse of the structure. If identified, the specific element can either be weakened or strengthened to prevent the collapse of the structure. A somewhat similar approach was initially presented at the 14th WCEE by Kam & Pampanin (2008), by testing the effect of a counter-intuitive selective weakening technique to prevent brittle failure mechanisms.

One of the main advantages of selective retrofit is the capability to prevent the collapse of a certain structure with very limited economic resources, which could result in an efficient approach when dealing with the seismic retrofit of large seismic areas.

Among the four collapse cases presented in the previous chapters, the research particularly focused on the selective retrofit of the two RC buildings, the Champlain Towers Condo, a residential building, and the Pyne Gould Building, PBC, an office building; in fact, the two cases were considered to be largely representative of generic RC residential and office buildings; on other hands, infrastructures such as the Polcevera Viaduct and heritage structures such as the Basilica di Collemaggio were considered to be generally characterized from specific singularities, whose collapse would be mostly depending on the peculiar structural system, or the different construction techniques.

In fact, in the case of the Polcevera Viaduct, analyses shown how the strengthening of the strands would have been crucial in preventing the collapse of the viaduct. In addition, it was also highlighted how the installation of transversal ribs in the deck, would have provided additional torsional capacity in the case of strand loss.

With reference to the Basilica di Collemaggio, although the analyses focused mostly on damage representation, it was noticed how the different stiffnesses of the two parts of the structure, the nave, and the transept, would induce a concentration of stresses at the intersection with the main dome.

Thus, a peculiar retrofitting strategy would have been developed to reduce the stress concentration and avoid the collapse.

Because of that, the work was mostly focused on the selective retrofit of the two considered RC structures, the Champlain Towers South, and the Pyne Gould Building. Non-linear dynamic analyses were employed to test the response of the buildings both with the same load which determined the actual collapse, and with an exceptional seismic load that occurred at the moment the analysis presented in this chapter were carried out, the magnitude-7.8 Turkey earthquake occurred in February 2023 at the border between Turkey and Syria, which caused widespread damage in an area of about 350.000 km^2, Figure 65.
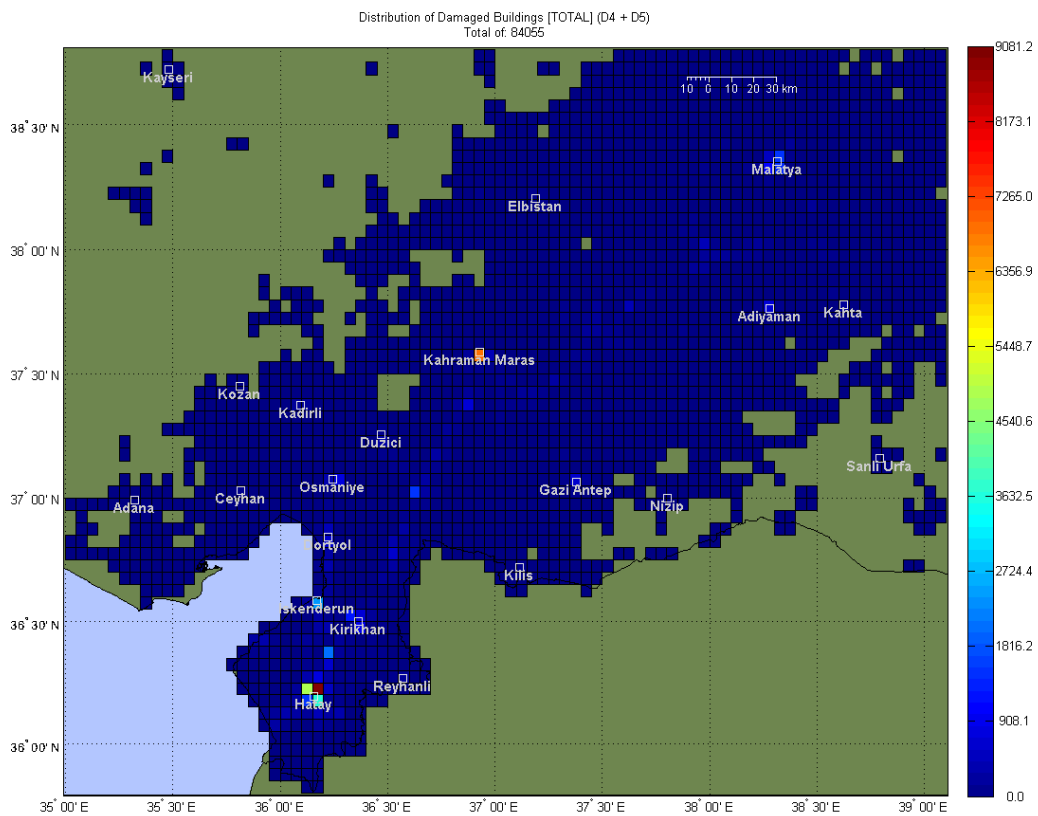
Figure 65. Distribution of Collapsed, to be immediately demolished and heavily damaged buildings (Hancılar et al. 2023).

More than 160,000 buildings collapsed during the event; although most of the collapsed buildings were of poor construction quality and built with no reference to the current seismic standards, also several newly constructed buildings stroke to the ground, (Hancılar et al. 2023). The time history record from the station near Kahramanmaras, Pazarck, Turkey, Station code 4615 (AFAD - Disaster And

Emergency Management Presidency 2023), was employed in the presented analyses (Figure 66).
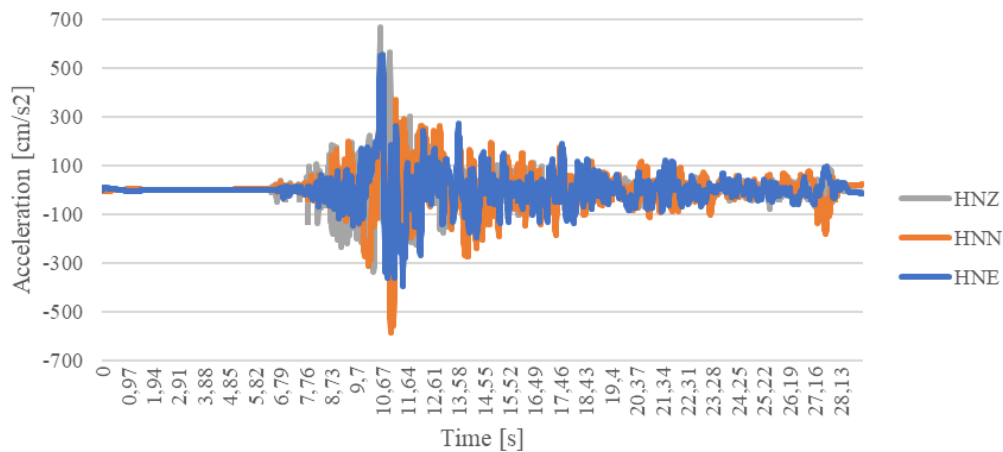
Figure 66. Recorded time-history of the February 2023 Turkey event, Kahramanmaras, Pazarck, Turkey, Station code 4615 (AFAD - Disaster And Emergency Management Presidency 2023)

The analysis results are discussed in the following chapters.

The selective retrofit of the Champlain Tower South residential building

Concerning the collapse of the Champlain Towers Condo, it was noted previously how the presence of high-depth beams at the pool deck level could have led to the instability of the perimeter columns and ultimately caused the disproportionate collapse of the building.

Thus, the first alternative scenario for collapse retrofitting assessment was to remove the deep beams connecting the slab to the perimeter columns (Figure 67, a, b).

In fact, as briefly explained earlier, the three deep beams were provided in the design as "slab drop", to cover the different elevations at the pool deck area. The slab reinforcement in this area was the same as the surrounding spans, having similar span lengths and loads but with no provision of deep beams. Therefore, the scenario only pertains to the removal of the "slab drops" and related differences in elevation, without modifications to the original design of the slabs.

In this configuration, even when assuming high degradation of the pool deck slab, perimeter beams, and columns, the failure of the slab did not affect the rest of the structure (Figure 67, c). Because the slab has a substantially smaller depth compared to one of the deep beams, the bending moment induced to the column - beams connection is considerably smaller. Therefore, when the slab fails, punching shear failure occurs and the slab detaches from the perimeter columns without compromising their load-bearing capacity (Figure 67, d).

a: Original design   b: Revised design

c: Revised design, analysis results
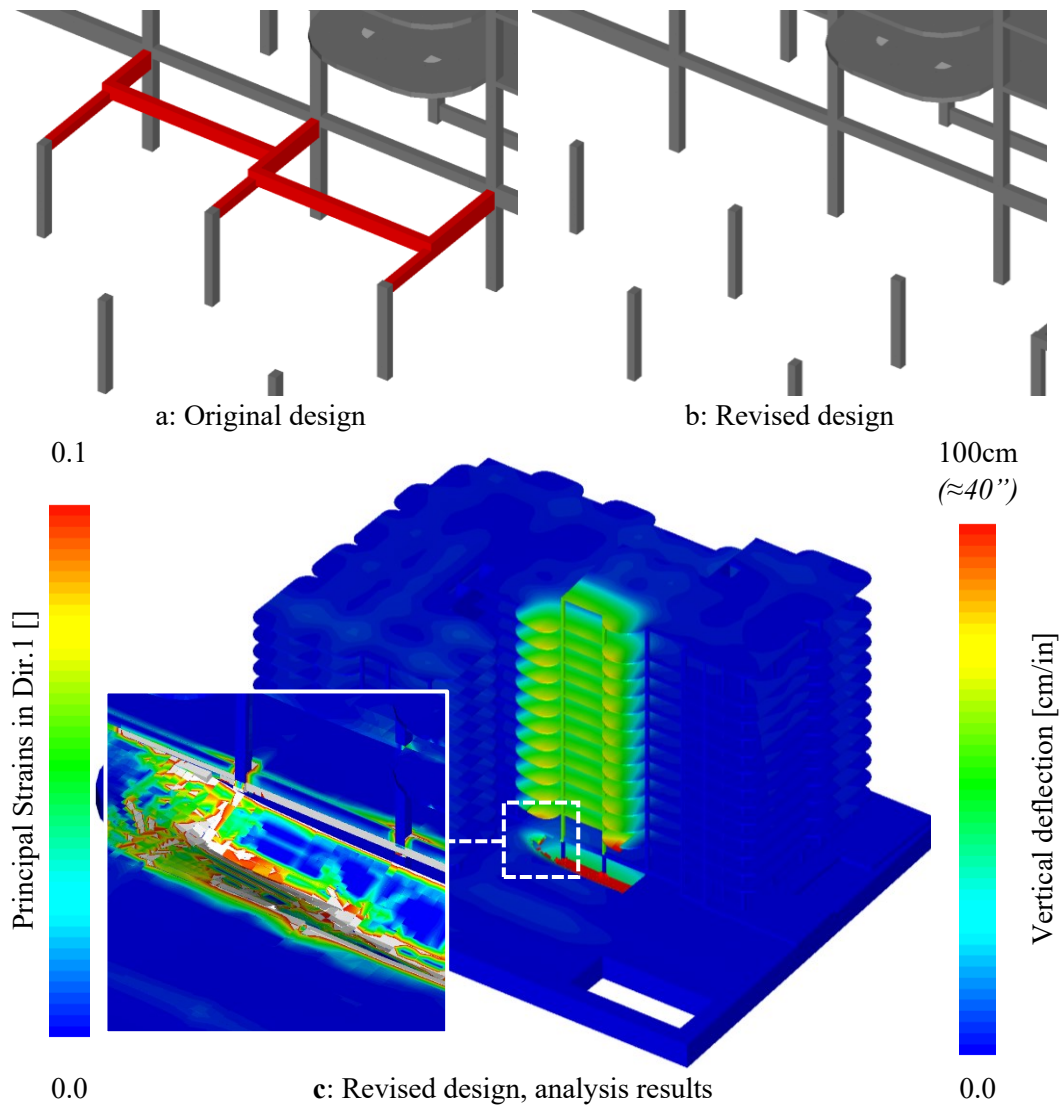
Figure 67. Original design (a), and alternative scenario (b), assuming the absence of beams connecting perpendicularly the pool deck to the perimeter column of the structure, Analysis results, Vertical displacement (c) [cm (in)], and Principal strains at slab failure (d) [-]

In terms of progressive collapse design, it is clear how the structural separation between the main twelve-story building and the secondary structure (i.e., one-story basement), could be an effective strategy in avoiding collapse propagation, especially when the secondary structure is naturally subject to deterioration (e.g., terraces, pool decks, etc.).

The second alternative design scenario considers the introduction of additional shear walls in the East core of the building (Figure 69, a). The objective is to reduce the torsional behavior observed during the collapse of the eastern wing of the building and avoid its failure (Figure 68, b, c).

In fact, the reason why, after the collapse of the central portion of the building, the collapse propagated to the eastern wing only, is related to the different torsional stiffness resulting from the structural layout. While the West core of the building consisted of RC shear walls oriented both in the North-South and East-West directions, the East RC core of the structure was composed of only one shear wall oriented in the North-South direction. Therefore, the torsional capacity of the

western core was significantly larger than the one of the eastern core. When the central block of the building starts failing, it was observed that slabs were detaching from the western and eastern wings at the interface of the shear wall. Afterward, the eastern wing fails, due to the lack of torsional capacity.

a: Original core

b. As-built results

c: Original design, Plan
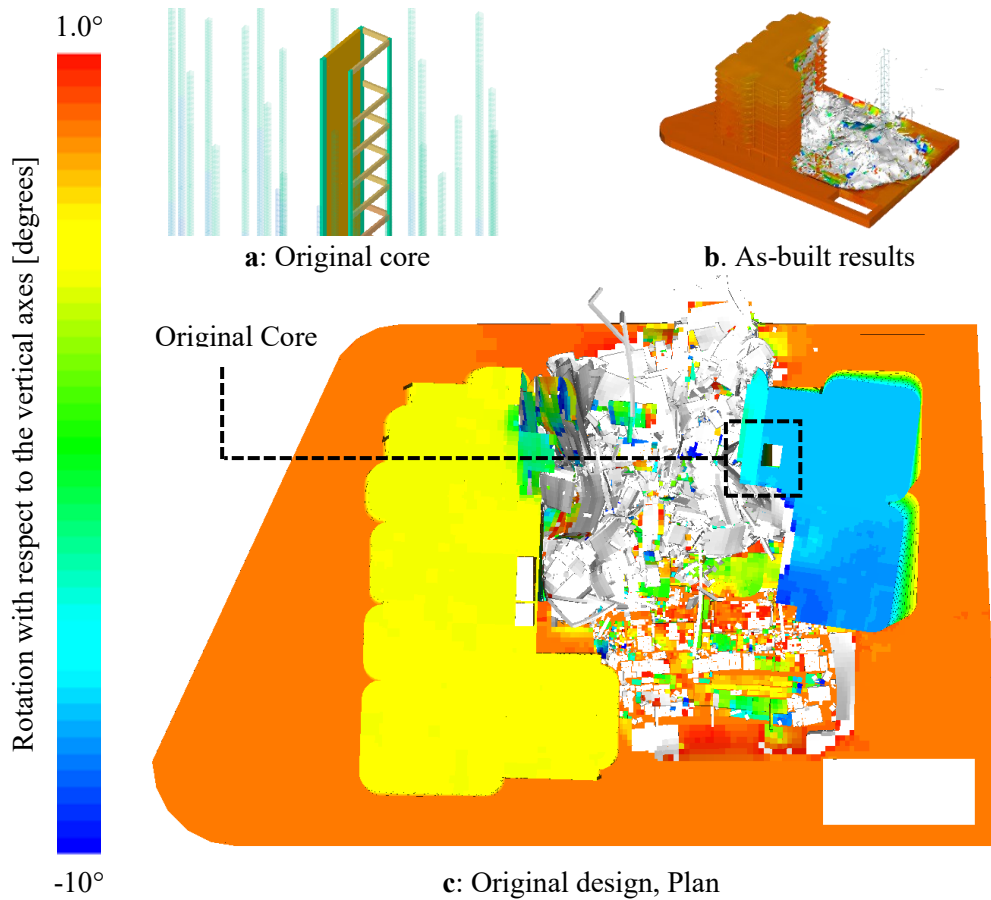
Figure 68. Original design of the easter core (a), results of the collapse analysis in the as-built configuration (b) and torsional behavior of the eastern portion of the building observed during the collapse (c).

Considering that, two additional shear walls were introduced in the East-West direction (Figure 69, a). Results show that the two small additional shear walls are effective in avoiding the collapse of the eastern wing (Figure 69, b, c). The difference in terms of rotation observed both in the original model and in the new design configuration can be evaluated comparing Figure 68, (c) and Figure 69, (c).

a: Retrofitted core   **b**. Retrofitted results

Rotation with respect to the vertical axes [degrees]

1.0°

-10°

Revised Core

c: Results in the retrofitted configuration, Plan
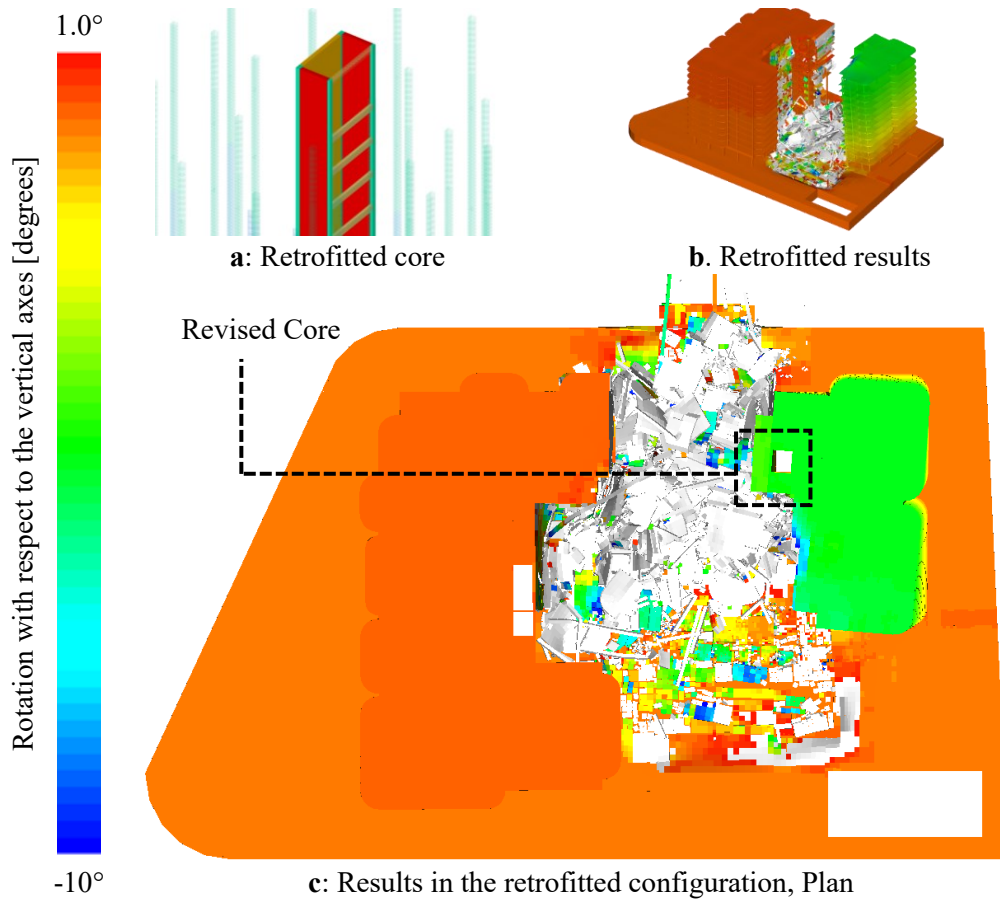
Figure 69. Retrofitted design of the easter shear core (a), 3D (b), and plan view (c) of the analysis results in the retrofitted configuration.

In terms of progressive collapse design, these results highlighted that providing RC cores with enough torsional capacity can be effective in preventing collapse propagation between different parts of the structure.

To assess the effect of retrofitting strategies, non-linear dynamic analyses were also carried out employing the February 2023 Turkey earthquake. Analysis results considering the as-built configuration of the structure, shown a catastrophic failure of the building (Figure 70).
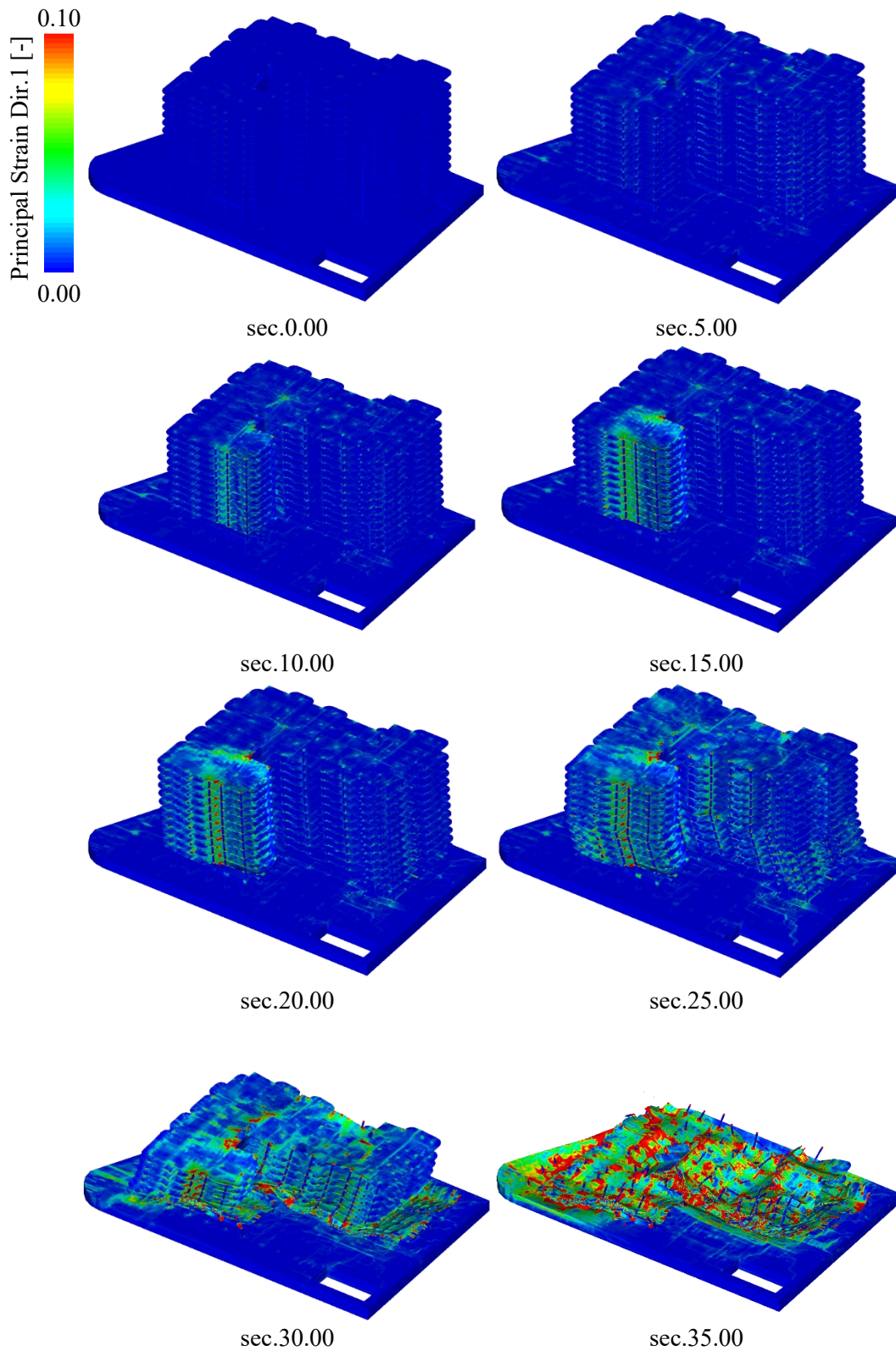
Figure 70. Champlain Towers, as-built, Time history analysis, February 2023 Turkey record, Principal strain.

It was observed hot the lack of shear walls oriented east-west would induce an evident torsional behavior in the structure, ultimately leading to its collapse (Figure 71).
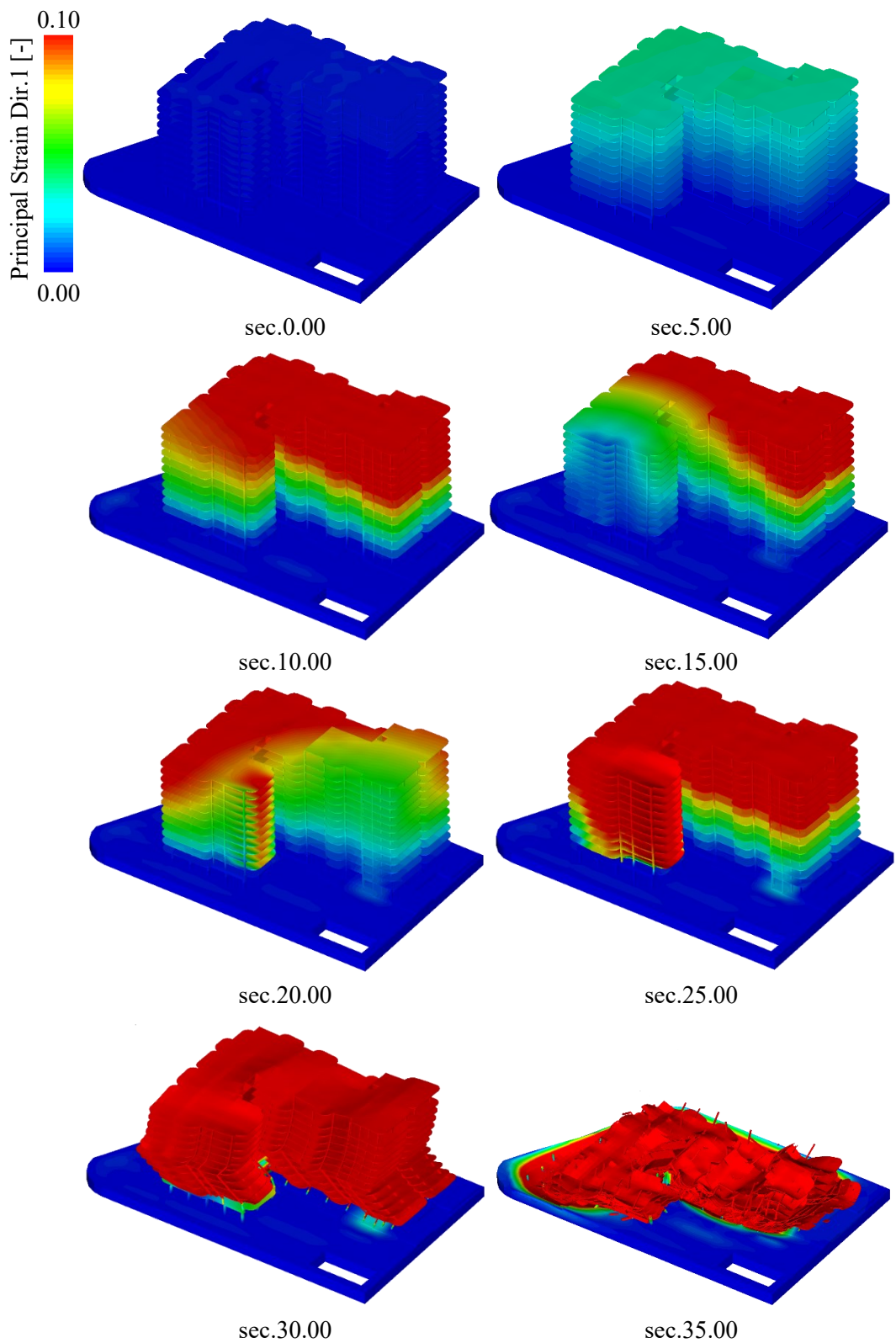
Figure 71. Champlain Towers, as-built, Time history analysis, Turkey record, Total displacement.

Figure 72 shows a comparison between the as built and the retrofitted configuration considered in the analyses. The retrofitting strategy consisted in adding limited portion of RC walls connected to the existing core of the building.
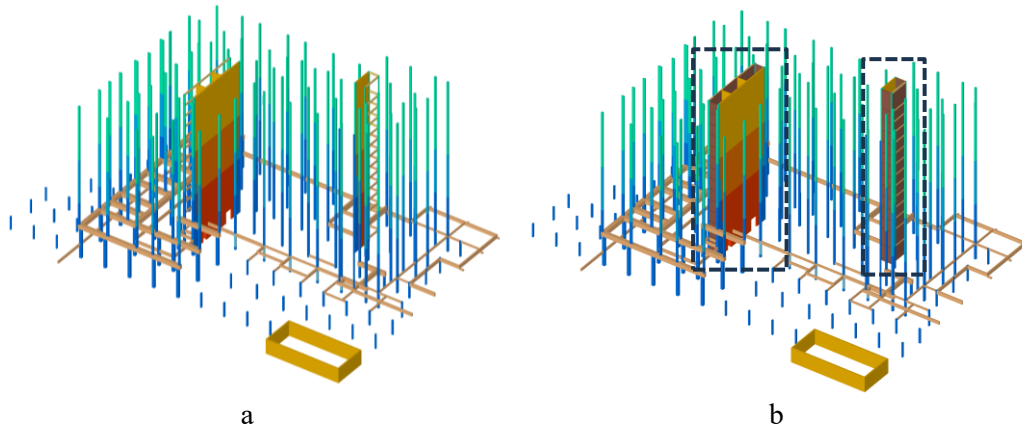
Figure 72. As-built (a) and retrofitted (b) configuration.

Consistently, the same amount of reinforcement and the same structural details were included in the additional RC walls. The analysis results are shown in Figure 73.
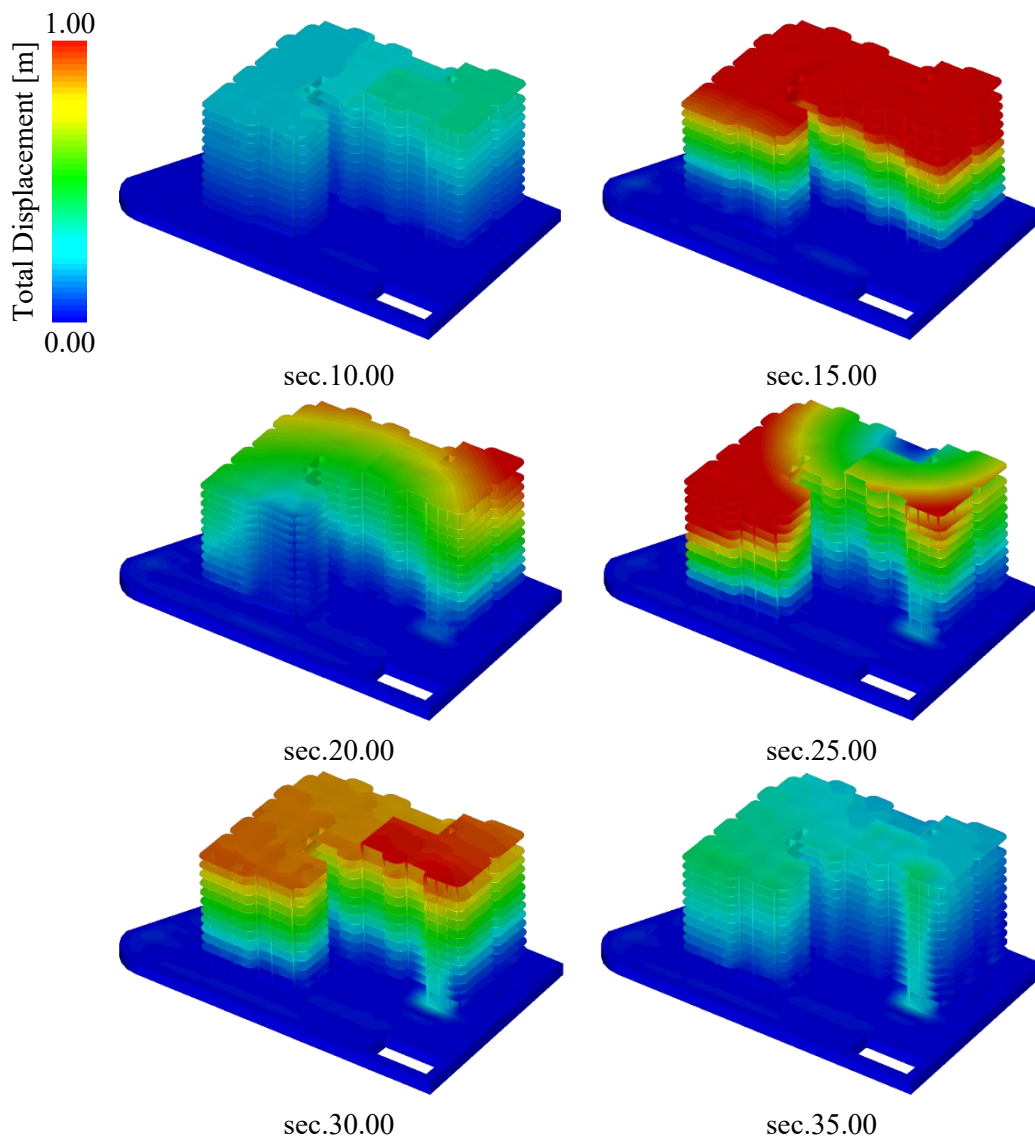
Figure 73. Champlain Towers, as-built, Time history analysis, Turkey record, Total displacement, retrofitted configuration.

Comparing Figure 71 and Figure 73 it can be clearly observed how the retrofitting strategy was effective in reducing the torsional behavior of the building and consequently avoid its collapse. Figure 74 also shown a direct comparison of the damage distribution in the shear core of the building in the as built (a) and retrofitted configuration (b).
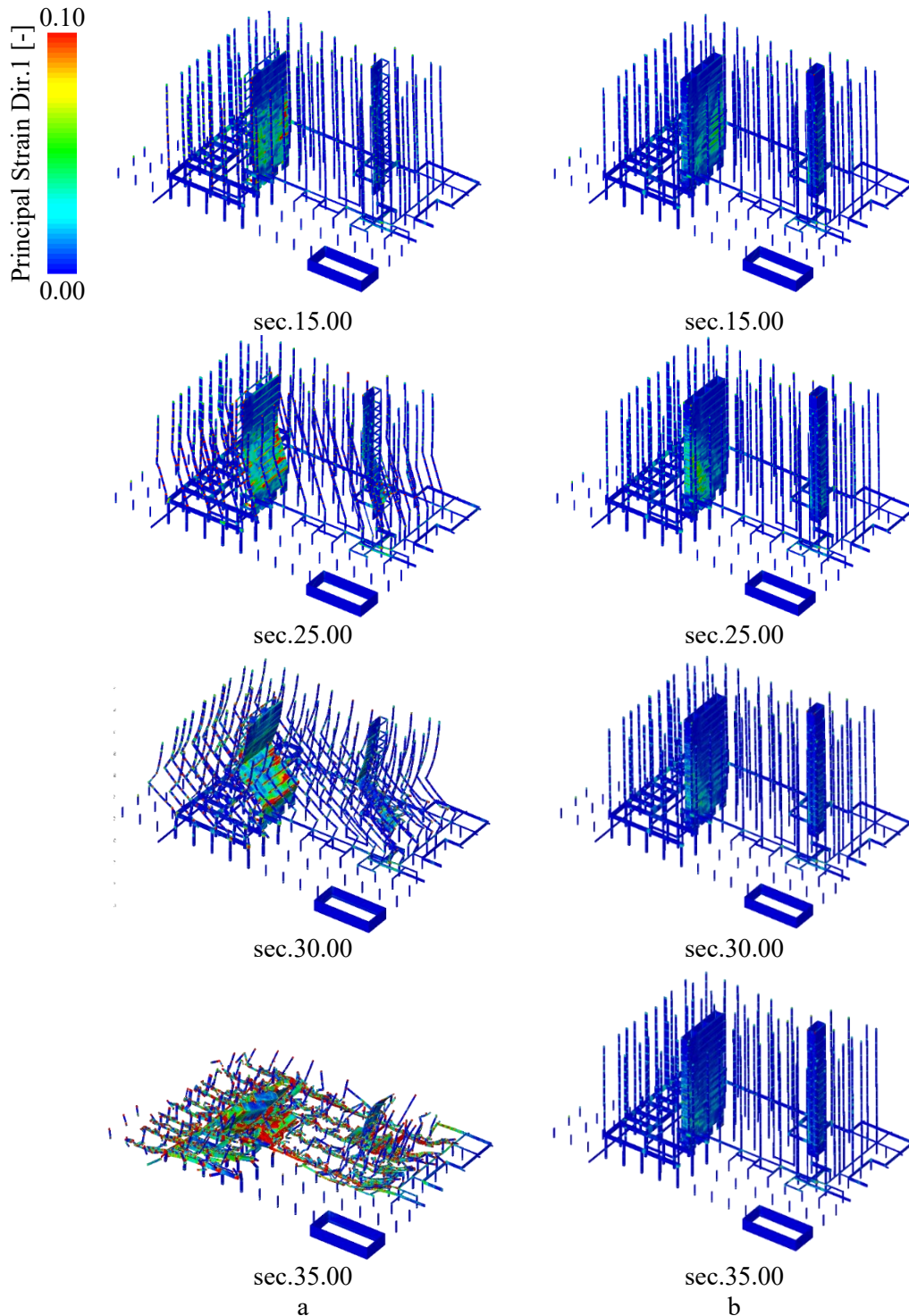
Figure 74. Comparison between as-built (a) and retrofitted configuration (b).

As it ca be observed the retrofitting strategy was effective in preventing the collapse of the building.

The selective retrofitting of the Pyne Gould Building

It was discussed in the previous chapter how it was found that a vertical misalignment in the shear core of the Pyne Gould Building could have led to a principle of buckling failure in the east wall of the core (Figure 75).
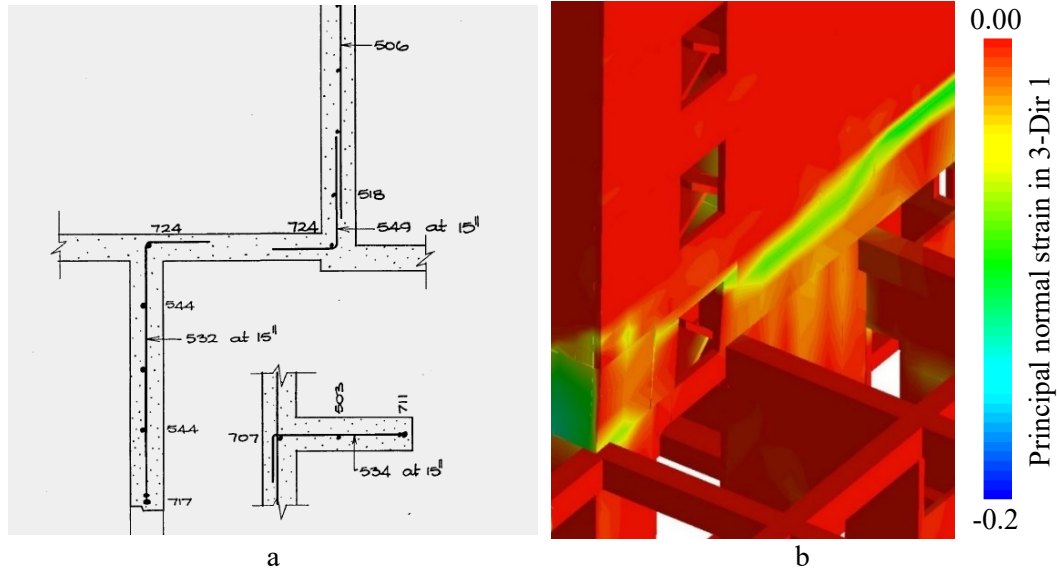
Figure 75. Vertical misalignment in the east portion of the Pyne Gould Building's shear core (a) and resultant distribution of compressive stresses in the non-linear dynamic analysis (b).

As observed, the initial failure would ultimately lead to the collapse of the structure (Figure 76).
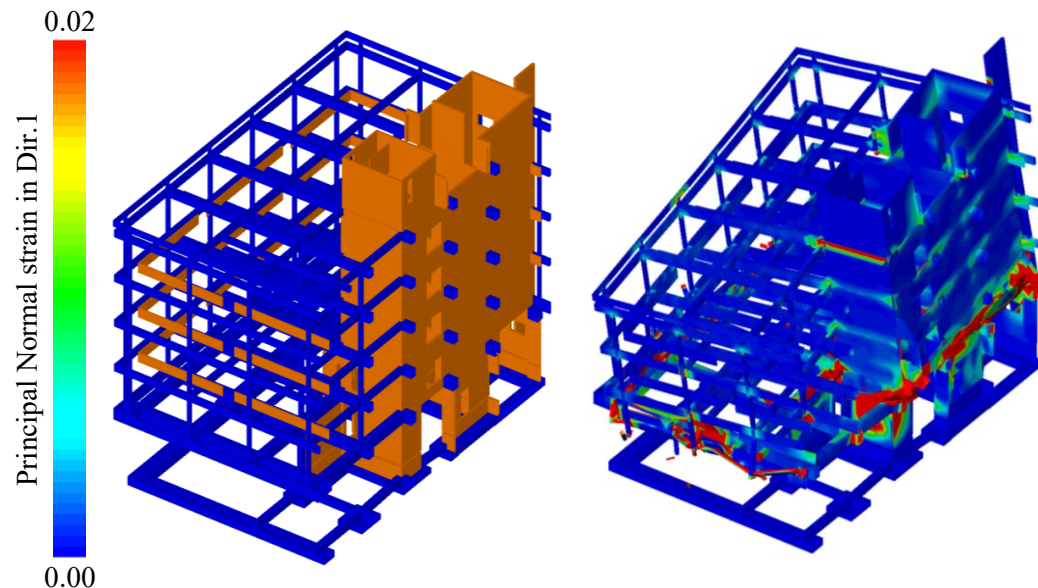
Figure 76. Pyne Gould Building, PBC, detected failure mechanism.

The adopted retrofitting strategies considered the introduction of ad additional RC wall to restore the vertical alignment in the east wall of the core. Consistently with the rest to the existing core, the same amount of reinforcement and the same

structural details were used in the additional wall in the retrofitted configuration (Figure 77).
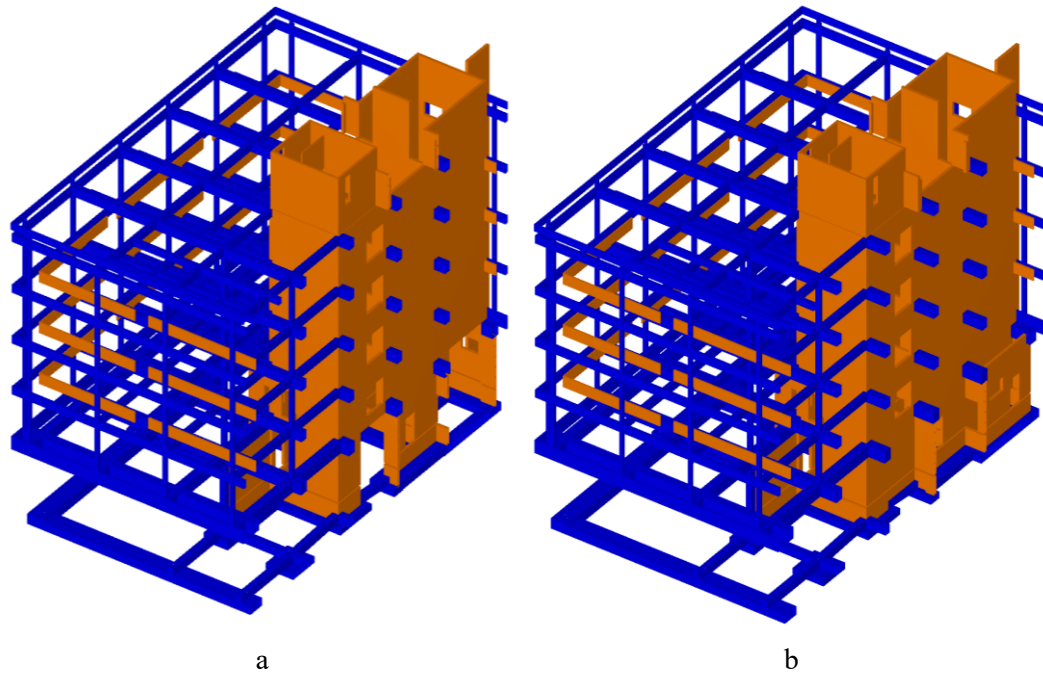
Figure 77. Pyne Gould Building, as-built (a) and retrofitted (b) configuration.

After defining a retrofitted strategy, the structure undergoes to the same time-history record which determined it's collapse during the February 2011 New Zealand earthquake. The analysis results shown that the correction of the vertical misalignment in the east wall of the core would have been effective in preventing the collapse of the structure (Figure 78).
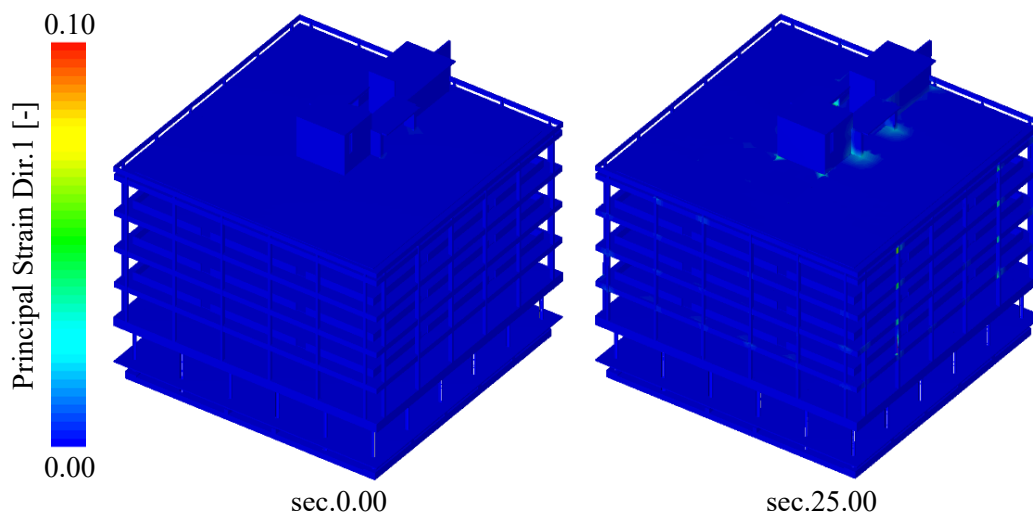
Figure 78. Non-linear time history analysis results employing the February 2011 New Zealand earthquake record.

The analysis in the as-built configuration was also carried out employing the February 2023 Turkey event. Results highlighted how the collapse would originate

and propagate from the same buckling failure observed using the 2011 New Zealand earthquake (Figure 79).
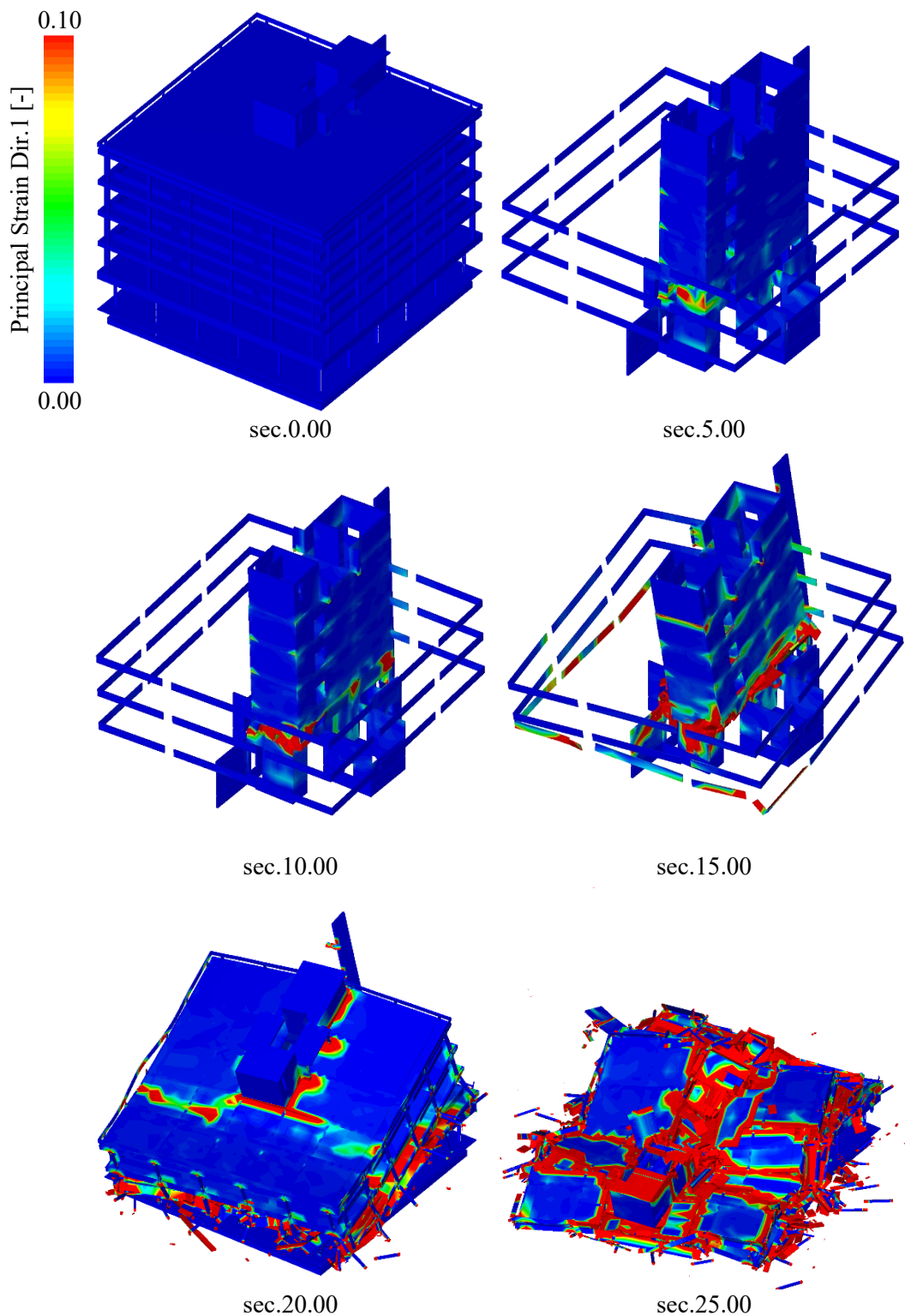
Figure 79. Pyne Gould Building, PBC, as-built configuration, non-linear dynamic analysis results employing the February 2023 Turkey record.

However, it was also observed that, when considering the retrofitted configuration, the buckling failure in the shear core did not occur and the building was able to withstand the February 2023 Turkey record with limited damage.
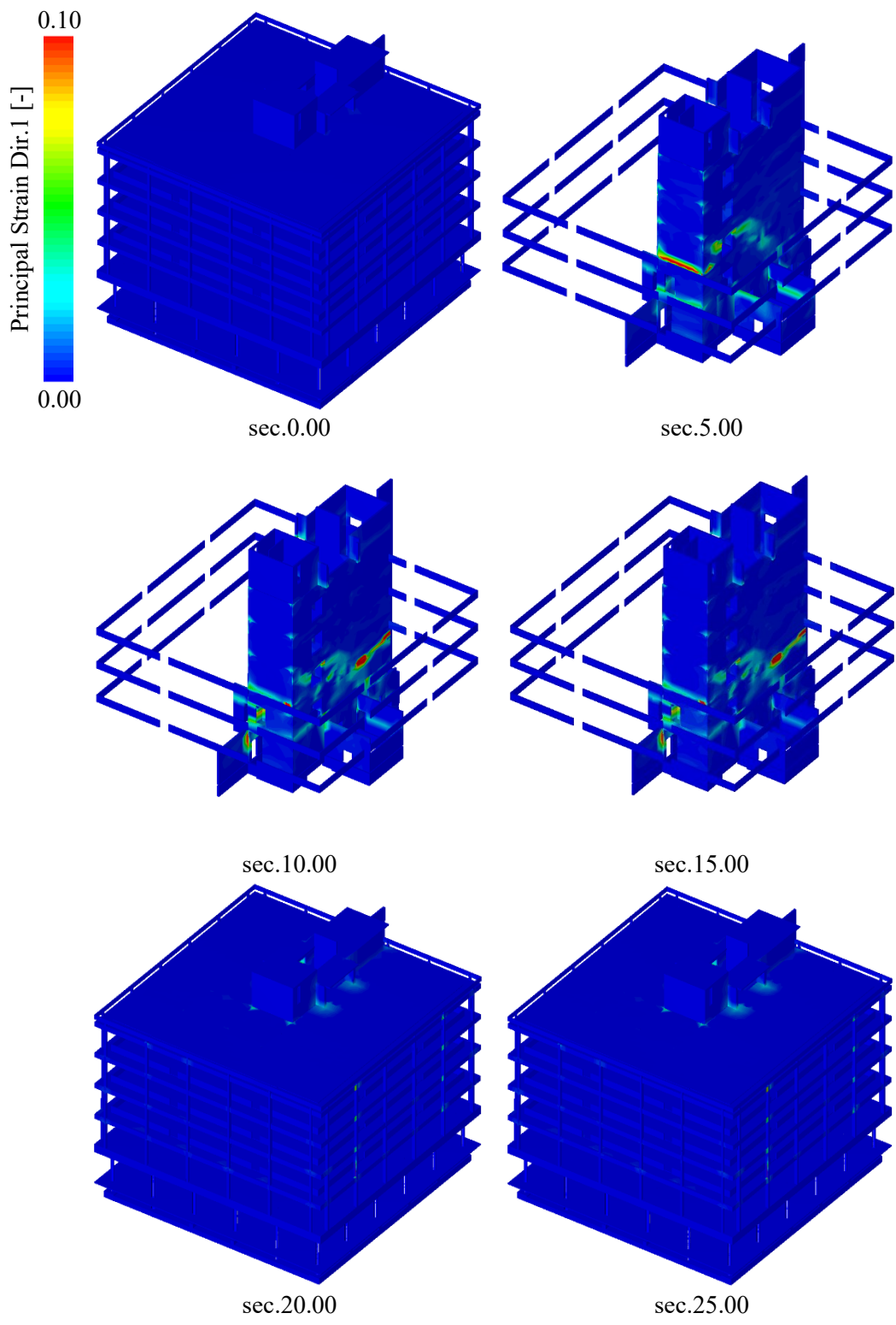
Figure 80. Pyne Gould Building, PBC, retrofitted configuration, non-linear dynamic analysis results employing the February 2023 Turkey record.

Therefore, the selective retrofit of the office building, known as Pyne Gould Building, collapsed during the 2011 New Zealand earthquake, which was obtained by simply adding a small portion of shear wall in the core of the building, would have been effective not only in the prevention of the actual collapse in 2011, but also in preventing the collapse of the building when subject to much more catastrophic events, such as the February 2023 Turkey record.

Findings

This chapter detailed the selective retrofit approach to the seismic retrofit of two RC buildings, the Champlain Towers South, a residential building, and the Pyne Gould Building, an office building.

In the case of the Champlain Towers South, two retrofitting strategies were introduced aiming at avoiding the collapse propagation from the pool deck to the main structure first, and the collapse of the eastern wing of the building after. It was found that the removal of the deep beams connecting the perimeter columns to the pool deck, it was effective in preventing the initial failure of the pool deck slab from propagating to the rest of the building. In addition, increasing the torsional capacity of the eastern wing by introducing two shear walls oriented in the East-West direction, was proven to be effective in preventing its collapse. The overall separation between structures of different natures, such as one-story basements and twelve-story buildings, and RC cores consisting of shear walls oriented along the two principal directions, are the main lessons learned from the progressive collapse analysis of the tragic Champlain Towers South collapse.

In addition, the seismic behavior of the Champlain Towers South was also tested employing the recent February 2023 Turkey earthquake record. It was noted how the reduced torsional capacity deriving from the lack of shear walls oriented east-west would lead to increasing damage to the existing shear core till collapse occurred.

The introduction of additional shear walls oriented east-west was effective in reducing stresses and crack propagation in the core of the building, preventing its collapse.

In the case of the Pyne Gould Building, it was found that a misalignment in the east wall of the shear core would lead to a buckling failure of the RC core, ultimately leading to the collapse of the building. By correcting the misalignment, the building was able to withstand the same time history that caused its collapse in 2011, the February 2011 New Zealand earthquake record.

In addition, the strategy was effective in preventing the collapse of the building even when considering the recent February 2023 Turkey record.

Conclusions

The main objective of the research was to develop a strategy for selective retrofitting against progressive collapse. In other words, to understand if it was possible to detect any specific path in collapse propagation, and if any specific lack of structural details or structural design mistake could be selected and fixed to prevent the initial failure and its spreading to the rest of the structure. In fact, while the aging and degradation of our current structure and infrastructure is a known concern, this approach would allow the selective retrofit of several structures with limited economic resources. A selective retrofitting strategy was derived for the investigated case studies: the Polcevera Viaduct clearly lacked transversal ribs in the deck, which would have provided additional torsional capacity in the case of strand loss, a small detail that could have prevented the final catastrophic outcome. As for the Champlain Towers Condo, it was observed how the connection of the one-floor basement structure (a pool deck slab and therefore also clearly exposed to degradation phenomenal) to the twelve-story building itself, using high-dept beam, was plainly a design mistake as the loss of one single slab would have destabilized up to three perimeters columns, spreading the collapse to the rest of the building. Analysis has shown that a structural separation between the two structures or a reduction of the depth of the beams would have prevented the collapse of the slab at the basement floor from spreading to the rest of the building. Analyses also highlighted a substantial lack of torsional capacity in the east portion of the building. In fact, both in the analysis and in the footage captured from a security camera it was possible to observe the easter portion of the building failing a few moments after the initial collapse while experiencing a substantial rotation around the vertical axes. In addition, analysing the original structural drawings it could be noticed how shear walls in that portion of the building were aligned in one direction only. It was demonstrated how the introduction of additional shear walls aligned in the opposite direction would have prevented the collapse of that portion of the building. In the case of the Pyne Gould building, analyses showed how the collapse would originate from a discontinuity in the shear walls of the building, even when considering different time-history loads. Simply closing the discontinuity at the ground floor, resulted sufficient to prevent the collapse of the Pyne Gould building not only with the actual 6.3 Magnitude earthquake that occurred the 22 February 2011 but also with seismic load significantly higher such as the time history record of the 7.8 Magnitude earthquake occurred in Turkey-Syria in 2023. Finally, the research also investigated an innovative AEM micro-modelling approach to the analysis of heritage buildings, such as the Basilica di Collemaggio. The technique allowed for a detailed reconstruction of masonry patterns, stone's edge interlocking, vaults reconstructions and retrofitting elements such as rods and steel meshes were introduce as implicit springs, reducing the computational burden of the entire Basilica's numerical model. Damage pattern analyses carried out employing the

nearest 2009's L'Aquila earthquake record revealed a good accordance with the actual damage state of the Basilica, captured after the seismic event using a combined laser-scanning and orthophoto technique.

Notations

The following symbols are used in this paper:

E = elastic modulus (GPa);

f_c = compressive strength of concrete (MPa);

f_t = tensile strength of concrete (MPa);

G = shear modulus (GPa);

G_i = element's centroid;

$k_{c,n}$ = normal stiffness of concrete springs

$k_{c,s}$ = shear stiffness of concrete springs

$k_{r,n}$ = normal stiffness of reinforcement springs

$k_{r,s}$ = shear stiffness of reinforcement springs

RTF = reinforcing bars;

u_i = element's degree of freedom;

ε_u = ultimate strain of steel;

μ = friction coefficient;

σ_y = yield stress of steel (MPa);

σ_u = ultimate stress of steel (MPa);

τ_s = shear strength of concrete (MPa);

References

Admane, Harshal, and Pranesh Murnal. 2017. "ANALYSIS OF MASONRY STRUCTURES: A REVIEW," November.

AFAD - Disaster And Emergency Management Presidency. 2023. "Turkish Accelerometric Archive v 1.0." Disaster And Emergency Management Presidency, Earthquake Department.

AISCAT. 2019. "AISCAT - Italian Association of Motorway and Tunnel Dealers." http://www.aiscat.it/pubblicazioni.htm?ck=1&nome= pubblicazioni&idl=4.

Alashker Yasser, Li Honghao, and El-Tawil Sherif. 2011. "Approximations in Progressive Collapse Modeling." *Journal of Structural Engineering* 137 (9): 914–24. https://doi.org/10.1061/(ASCE)ST.1943-541X.0000452.

ASCE. 2013. *ASCE 7-05 Minimum Design Loads for Buildings and Other Structures*. ASCE Standard. American Society of Civil Engineers. https://books.google.it/books?id=F9t_ngEACAAJ.

———. 2021. "ASCE/SEI 7-22 Minimum Design Loads and Associated Criteria for Buildings and Other Structures." American Society of Civil Engineers.

"AS/NZS 4671:2001." 2001. Standards Australia.

Bazzucchi, Fabio, Luciana Restuccia, and Giuseppe Ferro. 2018. "Considerations over the Italian Road Bridge Infrastructure Safety after the Polcevera Viaduct Collapse: Past Errors and Future Perspectives." *Frattura Ed Integrità Strutturale* 12 (46): 400–421. https://doi.org/10.3221/IGF-ESIS.46.37.

Beca Carter Hollings & Ferner Ltd. 2011. "Investigation into the Collapse of the Pyne Gould Corporation Building on 22nd February 2011."

Belmouden, Y., and P. Lestuzzi. 2009. "An Equivalent Frame Model for Seismic Analysis of Masonry and Reinforced Concrete Buildings." *Construction and Building Materials* 23 (1): 40–53. https://doi.org/10.1016/j.conbuildmat.2007.10.023.

Bomarito, Geoffrey, Jacob Hochhalter, Tim Ruggles, and Andrew Cannon. 2017. "Increasing Accuracy and Precision of Digital Image Correlation through Pattern Optimization." *Optics and Lasers in Engineering* 91 (April):73–85. https://doi.org/10.1016/j.optlaseng.2016.11.005.

Breyer, Donald E., Kelly E. Cobeen, and Zeno Martin. 2020. "APPENDIX B: Weights of Building Materials." In , 8th Edition. New York: McGraw-Hill Education. https://www.accessengineeringlibrary.com/content/book/9781260128673/back-matter/appendix2.

Calvi, Gian Michele, Matteo Moratti, Gerard J. O'Reilly, Nicola Scattarreggia, Ricardo Monteiro, Daniele Malomo, Paolo Martino Calvi, and Rui Pinho. 2019. "Once upon a Time in Italy: The Tale of the Morandi Bridge." *Structural Engineering International* 29 (2): 198–217. https://doi.org/10.1080/10168664.2018.1558033.

Cardoni, Alessandro, and Gian Paolo Cimellaro. 2020. "The Role of Reinforced Concrete Roofs in the Seismic Performance of Masonry Buildings." *Journal of Building Engineering* 28 (March):101056. https://doi.org/10.1016/j.jobe.2019.101056.

Carol Ignacio, Prat Pere C., and López Carlos M. 1997. "Normal/Shear Cracking Model: Application to Discrete Crack Analysis." *Journal of Engineering Mechanics* 123 (8): 765–73. https://doi.org/10.1061/(ASCE)0733-9399(1997)123:8(765).

CEN. 2006. "Actions on Structures-Part 1-7: General Actions-Accidental Actions. EN 1994-1-1, Eurocode 4." Brussels, Belgium: European Commission for Standardization.

Cervera, M., and M. Chiumenti. 2006. "Smeared Crack Approach: Back to the Original Track." *International Journal for Numerical and Analytical Methods in Geomechanics* 30 (12): 1173–99. https://doi.org/10.1002/nag.518.

Croci, G. 1998. *The Conservation and Structural Restoration of Architectural Heritage*. Advances in Architecture Series. Computational Mechanics Publications. https://books.google.it/books?id=nPVPAAAAMAAJ.

Domaneschi, M., C. Pellecchia, E. De Iuliis, G.P. Cimellaro, M. Morgese, A.A. Khalil, and F. Ansari. 2020. "Collapse Analysis of the Polcevera Viaduct by the Applied Element Method." *Engineering Structures* 214 (July):110659. https://doi.org/10.1016/j.engstruct.2020.110659.

Domaneschi, Marco, G. Cimellaro, Giuseppe Marano, Maurizio Morgese, Cosimo Pellecchia, and Ahmed Khalil. 2021. "Numerical Simulations of Collapse Tests on RC Beams." In , 286–87. https://doi.org/10.1201/9780429279119-171.

"Extreme Loading for Structures." 2021. Applied Science International, ASI. https://www.extremeloading.com/.

Fiorillo Graziano and Ghosn Michel. 2022. "Structural Redundancy, Robustness, and Disproportionate Collapse Analysis of Highway Bridge Superstructures." *Journal of Structural Engineering* 148 (7): 04022075. https://doi.org/10.1061/(ASCE)ST.1943-541X.0003369.

Gatti, Fabrizio. 2018. "Ponte Morandi, Le Foto Shock Prima Del Crollo: Travi Rotte e Cavi Ridotti Del 75 per Cento." *L'Espresso*, September. https://lespresso.it/c/attualita/2018/9/12/ponte-morandi-le-foto-shock-prima-del-crollo-travi-rotte-e-cavi-ridotti-del-75-per-cento/10861.

Gerasimidis Simos and Ellingwood Bruce. 2023. "Twenty Years of Advances in Disproportionate Collapse Research and Best Practices since 9/11/2001." *Journal of Structural Engineering* 149 (2): 02022002. https://doi.org/10.1061/JSENDH.STENG-12056.

Goulet, Christine, Tadahiro Kishida, Timothy Ancheta, Chris Cramer, Robert Darragh, Walter Silva, Youssef Hashash, et al. 2014. *PEER NGA-East Database*.

GPL software 2019. n.d. "CloudCompare." http://www.cloudcompare.org/.

Grunwald, Christoph, Ahmed A. Khalil, Benjamin Schaufelberger, Erik Maria Ricciardi, Cosimo Pellecchia, Emiliano De Iuliis, and Werner Riedel. 2018. "Reliability of Collapse Simulation – Comparing Finite and Applied Element Method at Different Levels." *Engineering Structures* 176 (December):265–78. https://doi.org/10.1016/j.engstruct.2018.08.068.

GSA. 2013. "ALTERNATE PATH ANALYSIS & DESIGN GUIDELINES FOR PROGRESSIVE COLLAPSE RESISTANCE." General Service Administration.

Guardia di Finanza Genova, dir. 2019. *Police Release New Footage of Doomed Morandi Bridge Collapse in Genoa.* https://www.youtube.com/watch?v=V479srTBlAk.

Hakuno Motohiko and Meguro Kimiro. 1993. "Simulation of Concrete-Frame Collapse Due to Dynamic Loading." *Journal of Engineering Mechanics* 119 (9): 1709–23. https://doi.org/10.1061/(ASCE)0733-9399(1993)119:9(1709).

Hancılar, Ufuk, Karin Şeşetyan, Eser Çaktı, Erdal Şafak, Nesrin Yenihayat, Fatma S. Malcıoğlu, Kökcan Dönmez, Tuğçe Tetik, and Hakan Süleyman. 2023. "Kahramanmaraş - Gaziantep Türkiye M7.7 Earthquake, 6 February 2023 (04:17 GMT+03:00) - Strong Ground Motion and Building Damage Estimations Preliminary Report (V6)." Department of Earthquake Engineering – Bogazici University. https://eqe.bogazici.edu.tr/sites/eqe.boun.edu.tr/files/kahramanmaras-gaziantep_earthquake_06-02-2023_large_hist_eqs_v1.pdf.

Hyland Fatigue and Earthquake Engineering for the Department of Building and Housing. 2011. "CTV Building Hearing: CTV Building: Site Examination and Material Test, Interim Report."

Invernizzi, Stefano, Francesco Montagnoli, and Alberto Carpinteri. 2019. "Fatigue Assessment of the Collapsed XXth Century Cable-Stayed Polcevera Bridge in Genoa." *25th International Conference on Fracture and Structural Integrity* 18 (January):237–44. https://doi.org/10.1016/j.prostr.2019.08.159.

Ismail, Najif, Hamid Mahmoud, Hossein Derakhshan, Win Clark, and Jason Ingham. 2009. *Case Study and Development of Retrofit Application Strategy for a Heritage Building.*

Italian Technical Standards Circolare C.S.LL.PP., 21/01/2019, n.7. 2019.

Kam, Weng Yuen, and Stefano Pampanin. 2008. "Selective Weakening Techniques for Retrofit of Existing Reinforced Concrete Structures." In .

Khalil, Ahmed, Cosimo Pellecchia, and Emiliano De Iuliis. n.d. "High Fidelity Numerical Seismic Modeling of Ancient Brick Structures." In *Structures Congress 2020*, 399–411. https://doi.org/10.1061/9780784482896.037.

Kiakojouri, Foad, Valerio De Biagi, Bernardino Chiaia, and Mohammad Reza Sheidaii. 2020. "Progressive Collapse of Framed Building Structures: Current Knowledge and Future Prospects." *Engineering Structures* 206 (March):110061. https://doi.org/10.1016/j.engstruct.2019.110061.

Kiakojouri, Foad, Mohammad Reza Sheidaii, Valerio De Biagi, and Bernardino Chiaia. 2021. "Progressive Collapse of Structures: A Discussion on Annotated Nomenclature." *Structures* 29 (February):1417–23. https://doi.org/10.1016/j.istruc.2020.12.006.

Lakshmish Kumar, Srinidhi, Aravind H B, and Nabil Hossiney. 2019. "Digital Image Correlation (DIC) for Measuring Strain in Brick Masonry Specimen Using Ncorr Open Source 2D MATLAB Program." *Results in Engineering* 4 (November):100061. https://doi.org/10.1016/j.rineng.2019.100061.

Lalkovski Nikolay and Starossek Uwe. 2022. "The Total Collapse of the Twin Towers: What It Would Have Taken to Prevent It Once Collapse Was Initiated." *Journal of Structural Engineering* 148 (2): 04021276. https://doi.org/10.1061/(ASCE)ST.1943-541X.0003244.

Lang, Kerstin, and Hugo Bachmann. 2004. "On the Seismic Vulnerability of Existing Buildings: A Case Study of the City of Basel." *Earthquake Spectra* 20 (1): 43–66. https://doi.org/10.1193/1.1648335.

Le Jia-Liang and Bažant Zdeněk P. 2022. "Spontaneous Collapse Mechanism of World Trade Center Twin Towers and Progressive Collapse in General."

Journal of Structural Engineering 148 (6): 04022065. https://doi.org/10.1061/(ASCE)ST.1943-541X.0003342.

Li, Jun, and Hong Hao. 2013. "Numerical Study of Structural Progressive Collapse Using Substructure Technique." *Engineering Structures* 52 (July):101–13. https://doi.org/10.1016/j.engstruct.2013.02.016.

Lu, Naiwei, Mohammad Noori, and Yang Liu. 2017. "First-Passage Probability of the Deflection of a Cable-Stayed Bridge under Long-Term Site-Specific Traffic Loading." *Advances in Mechanical Engineering* 9 (1): 1687814016687271. https://doi.org/10.1177/1687814016687271.

Lu, Xinzheng, Hong Guan, Hailin Sun, Yi Li, Zhe Zheng, Yifan Fei, Zhi Yang, and Lingxiao Zuo. 2021. "A Preliminary Analysis and Discussion of the Condominium Building Collapse in Surfside, Florida, US, June 24, 2021." *Frontiers of Structural and Civil Engineering* 15 (5): 1097–1110. https://doi.org/10.1007/s11709-021-0766-0.

Lu, Xinzheng, Xuchuan Lin, and Lieping Ye. 2009. "Simulation of Structural Collapse with Coupled Finite Element-Discrete Element Method." In *Computational Structural Engineering*, edited by Yong Yuan, Junzhi Cui, and Herbert A. Mang, 127–35. Dordrecht: Springer Netherlands.

Lu, Zheng, Xiangdong He, and Ying Zhou. 2018. "Discrete Element Method-Based Collapse Simulation, Validation and Application to Frame Structures." *Structure and Infrastructure Engineering* 14 (5): 538–49. https://doi.org/10.1080/15732479.2017.1373133.

Maekawa, Kouichi, and Hajime Okamura. 1983. "The Deformational Behavior and Constitutive Equation of Concrete Based on the Elasto-Plastic and Fracture Model." In . https://api.semanticscholar.org/CorpusID:109351922.

Malomo, Daniele, Rui Pinho, and Andrea Penna. 2020a. "Applied Element Modelling of the Dynamic Response of a Full-Scale Clay Brick Masonry Building Specimen with Flexible Diaphragms." *International Journal of Architectural Heritage* 14 (10): 1484–1501. https://doi.org/10.1080/15583058.2019.1616004.

———. 2020b. "Simulating the Shake Table Response of Unreinforced Masonry Cavity Wall Structures Tested to Collapse or Near-Collapse Conditions." *Earthquake Spectra* 36 (2): 554–78. https://doi.org/10.1177/8755293019891715.

Menegotto, Marco, and Paolo Emilio Pinto. 1973. "Method of Analysis for Cyclically Loaded R.C. Plane Frames Including Changes in Geometry and Non-Elastic Behaviour of Elements under Combined Normal Force and Bending." *Rapports Des Commissions de Travail AIPC = IVBH Berichte Der Arbeitskommissionen = IABSE Reports of the Working Commissions* 13:15. https://doi.org/10.5169/seals-13741.

MIT. 2018. "Comune Di Genova, Autostrada A10 – Crollo Del Viadotto Polcevera, Evento Accaduto Il 14 Agosto 2018." Ministero delle Infrastrutture e dei Trasporti, Commissione Ispettiva Ministeriale. http://www.mit.gov.it/comunicazione/news/ponte-crollo-ponte-morandi-commissione-ispettiva-genova/ponte-morandi-online-la.

Morandi, Riccardo. 1967. "Il Viadotto Sul Polcevera per l'autostrada Genova-Savona." *L'Industria Italiana Del Cemento* XXXVII:849–72.

———. 1968. "Viaducto Sobre El Polcevera, En Génova Italia." *Informes de La Construcción* 21 (200).

Morgese, Maurizio, Farhad Ansari, Marco Domaneschi, and Gian Paolo Cimellaro. 2020. "Post-Collapse Analysis of Morandi's Polcevera Viaduct in Genoa

Italy." *Journal of Civil Structural Health Monitoring* 10 (1): 69–85. https://doi.org/10.1007/s13349-019-00370-7.

Mpidi Bita Hercend, Huber Johannes A. J., Palma Pedro, and Tannert Thomas. 2022. "Prevention of Disproportionate Collapse for Multistory Mass Timber Buildings: Review of Current Practices and Recent Research." *Journal of Structural Engineering* 148 (7): 04022079. https://doi.org/10.1061/(ASCE)ST.1943-541X.0003377.

Orgnoni, Andrea, Rui Pinho, Matteo Moratti, Nicola Scattarreggia, and G. Calvi. 2019. "Revisione Critica e Modellazione Della Sequenza Di Costruzione Del Viadotto Sul Polcevera" Digital Modeling 25 (November).

Pasticier, Laurent, Claudio Amadio, and Massimo Fragiacomo. 2008. "Non-Linear Seismic Analysis and Vulnerability Evaluation of a Masonry Building by Means of the SAP2000 V.10 Code." *Earthquake Engineering & Structural Dynamics* 37 (3): 467–85. https://doi.org/10.1002/eqe.770.

Pellecchia, Cosimo, Alessandro Cardoni, G. Cimellaro, and Ahmed Khalil. 2023. *DAMAGE PATTERN ANALYSIS OF THE BASILICA DI COLLEMAGGIO USING AEM MICRO-MODELING*. https://doi.org/10.7712/120123.10531.21426.

Pellecchia Cosimo, Cardoni Alessandro, Cimellaro Gian Paolo, Domaneschi Marco, Ansari Farhad, and Khalil Ahmed Amir. 2024. "Progressive Collapse Analysis of the Champlain Towers South in Surfside, Florida." *Journal of Structural Engineering* 150 (1): 04023211. https://doi.org/10.1061/JSENDH.STENG-12485.

Petrangeli Marco and Ožbolt Joško. 1996. "Smeared Crack Approaches—Material Modeling." *Journal of Engineering Mechanics* 122 (6): 545–54. https://doi.org/10.1061/(ASCE)0733-9399(1996)122:6(545).

Praxedes Conrado and Yuan Xian-Xun. 2021. "Robustness Assessment of Reinforced Concrete Frames under Progressive Collapse Hazards: Novel Risk-Based Framework." *Journal of Structural Engineering* 147 (8): 04021119. https://doi.org/10.1061/(ASCE)ST.1943-541X.0003075.

Report prepared for Department of Building and Housing, by Hyland Fatigue and Earthquake Engineering. 2011. "Pyne Gould Corporation Building Site Examination and Material Tests." Auckland, New Zealand.

Rota, M., A. Penna, and G. Magenes. 2010. "A Methodology for Deriving Analytical Fragility Curves for Masonry Buildings Based on Stochastic Nonlinear Analyses." *Engineering Structures* 32 (5): 1312–23. https://doi.org/10.1016/j.engstruct.2010.01.009.

Russo, E., C. Felicetta, M. D'Amico, S. Sgobba, G. Lanzano, C. Mascandola, F. Pacor, and L. Luzi. 2022. "Italian Accelerometric Archive v 3.2 - Istituto Nazionale Di Geofisica e Vulcanologia, Dipartimento Della Protezione Civile Nazionale." https://doi.org/10.13127/itaca.3.2.

Sadek Fahim, Bao Yihai, Main Joseph A., and Lew H. S. 2022. "Evaluation and Enhancement of Robustness for Reinforced Concrete Buildings." *Journal of Structural Engineering* 148 (1): 04021248. https://doi.org/10.1061/(ASCE)ST.1943-541X.0003226.

Salonikios, T, C Karakostas, V Lekidis, and A Anthoine. 2003. "Comparative Inelastic Pushover Analysis of Masonry Frames." *Engineering Structures* 25 (12): 1515–23. https://doi.org/10.1016/S0141-0296(03)00118-4.

Slater, Andy. 2021. "JUST IN: Video I've Obtained of the Building Collapse in Surfside, Florida." https://twitter.com/AndySlater/status/1408051917964595202.

Stylianidis Panagiotis M. and Nethercot David A. 2021. "Simplified Methods for Progressive Collapse Assessment of Frame Structures." *Journal of Structural Engineering* 147 (11): 04021183. https://doi.org/10.1061/(ASCE)ST.1943-541X.0003190.

Tagel-Din, Hatem, and Kimiro Meguro. 2000. "APPLIED ELEMENT METHOD FOR DYNAMIC LARGE DEFORMATION ANALYSIS OF STRUCTURES." *Doboku Gakkai Ronbunshu* 2000:1–10.

Tomazevic, Miha. 1999. *Earthquake-Resistant Design of Masonry Buildings*. Vol. Volume 1. Series on Innovation in Structures and Construction, Volume 1. PUBLISHED BY IMPERIAL COLLEGE PRESS AND DISTRIBUTED BY WORLD SCIENTIFIC PUBLISHING CO. https://doi.org/10.1142/p055.

Tracciatori srl. 2021. "Ortofoto Pareti Abside Di Collemaggio."

UFC. 2016. "UFC 4-023-03: Design of Buildings to Resist Progressive Collapse." Washington, DC: Department of Defense.

Vrouwenvelder Ton. 2021. "The Weakness of Robustness." *Journal of Structural Engineering* 147 (11): 04021193. https://doi.org/10.1061/(ASCE)ST.1943-541X.0003187.

William M. Friedman & Associates Architects. 1979. "As-Built Drawings of the Champlain Tower South Project." https://townofsurfsidefl.gov/departments-services/town-clerk/champlain-towers-public-records-documents.